



***Conjugated Metallopolymer Systems for Electrochemiluminescence  
Enhancement;***

***New Approaches and Materials***

***Emmet O'Reilly B.Sc. (Hons)***

***A thesis submitted for the degree of Doctor of Philosophy***

***Supervisor : Prof. Robert J. Forster  
School of Chemical Sciences  
Dublin City University***

***September 2008***

## ***Abstract***

The goal of this work is to produce new materials with enhanced Electrochemiluminescence by tuning the properties of the material itself. The electrochemical and photophysical properties of films of the conjugated ruthenium metallopolymers  $[\text{Ru}(\text{bpy})_2(\text{PPyBBIM})_n]^{2+}$  ( where  $n = 1,10,20$ ) and composite films of  $[\text{Ru}(\text{bpy})_3]^{2+}$  with either high or low molecular weight fractions of the conducting polymer (PMAS) have been investigated with the goal of enhancing ECL production. It has demonstrated that it is possible to tune both the electrochemical and photophysical properties of a material to favor ECL production, but that there often exists a “trade off” between the two, e.g. enhanced charge transport resulting in decreased luminescent lifetime.

Both the Ru(2,2-bipyridyl)poly[2-(2-pyridyl)-bibenzimidazole metallopolymers and the Ru-PMAS films displayed charge transfer diffusion coefficients ( $D_{\text{CT}}$ ) of up to  $1.44 \pm 0.2 \times 10^{-10} \text{ S cm}^{-2}$ . The benzimidazole based metallopolymer displayed dual emission resulting from both the polymer backbone and the ruthenium metal centre. Given the spectra overlap quenching of the polymer based emission via electron transfer to the ruthenium centered emission was expected however it was shown that this was not thermodynamically feasible. Electron transfer from the polymer to the ruthenium has been shown to occur within the Ru-LMWT PMAS film resulting in an enhancement of ruthenium based emission. The Ru-HMWT displayed the fastest rates of charge transport however it has been shown to deactivate the ruthenium excited state via energy transfer to acceptor states on the polymer itself resulting in decreased photoluminescence and luminescence lifetimes. ECL efficiencies were calculated for each of the films, the Ru-LMWT PMAS film was shown to enhance ECL efficiency by approximately 25 % compared to the non conjugated metallopolymer  $[\text{Ru}(\text{bpy})_2(\text{PVP})_{10}]^{2+}$  demonstrating that conjugated metallopolymer systems represent a promising future of ECL.

## ***Table of Contents***

### ***Chapter 1; Theoretical Framework and Survey of Literature***

1.1 Electrochemiluminescence; Principles and Occurrence;	2
1.1.1 General Principles	2
1.1.2 Analytical Applications	14
1.1.3 ECL limitations	18
1.2 Conjugated Conducting Metallopolymers for ECL enhancement	19
1.2.1 Introduction	19
1.2.2 Charge Transport Mechanism of Conjugated Metallopolymers	22
1.2.3 Examples of Conjugated Metallopolymers with Enhanced Charge Transport	26
1.6 Conclusions	32

### ***Chapter 2; Characterisation of [Ru(bpy)<sub>2</sub>(PPyBBIM)<sub>n</sub>]<sup>2+</sup> and [poly(2-methoxyaniline-5-sulfonic acid)]***

2.1 Introduction	39
2.2 Apparatus and Reagents	43
2.3 Characterisation of [Ru(bpy) <sub>2</sub> (PPyBBIM) <sub>n</sub> ] <sup>2+</sup>	47
2.3.1 General	47
2.3.2 UV- Visible Spectroscopy	49
2.3.3 pH Dependence of UV-Vis Spectroscopy	51
2.3.4 Emission Spectroscopy	53
2.3.5 Excited State Lifetimes	57
2.3.6 Cyclic Voltammetry	61
2.4 Characterisation of Poly(2-methoxyaniline-5-sulfonic acid)	69
2.4.1 General	69
2.4.2 Uv-Visible Spectroscopy	70

2.4.3 Emission Spectroscopy	72
2.4.4 Photoluminescent yields and excited state lifetimes	74
2.4.5 Cyclic Voltammetry	76
2.5 Conclusions	79
2.6 References	84

***Chapter 3; Ground vs. Excited state electron transfer in***

***[Ru(bpy)<sub>2</sub>(PPyBBIM)<sub>n</sub>]<sup>2+</sup> Films***

3.1 Introduction	86
3.2 Apparatus and Reagents	88
3.3 Results and Discussion	91
3.3.1 Ground State Electron Transfer	91
3.3.1.1 Effect of Scan Rate	94
3.3.1.2 Contribution of the metallopolymer backbone to charge transport	100
3.3.2 Excited State Electron Transfer	105
3.3.2.1 UV-Visible Spectroscopy	105
3.3.2.2 Emission Spectroscopy	107
3.3.2.3 Driving Force for Photoinduced Electron Transfer	112
3.3.2.4 Luminescence Lifetime measurements	114
3.4 Conclusions	117
3.5 References	118

***Chapter 4; Electrochemical and Photophysical Studies of***

***Ruthenium-PMAS Composite Films***

4.1 Introduction	121
4.2 Apparatus and Reagents	123
4.2.1 Apparatus	123

4.2.2 Materials and Reagents	124
4.2.3 Composite Formation	124
4.3 Results and Discussion	127
4.3.1 Electrochemical properties of $[\text{Ru}(\text{bpy})_3]^{2+}$ composite films	127
4.3.2 Effect of Scan Rate	130
4.3.3 Steady State Luminescence of Ru-PMAS Composite Films	135
4.3.4 Solution Phase Quenching Studies	138
4.3.5 Luminescent Lifetime Measurements	144
4.3.6 Fluorescent Lifetime Imaging Spectroscopy	149
4.4 Conclusions	153
<b><i>Chapter 5.0; Electrochemiluminescent Properties of</i></b>	
<b><i><math>[\text{Ru}(\text{bpy})_2(\text{PPYBBIM})_n]^{2+}</math> and Ruthenium-PMAS Composite Films.</i></b>	
5.1 Introduction	157
5.2 Apparatus and Reagents	160
5.3 Discussion	164
5.3.1. Charge transport properties of ruthenium containing polymers and composite films	164
5.3.2 Sodium Oxalate as a co-reactant	167
5.3.3 ECL Generation with Sodium Oxalate	173
5.3.4 Electrochemiluminescent efficiencies of the metallopolymer films.	177
5.4 Conclusions	180
5.5 References	182
<b>Chapter 6; Conclusions</b>	
6.0 Conclusions	184
Appendix	

## *Chapter 1*

### *Literature Review and Theoretical Framework*

## ***1.4 Electrochemiluminescence; Principles and Occurrence:***

### ***1.4.1 General Principles:***

Chemiluminescence (CL) is a powerful analytical technique that exhibits high sensitivity and selectivity<sup>1,2</sup> compared to other luminescence based detection systems. Electrochemiluminescence or electrogenerated chemiluminescence (ECL) is a form of chemiluminescence in which the light emitting chemiluminescent reaction is preceded by an electrochemical reaction. The light emission is caused by relaxation of the ruthenium excited state having been created via energetic electron transfer reactions of electrogenerated species in solution. ECL has important advantages over more conventional CL in that the reagents needed for the reaction are produced *in situ* when required at the electrode. The reaction can therefore be controlled and manipulated by controlling the applied potential. This allows unstable reagents to react as soon as they are formed. By controlling the potential, light emission can be delayed until events such as immune or enzyme catalyzed reactions have taken place. Although similar control can be exercised over alternative detection methods, such as fluorescence, the equipment is considerably more sophisticated and expensive. ECL has a further advantage over optically driven luminescence in that no external light source is required for excitation thereby significantly reducing background interference. An illustration of ECL with current transduction methods can be seen in Figure 1.1.

ECL has another notable advantage in that it allows control over the position at which light is emitted. Control over position can be used to confine light emission to a region that is precisely located with respect to the detector, improving sensitivity by increasing the signal to noise ratio. A good example of this is the combination of ECL with magnetic bead technology, which allows bound label to be distinguished from unbound labels without a separation step. Control over position could also be used to determine the results of more than one analytical reaction in the same sample by interrogating each electrode in an array, either in sequence, or simultaneously using a position sensitive detector.

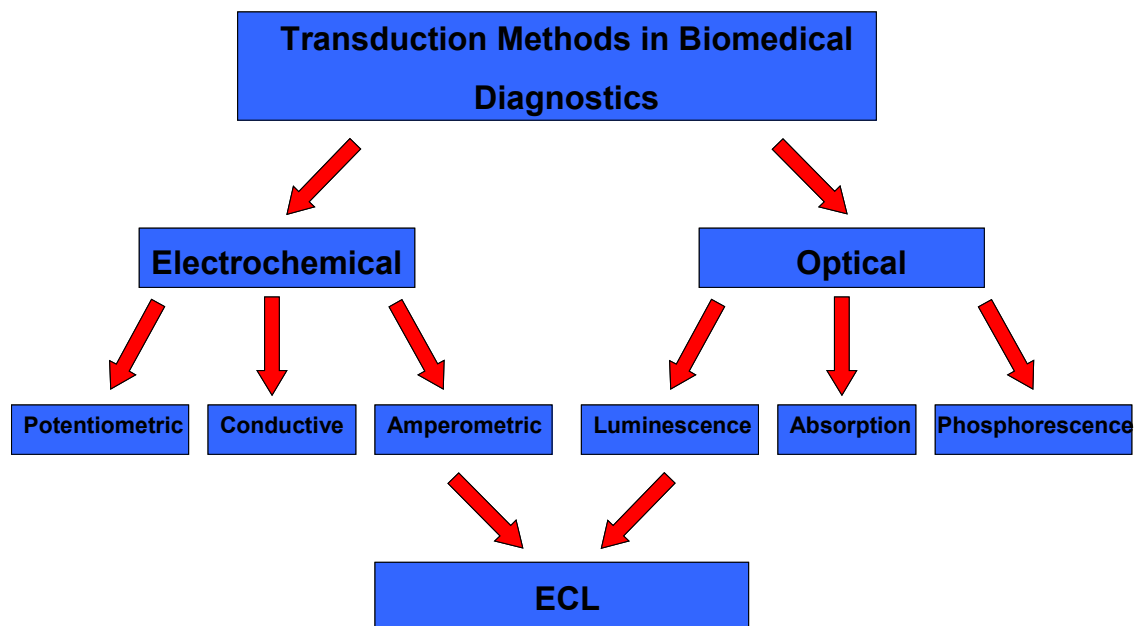
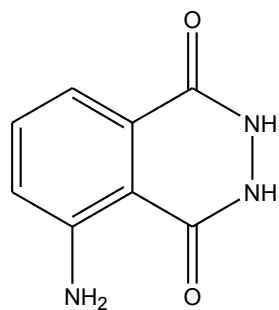


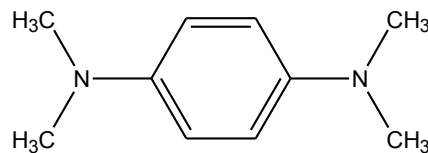
*Figure 1.1: Illustration of ECL within current transduction methods.*

Due to the aforementioned advantages, the study of ECL systems has attracted across different research fields, such as electrochemistry, spectroscopy and photochemistry that it entails, as well as by their potential as the basis for highly sensitive detection techniques in analytical chemistry. Indeed this increased interest is reflected in the number of reviews<sup>3,4,5,6,7,8,9,10,11,12,13,14,15</sup> that report the usefulness of ECL detection methods and its analytical applications.

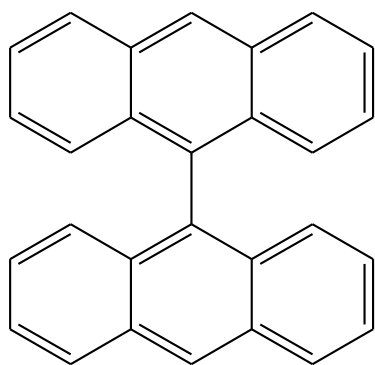
ECL can arise from organic as well as inorganic substances and can be produced by annihilation reactions between reduced and oxidised forms of the same species or by using a co-reactant that forms an energetic oxidant or reductant on bond cleavage. ECL provided the first evidence of the Marcus inverted region, where generation of the excited state rather than the energetically more favourable ground state was seen.<sup>16</sup> To generate ECL, AC as well as DC electrolysis may be used and the precursors may be generated sequentially at the electrode by CV or potential step techniques or simultaneously at a rotating ring disk<sup>17</sup> or double band electrode. Organic compounds known to produce ECL include luminol, anthracene, 9,10-diphenylanthracene (DPA) coronene and ruberene. A large number of inorganic metals and clusters are also able to produce ECL. Complexes of metals investigated include ruthenium<sup>11,12</sup> osmium<sup>18,19</sup> chromium<sup>20,21</sup> rhenium<sup>22,23</sup> cadmium<sup>24</sup> and copper.<sup>25</sup> The structures of some of the most widely studied organic and inorganic ECL active complexes can be seen in Figure 1.2 and Figure 1.3.



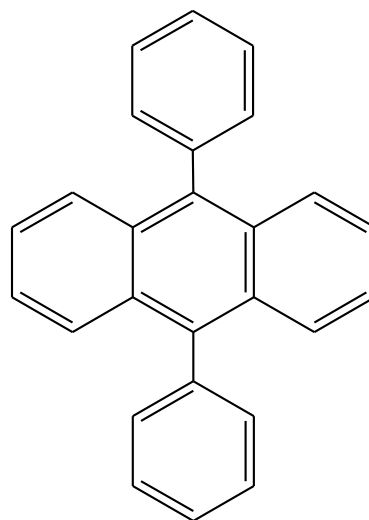
**Luminol**



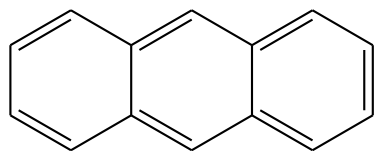
**TMPD**



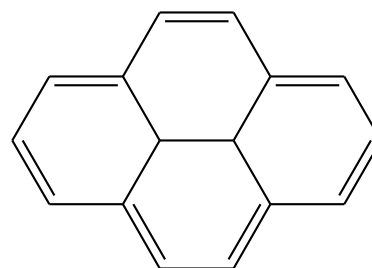
**Bianthryl**



**DPA**

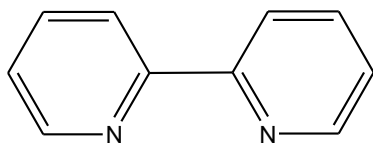


**Anthracene**

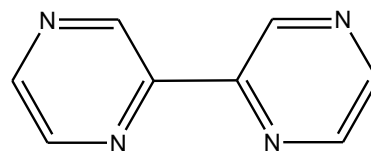


**Pyrene**

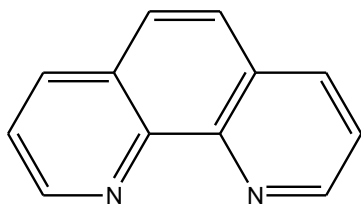
*Figure 1.2: Structure of some of the most commonly studied ECL-active organic species.*



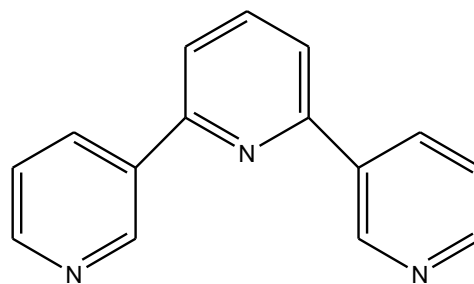
**bpy**



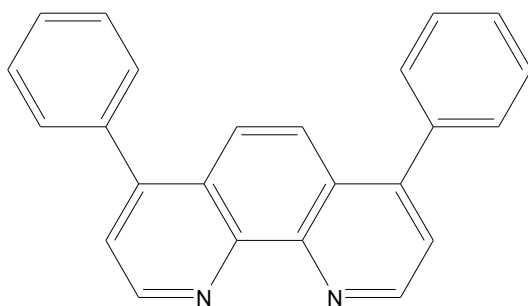
**bpz**



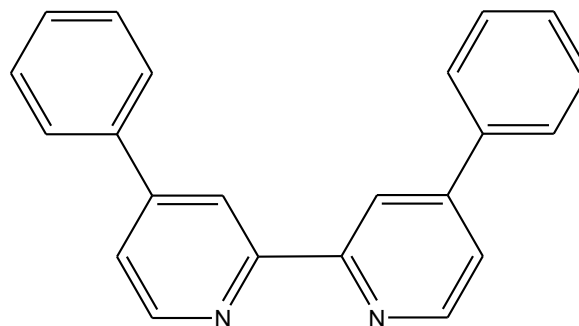
**phen**



**terpy**



**dp-phen**



**dp-bpy**

**Figure 1.3:** Structures of the ligands of some of the most commonly studied inorganic ECL-active complexes. The above ligands are commonly used to form ruthenium and osmium complexes.

The basic requirements for efficient annihilation ECL to occur are the formation of stable radical ions of the precursor molecules in the electrolyte of interest, good photoluminescence efficiency of a product of the electron transfer reaction and sufficient energy in the electron transfer reaction to produce the excited state. The precursors participating in the homogeneous electron transfer leading to the light emitting excited state are generated at electrodes through heterogeneous electron transfer reactions. In organic ECL systems these precursors are often in the form of oxidised and reduced radical ions, whereas in inorganic systems they are typically simply the reduced and/or oxidised forms of the parent complex. The oxidised precursor represents a ‘hole’ in the highest occupied molecular orbital (HOMO) which enhances its oxidative properties, while the reduced form represents an electron in the lowest unoccupied molecular orbital (LUMO), which enhances its capacity for reduction. In all cases the homogeneous reaction between these precursors is characterised by very fast ( $\sim 10^{10} \text{ M}^{-1}\text{s}^{-1}$ ) very energetic (typically 2-4 eV) electron transfer.<sup>26</sup>

As can be seen from Figure 1.4, there are two possible paths for the homogeneous reaction between the two radicals. Firstly, the electron transfer may take place from the now occupied LUMO of the reduced radical to the HOMO of the oxidised one (B). This is the path most favoured thermodynamically. However, if electron transfer is sufficiently rapid, this means that a large amount of energy would have to

be dissipated over a very short time scale in vibrational modes, which is very difficult for the reacting system. Here a kinetic manifestation of the Franck-Condon principle comes into play, and the path to electronically excited products becomes relatively attractive, because its demand for mechanical accommodation is not nearly so great.<sup>7</sup>

The luminescent path involves electron transfer between the LUMO of the reduced radical and the slightly less energetic LUMO of the oxidised radical (A). In this case only a small amount of energy needs to be dissipated in mechanical modes, this satisfies the Frank-Condon principle and leads to the formation of an excited state product, which emits light on relaxation, forming the stable ground state products.

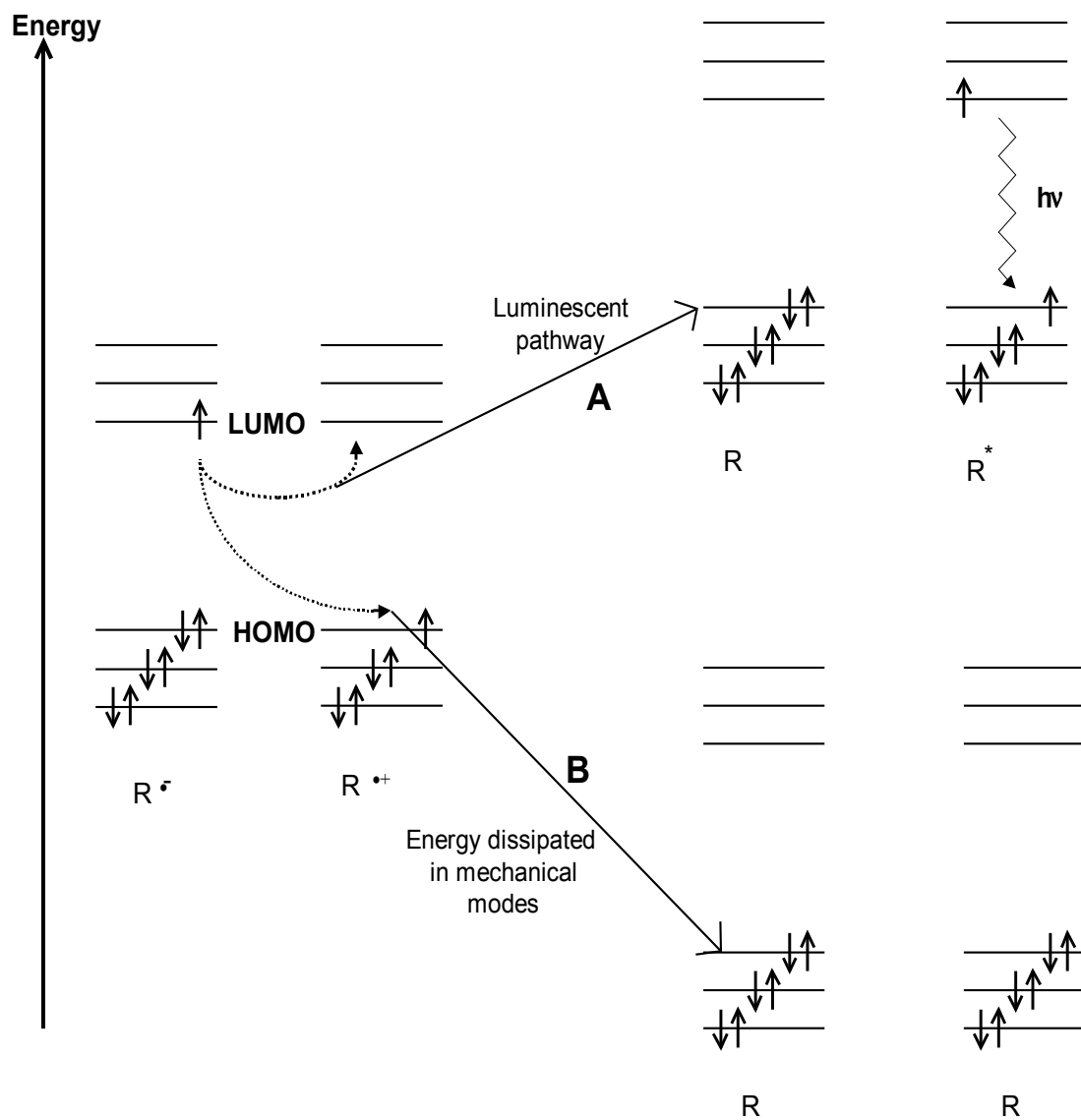
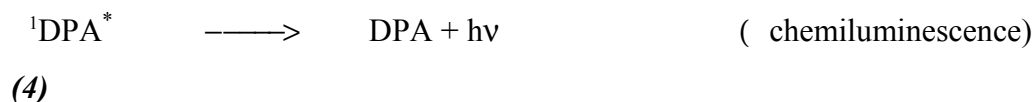


**Figure 1.4** Molecular orbital diagram showing two alternative pathways for electron transfer between oxidised and reduced precursors  $R^\bullet$  and  $R^{\bullet+}$ . (A) Formation of an excited state and (B) direct population of ground state products.

ECL mechanisms have been extensively studied and it has been found that there are at least five main pathways by which ECL can occur. These pathways are;

(i)S-Route: Reactions between oxidised and reduced precursors leading to the direct formation of an excited (usually singlet) state. This is known as the S-route and the system. A typical S-route system is the polyaromatic hydrocarbon; 9,10-diphenylanthracene (DPA). The radical cation and the anion of this species are produced by applying a double potential step to a platinum electrode in a solution of DPA dissolved in MeCN or DMF using a tetrabutylammonium salt as supporting electrolyte.<sup>27</sup> The reaction proceeds as follows;



where  $\text{DPA}^*$  is the excited singlet state. Emission is observed at  $\lambda_{\text{max}} = 420\text{nm}$ . As can be seen from Figure 1.4, the energy supplied by the ion annihilation reaction (reaction 3 above) is sufficient to directly populate the emitting singlet state.

(ii) T-Route: When radical annihilation reaction is 'energy deficient' and therefore unable to produce an excited singlet state directly, then an excited triplet may be formed, which may be able to generate a singlet for efficient light emission through triplet-triplet annihilation. This indirect pathway is known as the T-route. An example of the T-route is the DPA-TMPD ECL system, (where TMPD is N,N,N',N'-tetramethyl-p-phenylenediamine). In this system the following reactions take place;





These reactions are then followed by reaction 8. As can be seen from Figure 1.5 only the non-emitting triplet is energetically accessible following reaction 10, therefore the energy for the population of the first excited singlet comes from reaction 11 where the energy from two electron transfers is pooled to provide sufficient energy.

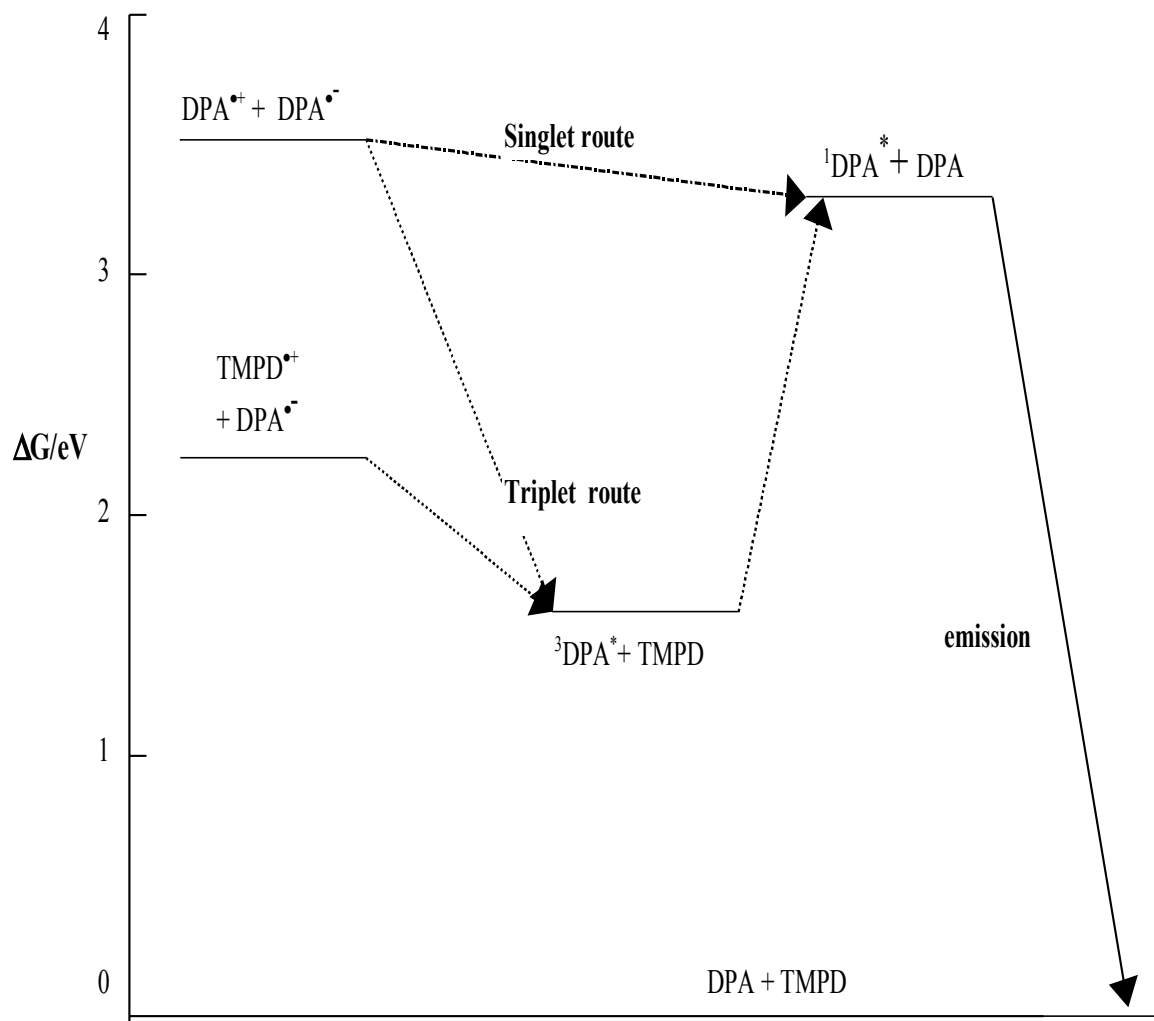
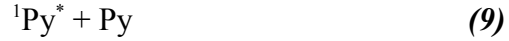


**Figure 1.5** Energy level diagram for DPA and DPA-TMPD ECL systems

- (iii) E-Route: In the two previous types of ECL considered, the annihilation reaction leading to the formation of the emitting species is said to proceed *via* a charge transfer or encounter complex. There is a third type where this molecular complex itself is responsible for emission. If the excited complex emitter is formed from two like molecules, it is known as an eximer, and if formed from two unlike molecules, it is an exiplex.<sup>28</sup> The mechanism involving emission originating from these types of complexes is sometimes known as the E-route.

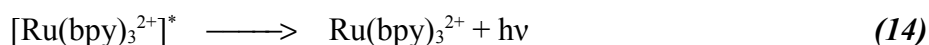
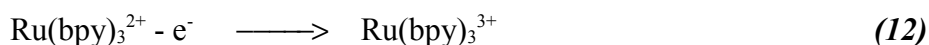
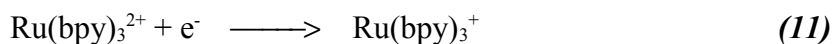
For example, the ECL of pyrene<sup>63</sup> (Py) plus TMPD produces a bimodel spectral emission with peaks at *ca.* 400nm from  $^1\text{Py}^*$ , and *ca.* 480nm from the  $\text{Py}_2^*$  eximer:



where  $^1\text{Py}^*$  and  $^3\text{Py}^*$  represent the excited singlet and triplet states of pyrene respectively and  $\text{Py}_2^*$  represents the eximer.

- (iv) A S-route system that involves direct population of triplets by homogeneous reaction between electrogenerated precursors, followed by phosphorescence to give ground state products. This path is most often encountered with transition metal complexes such as ruthenium(tris)bipyridine,  $[\text{Ru}(\text{bpy})_3]^{2+}$ . Here, spin allowed excited states undergo rapid deactivation due to spin-orbital coupling and emission originates from the lowest energy excited state via energy sufficient routes. The lifetime of this species being too short to take part in subsequent annihilation reactions, emission comes as phosphorescence from the spin-forbidden excited state.

If a solution of  $\text{Ru}(\text{bpy})_3^{2+}$  in acetonitrile (ACN) is subjected to a cyclic double step potential alternating between oxidation and reduction potential of the complex, an orange emission is observed from the vicinity of the electrode ( $\lambda_{\text{max}} = 610 \text{ nm}$ ). The reaction sequence is as follows;



Since the excited state triplet from which emission occurs is directly populated, the system is energy sufficient and is therefore classed as an S-Route system.

(v) Homogeneous reactions of electrogenerated precursors with electron donors/acceptors present in solution can also result in ECL. For instance, if a strong oxidising or reducing agent, such as oxalate ( $\text{C}_2\text{O}_4^{2-}$ ) or peroxodisulphate ( $\text{S}_2\text{O}_8^{2-}$ ) is introduced into solution in the  $[\text{Ru}(\text{bpy})_3]^{2+}$  system described above, then only half the oxidation-reduction cycle need be applied. However, it should be noted that being a strong oxidising/reduction agent is a necessary, but not sufficient condition for a co-reactant to produce ECL in these cases.<sup>8</sup>

#### ***1.4.2 Analytical Applications:***

The application of electrochemiluminescence (ECL) for the detection of biologically important analytes has seen substantial development over the last two decades. Due to its highly sensitive and selective detection methods Electrochemiluminescence (ECL) has proven to be a powerful tool for use within analytical applications. The increasing interest over the past two decades is reflected in some of the many ECL reviews.<sup>5,7</sup> Relatively inexpensive commercial instrumentation and ECL labels with linker groups that are easily attached to biomolecules have allowed researchers to quickly and easily develop numerous assay formats for a variety of applications. Many of the analytical applications of ECL have been based on the inorganic ruthenium chelate  $[\text{Ru}(\text{bpy})_3]^{2+}$  and its derivatives. This is due to the ability of these complexes to emit luminescence at room temperature in aqueous solutions and undergo reversible one-electron transfer reactions at easily attainable potentials thus producing stable reduced or oxidised species. Under certain conditions the efficiency of excited state production ( $\Phi_{\text{ES}}$ ) for these complexes has been known to approach 100%.<sup>29</sup>  $[\text{Ru}(\text{bpy})_3]^{2+}$  exhibits intense ECL with a range of co-reactants, both oxidants and reductants, which is relatively insensitive to the presence of oxygen and impurities. This makes the system a very attractive means of detection, and there are numerous such methods published in the literature for determination of a wide variety of analytes. These have been extensively reviewed.<sup>8,13,14</sup>

The occurrence of ECL in the reaction of  $[\text{Ru}(\text{bpy})_3]^{2+}$  with amines<sup>30</sup> enables the determination of a large number of analytes. Many amine containing analytes such as amino acids, proteins, aliphatic and cyclic amines and various pharmaceuticals have been determined with high sensitivity using this method.<sup>11</sup> The relationship between the ECL behaviour and the structure of the amine containing molecule has been intensively investigated and reviewed by Knight and Greenway.<sup>31</sup> It is found that ECL emission from the reaction with amines increases in the order  $1^\circ < 2^\circ < 3^\circ$  amines. Primary amines show the lowest ECL intensity and their detection is sometimes only possible after derivatisation with divinylsulfone. Upon reaction with divinylsulfone primary amines undergo a cycloaddition reaction resulting in the formation of the alicyclic tertiary amine.<sup>32</sup> Other factors that influence the ECL of amines are electron

donating or accepting substituents at the nitrogen or  $\alpha$ -carbon, chain length of the alkyl chains, a rigid cyclic or a non cyclic structure and the presence of aromatic groups. Electron withdrawing substituents close to the radical centre tend to modulate ECL intensity due to a stabilising or destabilising effect on the radical intermediate (which participates in the reaction leading to the excited state). Resonance stabilisation of the radical intermediate reduces its reactivity and thus ECL intensity (as is the case with aromatic amines). The molecular geometry and the radical species may also be a factor.

Danielson *et al*<sup>33</sup> have looked at a large number of amines with respect to their potential for producing ECL. They found a strong inverse correlation between ECL intensity and first ionisation potential, and also noted that the loss of a non-bonding electron for the electron transfer reaction leading to ECL was favoured.

The  $[\text{Ru}(\text{bpy})_3]^{2+}$ /oxalate system has also been used to determine oxalate in synthetic urine.<sup>34</sup> High oxalate concentrations in blood and urine are known to accompany a number of maladies including renal failure, vitamin deficiency and intestinal diseases. ECL intensity was linearly related to oxalate concentration over the range of  $10^{-6}$ - $10^{-4}$  M. This region encompasses the concentrations found in normal blood and urine.  $[\text{Ru}(\text{bpy})_3]^{2+}$  itself has been determined in the presence of oxalate and persulphite to levels as low as  $10^{-13}$  M, which allowed the authors to suggest its implementation as a novel ECL label.<sup>35</sup> Other organic species which have been determined using  $[\text{Ru}(\text{bpy})_3]^{2+}$  ECL include hydroxyl carboxylic acid,<sup>36</sup> monohydric alcohols both of which produce the excited state through broadly similar mechanisms to oxalate.

The combination of very sensitive ECL detection with extremely selective biological interactions such as enzymatic reactions, immunoassays and DNA probe assays has gained more and more interest over the past number of years and has resulted in a number of publications.<sup>33,37</sup> Ruthenium based systems have once again received much attention in this area. This is mainly due to the fact  $[\text{Ru}(\text{bpy})_3]^{2+}$  can be easily modified by attaching reactive groups to the bipyridyl ligands to form active labels

for proteins, nucleic acids and other biological molecules. This allows measurements in aqueous solutions at an optimal pH for immunoreactions. Impurities introduced with the biological matrix or dissolved oxygen do not interfere with the accurate detection of the ECL label. This technique allows even multi labelling of biomolecules without interfering with the biological activity. This approach has many distinct advantages, namely that problems of sample handling, disposal and lifetime decay inherent in radioimmunoassay are eliminated, since no radioactive isotope is used. Detection limits are extremely low, normally sub-picomolar, (a limit of  $5 \times 10^{-20}$  moles was reported for the HIV-1 *gag* gene), the linear dynamic range is greater than six orders of magnitude, the labels are extremely stable and can be stored for over a year at room temperature and their small size allows multiple labelling of the same molecule without affecting the immunoreactivity or hybridisation of the probes.

ECL technology has recently been commercially developed for the clinical diagnostics market.<sup>38</sup> Assays have been developed for a wide variety of applications such as monitoring pregnancy, thyroid diseases, and infectious diseases.<sup>39</sup> The sensitive detection of biotoxoids and bacterial spores such as anthrax in soil has also been described.<sup>40</sup> In this technology, ECL detection is combined with conventional antigen-antibody reactions which take part on streptavidin coated magnetic particles. The sample is combined with a reagent containing biotinylated antibody and a second ruthenium labelled antibody. During incubation the antibodies capture the target molecules, the microparticles are then added and during a second incubation period the biotinylated antibody attaches to the streptavidin coated particles (Figure 1.6). The sample is drawn into the ECL measuring cell along with a buffer containing tripropylamine. A magnet located under the electrode captures the microparticles at the electrode surface and all unbound reagent is washed from the cell. The magnet is then removed and a potential is applied to the electrode, initiating ECL.

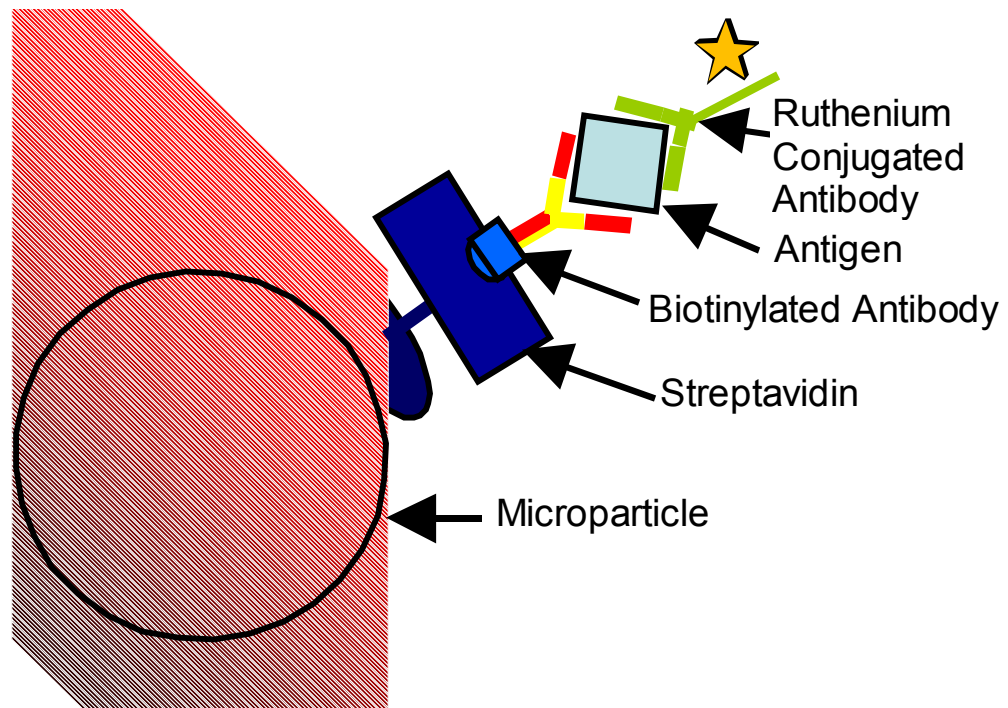


*Figure 1.6: Basis of Elecsys® ECL immunoassay technology.*

### ***1.4.3 ECL Limitations:***

Electrochemiluminescence has many distinct advantages over conventional Chemiluminescence such as the ability to generate the reactants in situ, the opportunity to gain additional information from monitoring the electrochemical activity of the analyte and removal of the need for an external light source thereby reducing background noise and increasing sensitivity. However like many other transduction methods it too suffers from certain disadvantages. Low photoluminescent yields and luminescence lifetimes can significantly reduce ECL in both organic and inorganic systems. In ruthenium based ECL systems certain criteria exist that favour ECL production such as film porosity. A rigid film prevents analyte diffusion to the mediating  $\text{Ru}^{3+}$  metal centres. If transport of the analyte is not rate limiting ECL production is highly dependent upon the rate of charge transfer ( $D_{CT}$ ). A fast rate of charge transfer ensures sufficient  $\text{Ru}^{3+}$  will be present to react with a given analyte and produce ECL. The non conjugated redox metallopolymers that have typically been used for ECL suffer from relatively slow charge transport compared to recently developed conducting metallopolymers.<sup>41</sup>

The metallopolymers currently utilised for ECL production such as  $[\text{Ru}(\text{bpy})_2(\text{PVP})_{10}]^{2+}$  consist of electrochemically active sites at each ruthenium metal centre tethered to a electrochemically inactive backbone. The ruthenium metal d-orbitals are isolated from one another and as such charge transfer occurs via a “through space mechanism”. By incorporating a conjugated backbone the electronic interactions between the polymers  $\pi$ -system and the metals d-orbitals will modulate the properties of both components in interesting and potentially useful ways. One of the anticipated benefits is to achieve several photons per luminophore in the measurement. A faster rate of charge transfer would therefore significantly increase the production of ECL leading to enhanced sensitivity.

## ***1.5 Conjugated Conducting Metallopolymers for ECL Enhancement:***

### ***1.5.1 Introduction:***

The study of conducting polymers has blossomed into a mature field over the last four decades. Tremendous progress has been made towards the goal of developing conjugated organic materials with delocalised  $\pi$  electrons serving as the means of electronic conductivity.<sup>42,43,44</sup> The extensive delocalization of  $\pi$  electrons is well known to be responsible for the array of remarkable characteristics that these polymers exhibit. These properties include non-linear optical behaviour and exceptional mechanical properties such as tensile strength and resistance to harsh environments. However the most remarkable characteristic of these polymers is their ability to act as electronic conductors.<sup>42</sup>

The first polymer capable of conducting electricity was prepared in the mid 1970s. Polyacetylene as shown in Figure 1.7 was prepared by accident by Shirakawa.<sup>45</sup> The subsequent discovery by Heeger and MacDiarmid<sup>46</sup> that the polymer would undergo an increase in conductivity of 12 orders of magnitude by oxidative doping with iodide quickly reverberated around the polymer and electrochemistry communities, and an intensive search for other conducting polymers soon followed.

The essential structural characteristic of all conjugated polymers is their quasi-infinite  $\pi$  system extending over a large number of recurring monomer units. This feature results in materials with directional conductivity, strongest along the axis of the chain.<sup>47</sup> Since the discovery by Heeger and McDiarmid many conjugated polymers with varying degrees of functionality have been produced. The aim of which is to produce a material that could combine the processibility, environmental stability, and weight advantages of a fully organic polymer with the useful electrical properties of a metal. Electronically conducting polymers are extensively conjugated molecules and as such it is believed that they possess a spatially delocalised band-like electronic structure.<sup>47</sup> These bands stem from the splitting of interacting molecular orbitals of

the constituent monomer units in a manner reminiscent of the band structure of solid-state semiconductors. The mechanisms of conductivity in these polymers have been shown to be based on the motion of charged defects within the conjugated framework. The charge carriers, either positive p-type or negative n-type, are the products of oxidising or reducing the polymer respectively. To date research into the applications of conducting polymers is ongoing within academic, industrial and governmental laboratories. Current applications of conducting polymers include solar cells,<sup>48</sup> lightweight batteries, sensors<sup>49,50</sup> and molecular electronic devices.<sup>51</sup>

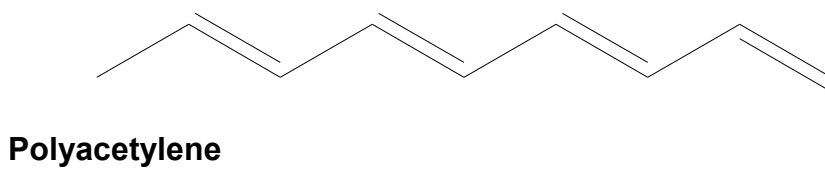
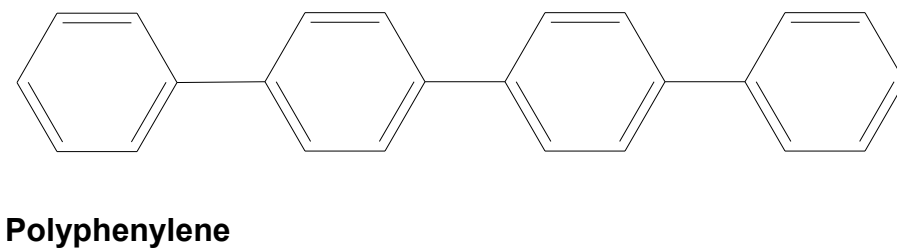
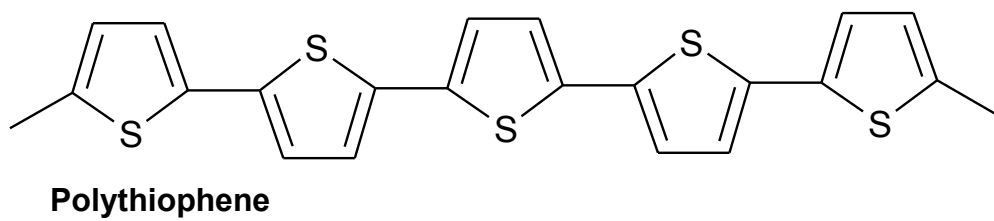
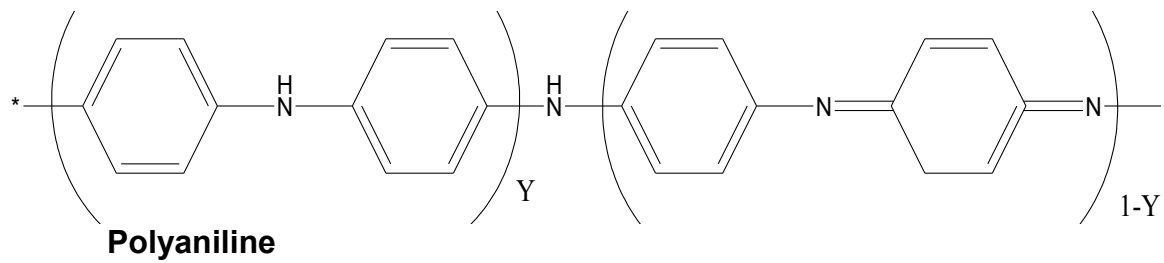
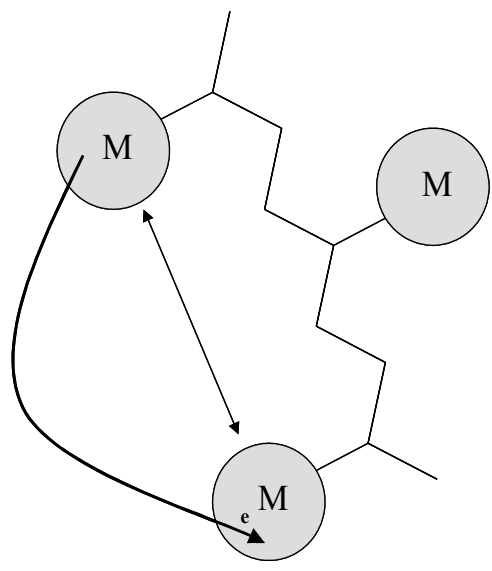


*Figure 1.7: Structure of some common conducting polymers.*

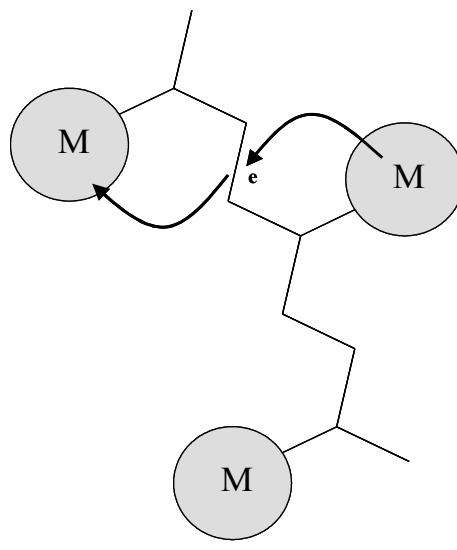
### **1.5.2 Charge Transport Mechanisms of Conjugated Metallopolymers:**

As previously discussed the primary rationale for creating conjugated metallopolymers is that electronic interactions between the polymers  $\pi$ -system and the metals d-orbitals will modulate the properties of both components in interesting and potentially useful ways. One of the anticipated benefits is fast charge transport to and from the metal centres so that multiple electrons can be rapidly exchanged with a substrate (e.g.  $O_2$ ) during electrocatalysis. The source of the extra electrons can be the polymer backbone itself, if it is electroactive over the appropriate potential range, or other nearby metal centres. In either case d- $\pi$  interactions would be expected to enhance the rate of electron transport. This would be especially advantageous in the area of electrochemiluminescent based sensing.

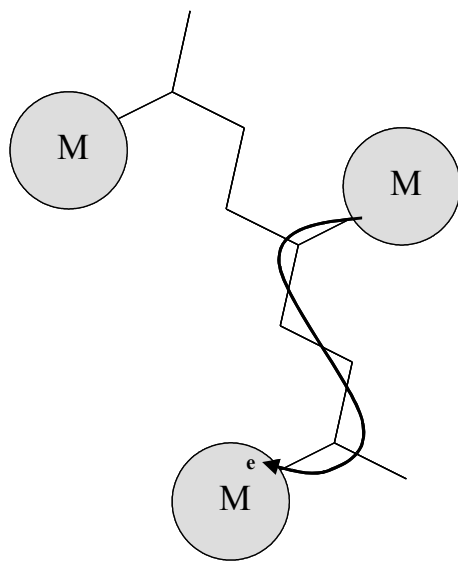
Electron transfer between immobilised metal centres in a polymer film has been shown to occur by at least three mechanisms,<sup>52</sup> outer sphere electron transfer between metal sites, as in conventional redox polymers,<sup>53,54</sup> electron transfer through the polymer backbone via a metal-metal electronic interaction (super-exchange pathway), and via polymer based charge carriers (polymer mediated pathway).<sup>55</sup> A schematic representation of these pathways can be seen in Figure 1.8. Electron transfer via polymer based charge carriers requires the polymer backbone to be electronically conductive and therefore either p-doped or n-doped at potentials close to the formal potential of the metal centre. The significance of this pathway can be assessed to some extent by cyclic voltammetry thereby showing the extent to which the polymer backbone's redox waves overlap with that of the metal complex.



(a)



(b)



(c)

**Figure 1.8:** Schematic diagram of the three electron transfer pathways between metal centres in metallopolymers. (a) Outer sphere electron transfer; (b) Superexchange pathway; (c) polymer mediated pathway.

Electron transfer through the polymer backbone via a metal-metal electronic interaction (superexchange pathway) can occur via two mechanisms,<sup>56</sup> electron type superexchange and hole type superexchange, as illustrated in Figure 1.9. In the former, mixing of the  $\pi^*$  LUMO of the polymer and the metal d orbitals is the major contributor to the metal-metal interaction, while in the latter mixing of the  $\pi^*$  HOMO of the polymer and the metal d orbitals is the major contributor. The extent of d- $\pi$  interactions in conjugated metallopolymers will depend on the relative energies of these orbitals, something that can be conveniently assessed from electrochemical studies.

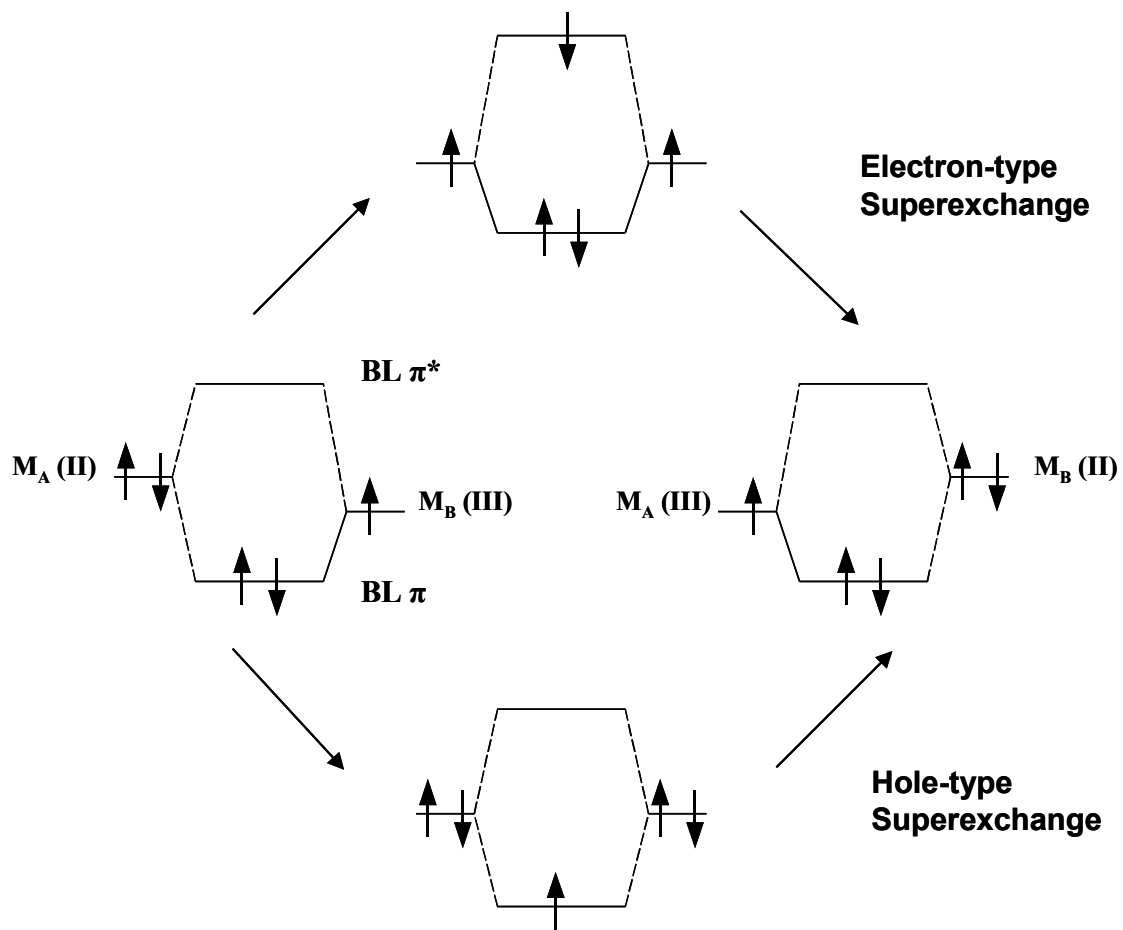
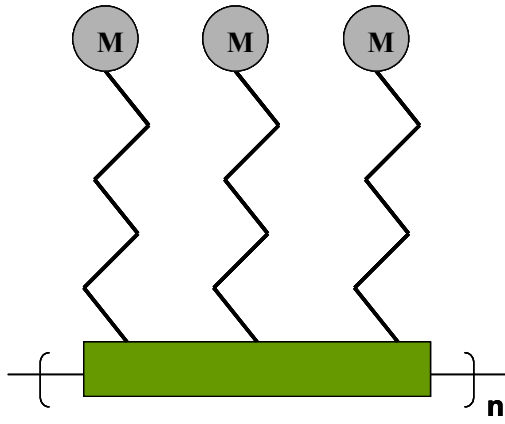


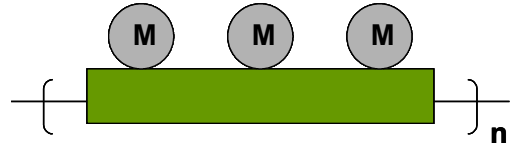
**Figure 1.9:** *Diagram illustrating electron type superexchange and hole type superexchange.*

### **1.5.3 Examples of Conjugated Metallopolymers with Enhanced Charge Transport.**

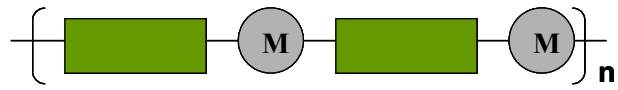
Metal containing conjugated or conducting metallopolymers can generally be divided into three types known as I, II, and III. The difference between these types depends on if the respective metal is tethered, coupled or incorporated. These three types of metallopolymers are illustrated in Figure 1.10. Type I polymers have the metal group tethered to the conjugated backbone by a linker moiety such as an alkyl group. In this case the polymer acts as a conductive electrolyte and the metal ions act in a similar way to an untethered group present in the polymer matrix. Type II polymers have the metal directly coupled to the polymer backbone or coupled to the backbone by a conjugated linker group. This makes it easier for the polymer and the metal group to affect each other's properties directly. If the conductive backbone and the metal ions are redox active, the systems can be electrochemically tuned. The third type of polymer has a metal group directly incorporated into the conjugated backbone. In this type of metallopolymer the metal group had the greatest influence on the properties of the conducting polymer.



**Type I**



**Type II**



**Type III**

 = Metal Group

 = Conjugated Backbone

*Figure 1.10: Diagram illustrating the three different types of conducting metallopolymers. Type I (tethered), Type II (coupled) and Type III (incorporated).*

Type I metallopolymers have included various cyclam<sup>57</sup> and porphyrin<sup>58</sup> complexes, ferrocene,<sup>59</sup> bipyridyl groups,<sup>60</sup> crown ether complexes<sup>61</sup> and sulfonic acid salts.<sup>62</sup> Due to the spatial difference between the metal complex and the polymer backbone type I metallopolymers exhibited very little metal-backbone conductivity. Within ferrocene tethered complexes redox conduction was only observed if the alkyl chain was very short.<sup>62,63</sup> Multicoloured electrochromism had been demonstrated with a copolymer of a thiophene bearing a tethered Ni<sup>2+</sup> cyclam and 3-methylthiophene synthesised electrochemically in acetonitrile.<sup>64</sup> The polymer was orange-red when neutral, green when the thiophene was oxidised and then turned blue when the nickel also became oxidised.

A number of type II polymers are known including diimine polymers, pendant ferrocene complexes, pendant bis(salicylidene) metal complexes, metallorotaxane polymers and complexed polythiophenes. Diamine groups such as bipyridyl, when they are a part of a polymer backbone have been used to complex with a number of metal ions. Metals that have been complexed include ruthenium, copper, osmium and rhenium. Pickup and co-workers<sup>41,55,65,66</sup> have made extensive use of impedance spectroscopy, rotating disk voltammetry, and dual sandwich electrode voltammetry to elucidate charge transport mechanisms in several ruthenium and osmium containing conducting polymers. They outlined how different conductivity mechanisms depend upon the nature of the interaction between the metal centres and the ligand backbone. A benzimidazole-based polymer as seen in Figure 1.11 has demonstrated strong polymer mediated communication between the metal centres.<sup>41,55</sup> The pH dependent nature of the charge delocalisation resulting from the protonation/deprotonation of the polymer backbone support its role in charge transport. Since the backbone of this polymer is not doped in the potential region of the Ru(III/II) formal potential it does not contribute directly to the electronic conductivity of the polymer in this region, the rate of the Ru(III/II) redox process is therefore determined by the rate of electron

exchange between the redox sites. This is conveniently measured and represented as the electron diffusion coefficient,  $D_e$ . These results showed for the first time that electron transport between metal centres is enhanced significantly when the metal sites are coordinated directly to the  $\pi$  backbone of a conjugated polymer.  $D_e$  rates for this metallopolymer were more than a factor of 10 greater than those in similar ruthenium systems where the metal is electronically isolated by saturated bonds.

Type II conducting metallopolymers have also displayed conductive properties. Organometallic heterocyclic polymers have been prepared by “metacycling” polymerisation reactions,<sup>67,68</sup> by Nishihara and coworkers. Both ruthenium and cobalt materials have been investigated,<sup>69,70</sup> The soluble cobalt containing polymer displayed redox conductivity of  $10^{-4}$  S  $\text{cm}^{-1}$  when doped with  $\text{I}_2$ . Metallopolymers with redox conductivity as high as  $10^{-3}$  s  $\text{cm}^{-1}$  have also been reported.<sup>71</sup> Although the most common method of polymerisation for types I and II polymers are electropolymerization this technique is much less common with type III polymers. For this type of polymer chemical polymerisation is more common. Type III metallopolymers were among some of the first metallopolymers to be synthesised. Type III metallopolymers can be either linear or three-dimensional and can be obtained with a wide range of physical and electronic properties. Polymer chains can be made through direct metal-metal bonding or through ligand-metal interactions and both semi-conductive and highly conductive materials have been produced. In the case of entwined metallopolymer systems,<sup>72</sup> two ligands have been studied that incorporate thiophene based electropolymerizable moieties in the 2,9 - positions of the copper binding 1,10-phenanthroline ligands. A 9 fold increase in conductivity was noted when alkyl chains were incorporated into the metallopolymer structure.

The creation of many of the metallopolymers mentioned above involved complex methods of synthesis and is labour intensive as well as time consuming. An alternative to such metallopolymers is the immobilisation of metal complexes either electrostatically or electrochemically in conducting polymer matrixes. This avoids complex synthetic procedures for covalently attaching the metal to the polymer

backbone and enables polymer films to be produced quickly and easily. Previous work by Forster *et al* has demonstrated the electrochemical polymerisation of methoxy-aniline in the presence of  $[\text{Ru}(\text{bpy})_3]^{2+}$  resulting in ruthenium based luminescence and electrochemiluminescence as well as enhanced rates of charge transport.<sup>73</sup> This method of preparing films represents a simplistic and effective approach to combining metal complexes with polymeric systems while maintaining many of the anticipated benefits of having both conducting backbone and metal centres.

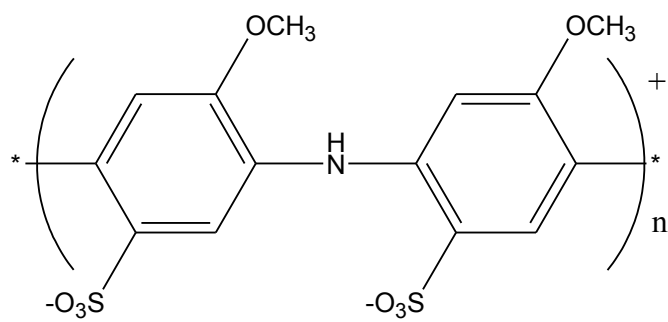
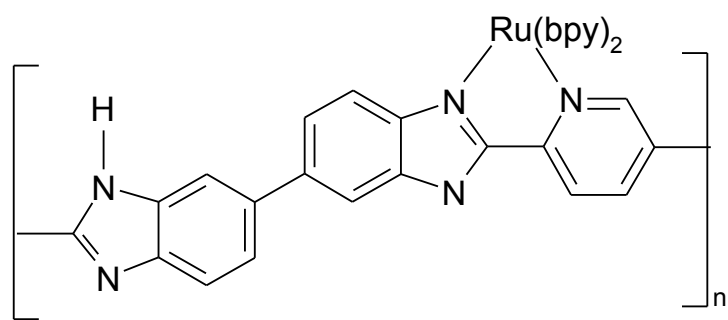


**Figure 1.11:** Structure of Ru(2,2-bipyridyl)poly[2-(2-pyridyl)-bibenzimidazole] and Poly-2-Methoxyaniline-5-sulfonic acid (PMAS).

## 1.6 Conclusions

The future of the biomedical diagnostics industry lies in the identification of disease biomarkers at very low concentrations often picomolar levels. In order to achieve the level of detection required a significant improvement over current transduction methods is required. Current approaches involve both optical and electrochemical methods however both suffer from inherent limitations. The inherent advantages of ECL make it an ideal technique for use within the biomedical diagnostics industry. ECL does not require external excitation and all reagents are generated in situ. ECL has the added advantage that as light emission occurs close to the electrode, the electrode shape and size can be altered to maximise the capture of light. ECL however is highly dependent on the rate of charge transfer ( $D_{CT}$ ) through the metallopolymer film. Traditionally the ruthenium redox metallopolymer that have been utilised for ECL production have shown a slow rate of charge transfer and this has limited ECL production. ECL intensity is also limited by low photoluminescent yields and short lived luminescence lifetimes. One solution to this problem is to utilise metallopolymer with a conjugated backbone. The delocalised  $\pi$  network along the backbone has been shown to increase charge transfer rates between metal centres. The possibility of energy or electron transfer from the polymer backbone to the metal may enhance luminescence or luminescence lifetimes. If applied to an ECL system this approach could result in enhanced ECL production.

This thesis attempts to tune the electrochemical and photophysical properties of 2 polymeric systems to produce enhanced ECL. The first system is a Ru(2,2-bipyridyl)poly[2-(2-pyridyl)-bibenzimidazole]  $(Ru(bpy)_2(PPyBBIM)_n)^{2+}$  metallopolymer whereby the ruthenium bipyridyl metal complex is covalently bound to the polymer backbone as seen in Figure 1.11. The second system involves electrostatically isolating  $[Ru(bpy)_3]^{2+}$  in films of both high and low molecular weight fraction of Poly-2-Methoxyaniline-5-sulfonic acid (PMAS).

Chapter 2 of this thesis characterises each system by comparison to previously reported photophysical and electrochemical characteristics. The PMAS polymers are characterised without the addition of ruthenium to ensure purity. Chapter 3 probes the driving forces for ground and excited state electron transport within the  $[\text{Ru}(\text{bpy})_2(\text{PPyBBIM})_n]^{2+}$  metallopolymer films as well as examining how these processes affect luminescent intensity and luminescent lifetimes. Chapter 4 examines the electrochemical and photophysical characteristics of ruthenium containing PMAS films. Chapter 5 then examines how if the electrochemical and photophysical characteristics reported in Chapters 3 and 4 translate into ECL enhancement. Chapter 6 summarizes the main conclusions of the thesis.

## *Chapter 2*

*Characterisation of  $[Ru(bpy)_2(PPyBBIM)_n]^{2+}$  and  
[poly(2-methoxyaniline-5-sulfonic acid)]*

## 2.1 Introduction

Electrically conducting (conjugated) polymers such as polyimidazole, polyaniline, polypyrrole and phenylene continue to be the subjects of intense research<sup>74</sup> with anticipated uses as sensors, rechargeable batteries, electrochromic displays and corrosion resistant coatings.<sup>75,76,77,78,79,80,81</sup> The use of polymers as supports for confining transition metal complexes at the electrode solution interface is also well known.<sup>82,83</sup> A significant area of interest involves using conducting polymers to enhance communication between metal centres either by covalently binding the metal to the polymers or via electrostatic interaction.

There has been sustained interest in  $\pi$ -conjugated metallopolymers over the last decade. The anticipated advantage of an arrangement where the metal is coordinated into the  $\pi$  backbone lies in the hypothesis that interactions between metal-based  $d\pi$  orbitals and ligand (polymer)  $L \pi$  or  $L \pi^*$  can occur. As a result, the  $\pi$  network can in essence act as an intramolecular electron conduit allowing the rapid movement of electrons necessary for high electrocatalyst performance such as that involved in the generation of Electrochemiluminescence. The ability of conjugated linkages to provide an effective pathway for electron transfer between metal sites has been demonstrated in a number of polymeric systems. For example Pickup *et al*<sup>84</sup> demonstrated increased electron transfer rates between metal centres via a superexchange mechanism through a conjugated backbone. An illustration of the superexchange mechanism can be seen in Figure 2.1

Polymers based on the benzimidazole fragment in particular have long been recognized for their useful engineering properties and resilience. The preferred method of synthesizing polymers based on the benzobisazole fragment is the condensation reaction between a carboxylic acid and an appropriate substituted

phenyl ring in polyphosphoric acid (PPA)<sup>85,86,87,88</sup> This approach is known to be significantly more reliable than older techniques such as high temperature melt reactions between diamines (for benzimidazoles) and acids or esters, and the interfacial polycondensation of diamines with acid chlorides<sup>89</sup>. Metallopolymers can then be prepared by simply refluxing the polymer backbone with the metal complex of interest. Materials of different metal loadings can be prepared by simply varying the relative molar ratio of reactants or by controlling the refluxing times. As these materials can be readily dissolved they can be investigated in great detail as solution phase species. Conventional spectroscopic and electrochemical methods can be used to probe the nature of the coordination sphere around the metal atom and also investigate the ground and excited state properties of the polymer itself.

Functionalised polyaniline has attracted immense interest over the years due to its unique electrochemical properties, water solubility and potential industrial applications.<sup>90,91</sup> The anticipated advantages of combining sulfonated polyaniline (SPAN) with transition metal complexes such as enhanced rates of metal to metal charge transport and increased luminescence due to energy transfer from the polymer to metal are significant. Sulfonated polyaniline was the first reported water soluble conducting derivative of polyaniline.<sup>92</sup> Substitution of methoxy groups onto the aniline ring has further improved the conducting and solubility properties of SPAN.<sup>93</sup>

Poly(2-methoxyaniline-5-sulfonic acid) (PMAS) has been shown to display interesting photophysical, electrochemical and synthetic characteristics. Unlike many other forms of polyaniline both the chemical and electrochemical synthesis of Poly(2-methoxyaniline-5-sulfonic acid) in aqueous media have been found to give two distinct polymer fractions, a high molecular weight polymer, referred to as (HMWT PMAS) with molecular weights of approximately 8-10 kDa and low molecular weight (LMWT PMAS) oligomers of approximately 2 kDa. As such, early attempts to isolate each fraction typically resulted in either fraction also containing a significant amount of the other. Recently however, these high and low molecular weight fractions have been separated utilising cross flow dialysis tubing providing samples of each fraction

with purity greater than 95%.<sup>94</sup> Once isolated, PMAS fractions have previously been demonstrated to display remarkable electrochemical and photoluminescent properties.<sup>95,96,97</sup> The unique features of such polymers provide increased scope in the area of metal based luminescent sensing. The isolation of a highly luminescent metal centre within such polymers may lead to increased cooperative effects between both the metal and the polymer thereby increasing the sensitivity of current luminescence based sensors. Prior to this however it is necessary to characterise each PMAS fraction to ensure purity.

This chapter aims to characterise the electrochemical and photophysical characteristics of the metallopolymer  $[\text{Ru}(\text{bpy})_2(\text{PPyBBIM})_n]^{2+}$  metallopolymers where n varies depending on the amount of ruthenium complex on the polymer backbone and the conducting polymer Poly(2-methoxyaniline-5-sulfonic acid) prior to the addition of ruthenium. The results of which are compared to those previously reported in the literature..

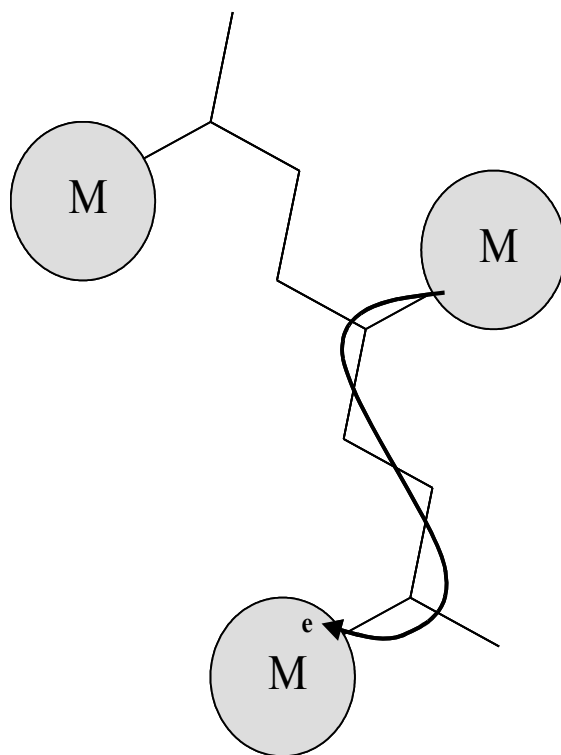


**Figure 2.1:** Illustration of the superexchange mechanism proposed by Pickup et al.<sup>83</sup>

## ***2.2 Apparatus and Reagents***

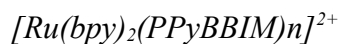
Ultraviolet-visible spectra were carried out in ethanol or acetonitrile using a UV-Visible Cary 50 Scan spectrophotometer and data analysed using a personal computer containing Cary Win UV software. Emission spectra were recorded using a Perkin Elmer LS-50 luminescence spectrometer, equipped with a red sensitive Hamamatsu R928 detector. In each case a 1 cm quartz cell was used. Samples were prepared at concentrations of 10  $\mu$ M in spectroscopic grade acetonitrile.

Emission lifetime measurements were performed on a PicoQuant Fluo Time 100 Time Correlated Single Photon Counting spectrometer (TCSPC) using a PDL-800B pulsed diode laser controller and employing 280, 370 and 450 nm pulsed laser sources with cut off filters of 400, 475 and 530 nm. All solutions were deaerated for 20 minutes using argon or nitrogen prior to use. Lifetimes were determined using PicoQuant FluoFit software.

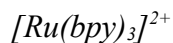
Electrochemical experiments were performed in a standard electrochemical cell using a CH instruments (Memphis TN.) model 440 potentiostat and were carried out using a 3 mm diameter glassy carbon working electrode in a conventional three-electrode assembly using a platinum flag as the counter electrode. Working electrodes were cleaned by polishing with alumina (0.3 and 0.05 micron) on felt pad, followed by sonication in distilled deionised water for 30 min. Potentials were measured versus a Ag/AgCl reference electrode (3M). All solutions were deoxygenated using nitrogen or argon prior to measurement. Electrochemical spectra were background corrected using CH instruments fitting software. As one of the goals of producing these materials is for use in ECL based sensors for detection of biological analytes extremes of pH are not desired. As such electrochemical measurements were performed in either 0.1M LiClO<sub>4</sub> (pH6) or 0.1 M H<sub>2</sub>SO<sub>4</sub> adjusted

to pH 6. All solutions were deoxygenated using nitrogen or argon prior to measurement.

Where appropriate, working electrodes were modified by applying a drop ( $\approx 15 \mu\text{L}$ ) of an ethanolic solution of the metallopolymer to the electrode surface which was allowed to dry in the dark for 10 to 24 hours. The surface coverage  $\Gamma$ , was determined by graphical integration of background corrected cyclic voltammograms ( $< 5 \text{ mV s}^{-1}$ ). Surface coverages ranged from  $2\text{-}5 \times 10^{-8} \text{ mol cm}^{-2}$  for  $[\text{Ru}(\text{bpy})_2(\text{PPyBBIM})_n]^{2+}$  metallopolymer, however in each case the respective surface coverage is listed in the figure legend. All electrochemical experiments were performed at room temperature ( $293^\circ\text{K}$ )



Imidazole based metallopolymer were kindly provided by Dr. Darren Griffith of the Keyes Research Group. The metallopolymer,  $[\text{Ru}(\text{bpy})_2(\text{PPyBBIM})_n]^{2+}$ , where n is 3, 10 or 20,  $\text{Ru}(\text{bpy})_2$  is Ruthenium-[2,2'-bipyridyl] and PPyBBIM is poly[2-(2-pyridyl)-bibenzimidazole] were prepared according to a literature method.<sup>98</sup> Polymers of various metal loadings were prepared by simply varying the relative molar amounts of reactants, e.g. n = 3 refers to one Ruthenium-[2,2'-bipyridyl] every three PPyBBIM monomeric units. The structure of these metallopolymer is illustrated in 2.2. All other chemicals were reagent grade or better and used as received.



$[\text{Ru}(\text{bpy})_3]^{2+}$  was purchased from sigma Aldrich and used as a reference model complex for ruthenium metallopolymer studies.



Poly(2-methoxyaniline-5-sulfonic acid) (PMAS) was provided by Dr. Peter Innis of the University of Wollongong, NSW, Australia and was synthesized chemically from the monomer MAS.<sup>99,97</sup> High and Low molecular weight fractions were separated using a cross flow dialysis system.<sup>97</sup> The polymerization process of PMAS is illustrated in Figure 2.3 where n refers to the degree of polymerization.

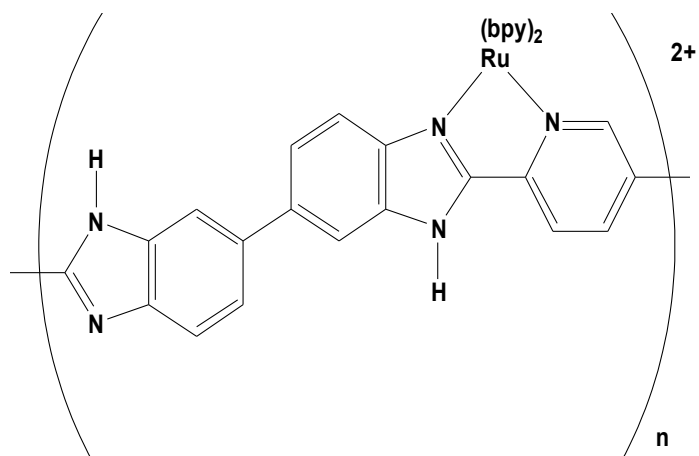


**Figure 2.2:** Structure of  $[Ru(bpy)_2(PPyBBIM)_n]^{2+}$

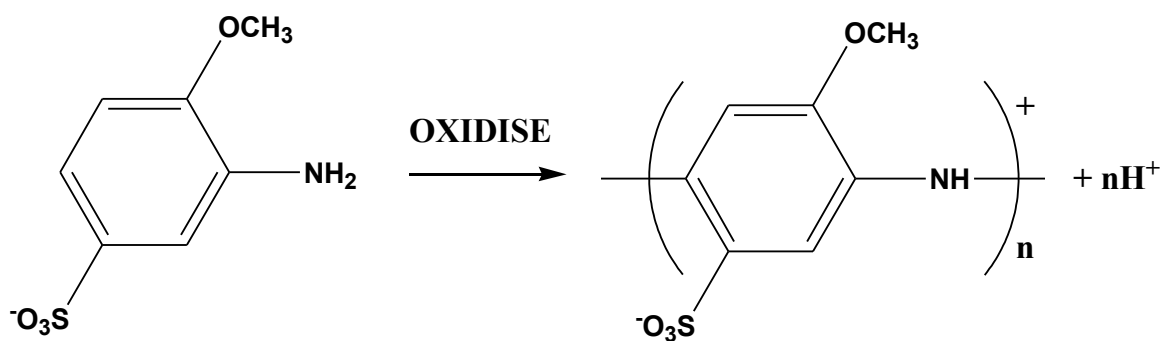


**Figure 2.3:** Oxidation of the monomer MAS to form PMAS.

### **2.3 Characterisation of $Ru(bpy)_2(PPyBBIM)_n]^{2+}$ based metallopolymers.**

### 2.3.1. General

Ruthenium ( $\Pi$ ) diimine complexes are stable low-spin  $d^6$  species where oxidation occurs on a metal centred orbital and reduction involves a ligand  $\pi^*$  orbital. Metal complexes also show rich photophysical properties which are depicted in Figure 2.4. The absorption spectrum of these species is characterised by intense absorption bands in the visible region, which are assigned to metal to ligand charge transfer (MLCT) transitions.<sup>100</sup> Emission is dominated by a closely spaced manifold of at least three triplet charge transfer states, but at ambient temperatures<sup>101</sup> these can be viewed as occurring from a single state ( $^3$ MLCT). Due to spin orbital coupling, fast intersystem crossing occurs from the singlet to triplet state with an efficiency of unity, followed by emission from the triplet state to the ground state ( $k_r$ ) or radiationless deactivation<sup>102</sup> to the ground state ( $k_{nr}$ ). An alternative deactivation is population of the  $^3$ MC (metal centred) state. If this occurs the electron occupies an anti-bonding metal-based orbital, resulting in distortion of the metal ligand axes and weakening the Ru-N bonds. This may cause photodecomposition of the complex, which manifests itself as ligand loss followed by co-ordination of a substitute ligand, often solvent or electrolyte.<sup>103,104</sup>

For a ruthenium containing metallopolymer, the nature of the co-ordination sphere around the central atom is of prime importance since it determines the reduction and oxidation potentials as well as the photophysical properties of the material obtained. Electronic spectroscopy has proven useful in the characterisation of these species.<sup>105</sup> In particular, the position of the lowest absorption maxima and the wavelength of emission are often characteristic of a particular ruthenium moiety. Ruthenium poly(pyridyl) compounds typically exhibits two bands in the visible region of the spectrum. As previously stated, these have been assigned to metal to ligand charge transfer (MLCT) transitions from the metal localised orbital, Ru ( $d\pi$ ), to the ligand localised orbital, bpy ( $\pi^*$ ) orbitals. The positions of the absorption maxima are governed by the  $\delta$ -donor and  $\pi$ -acceptor properties of the ligands. A ruthenium complex with a strong  $\delta$ -donating ligand such as chloride is electron rich and the

MLCT band is present at a lower energy. This also results in a lower oxidation potential for the compound.

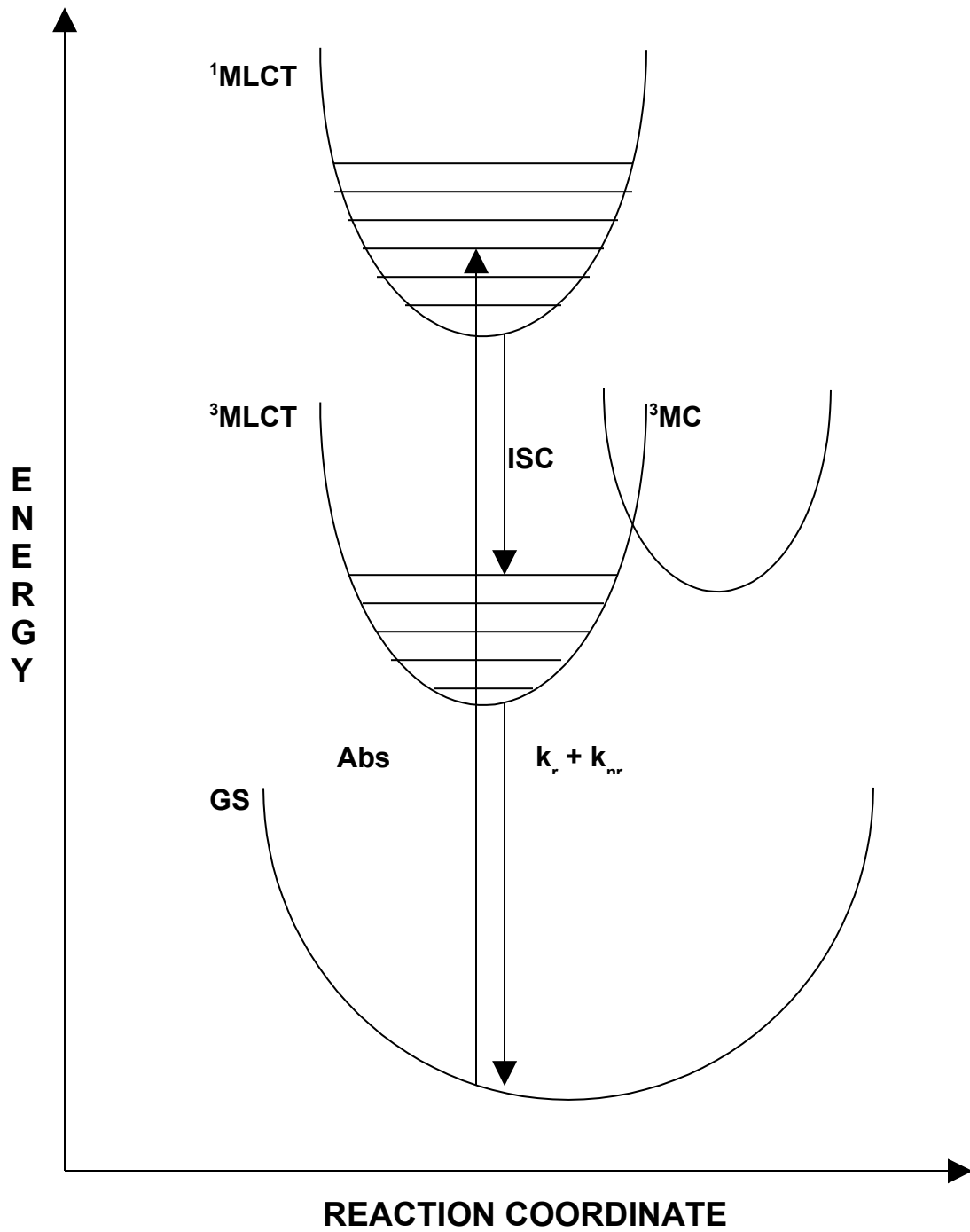


*Figure 2.4: Photophysical process of ruthenium polypyridyl compounds.*

### **2.3.2 UV-Visible Spectroscopy:**

The ultraviolet-visible spectra of transition metal complexes provide insights into the electronic transitions within the metallopolymer complex. Figure 2.5 depicts the absorption spectra of  $[\text{Ru}(\text{bpy})_2(\text{PPyBBIM})_{10}]^{2+}$  and  $[\text{Ru}(\text{bpy})_3]^{2+}$  which was obtained in order to assist in the characterisation of the polymer. The  $[\text{Ru}(\text{bpy})_2(\text{PPyBBIM})_{10}]^{2+}$  metallopolymer exhibits an intense absorption at 410 nm due to the  $\pi$ - $\pi^*$  transition of the polymer backbone. This absorption is slightly red shifted by  $\sim 10$  nm compared to the UV-Vis spectrum of the uncomplexed polymer reported by Pickup.<sup>84</sup> Absorptions at 245 and 280 nm can be attributed to bipyridine transitions and can also be seen on the  $[\text{Ru}(\text{bpy})_3]^{2+}$  model complex. Spin allowed metal to ligand charge transfer (MLCT) absorptions are visible at 345 and 470 nm and are indicative of the  $[\text{Ru}(\text{N})_6]^{2+}$  coordination-sphere. The MLCT absorption at 470 nm appears as a shoulder on the polymer  $\pi$ - $\pi^*$  peak.

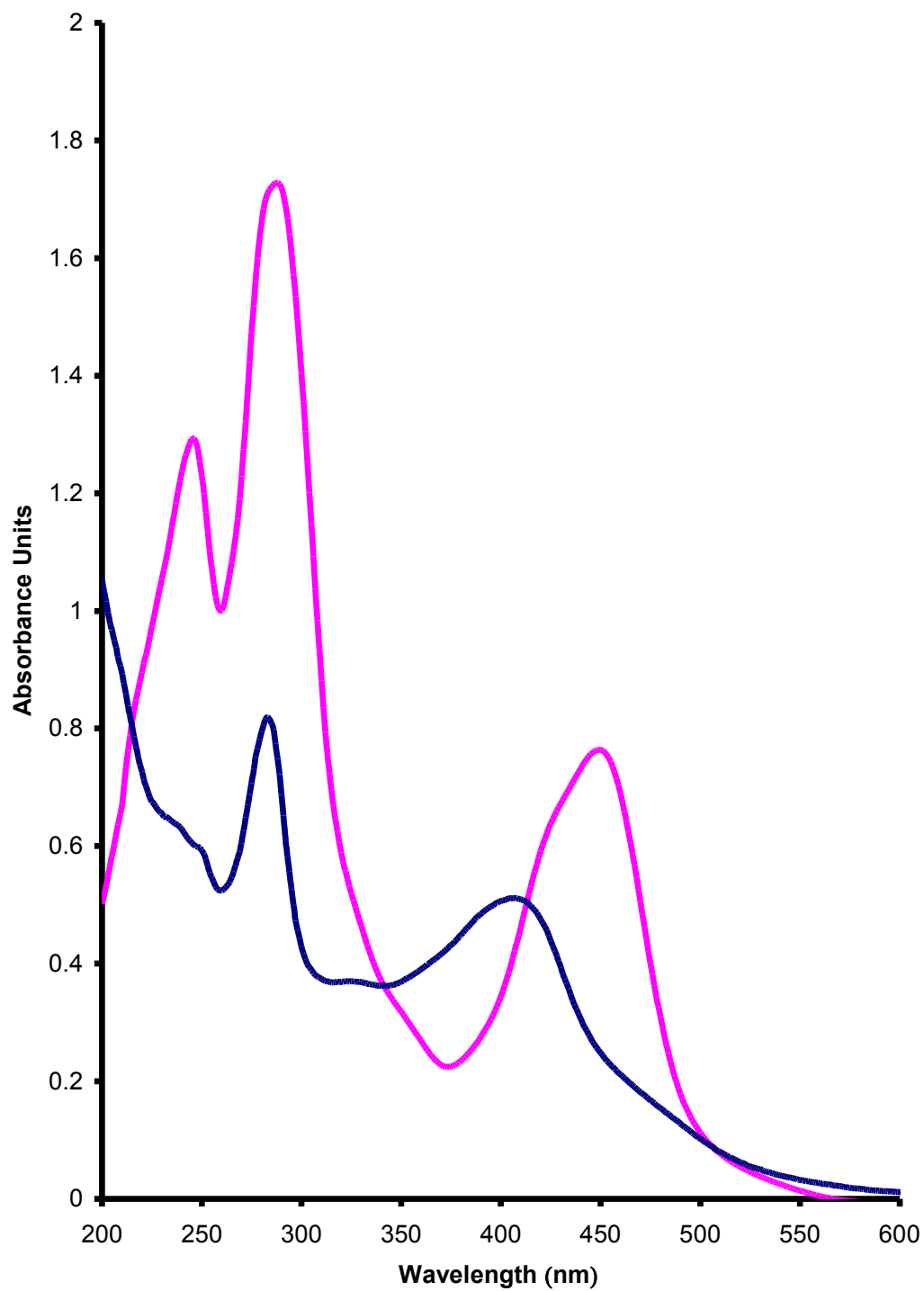


**Figure 2.5:** UV-visible absorption spectra of  $[Ru(bpy)_2(PPyBBIM)_{10}]^{2+}$  (blue) and  $[Ru(bpy)_3]^{2+}$  (pink) ( $10\mu\text{m}$ ) dissolved in acetonitrile.

### ***2.3.3 pH Dependence of UV-Vis Spectroscopy:***

Figure 2.6 depicts the absorption spectra of  $[\text{Ru}(\text{bpy})_2(\text{PPyBBIM})_3]^{2+}$  as a function of pH. Previous pH UV-Absorption studies carried out by Pickup on the  $[\text{Ru}(\text{bpy})_2(\text{PPyBBIM})]^{2+}$  polymer showed changes in the polymer absorption bands as a function of pH due to deprotonation of the lone hydrogen on the imidazole polymer. The UV spectrum of these metallopolymers was also found to change as a function of pH. In going from acidic to basic media the intensity of the  $\pi$ -  $\pi^*$  transitions in both the polymer and bipyridine ligands decrease while the MLCT grows in intensity. This behaviour strongly parallels that of previously reported results for ruthenium containing imidazole metallopolymers and is reported to be reversible<sup>106</sup>

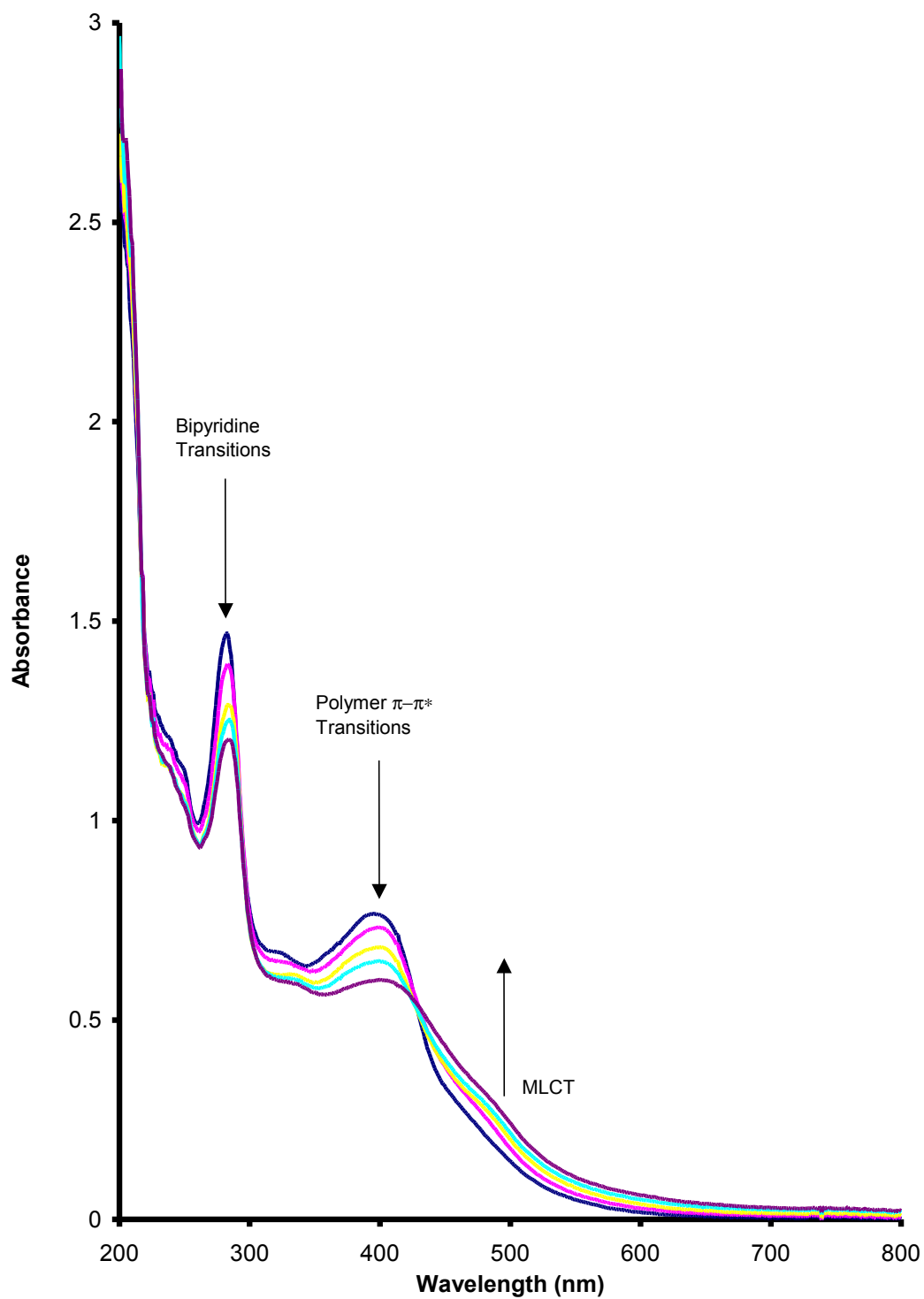


**Figure 2.6:** UV-Vis spectra of the  $[Ru(bpy)_2(PPyBBIM)_3]^{2+}$  ( $10\mu M$ ) polymer complex in phosphate buffer at pH values of 2, 4, 6, 8, and 10. Arrows indicate changes with increasing pH, pH of the solution has been altered by addition of 0.05M HCl.

### 2.3.4 Emission Spectroscopy

Further evidence of the Ru(N)<sub>6</sub> nature of the co-ordination sphere is provided by the luminescence spectra of the polymer, Figure 2.7 shows the solution phase luminescence spectra obtained for the different metal loadings in ACN excited at 450 nm. The spectrum shows two peaks at ca. 540 and 680 nm. As can be seen from Figure 2.8 the emission observed at 540 nm is a result of the poly[2-(2-pyridyl)-bibenzimidazole] polymer backbone while the 680 nm emission is attributed to the ruthenium metal centre. The intensities of the polymer backbone emission have been normalised in order to accurately compare the metal emission intensities.

The phenomenon of dual emission was quite unexpected since according to Kasha's rule one would ordinarily only expect emission from the lowest energy state. However further investigations are reported in Chapter 3. For each metallopolymer the ruthenium based emission at 680 nm exhibits a broader emission than that previously observed for non conjugated ruthenium containing metallopolymer. This may be due to the presence of more than one ruthenium emission process occurring within the metallopolymer film or microenvironment.

To assist in the assigning of the polymer based emission Figure 2.8 shows the overlapping UV-Visible spectra of [Ru(bpy)<sub>2</sub>(PPyBBIM)<sub>10</sub>]<sup>2+</sup> with the polymer backbone [(PPyBBIM)] and [Ru(bpy)<sub>2</sub>(PPyBBIM)<sub>10</sub>]<sup>2+</sup> emission spectra. Unlike the observed UV- visible results extremes of pH have no significant change in emission intensity as illustrated in Figure 2.9.

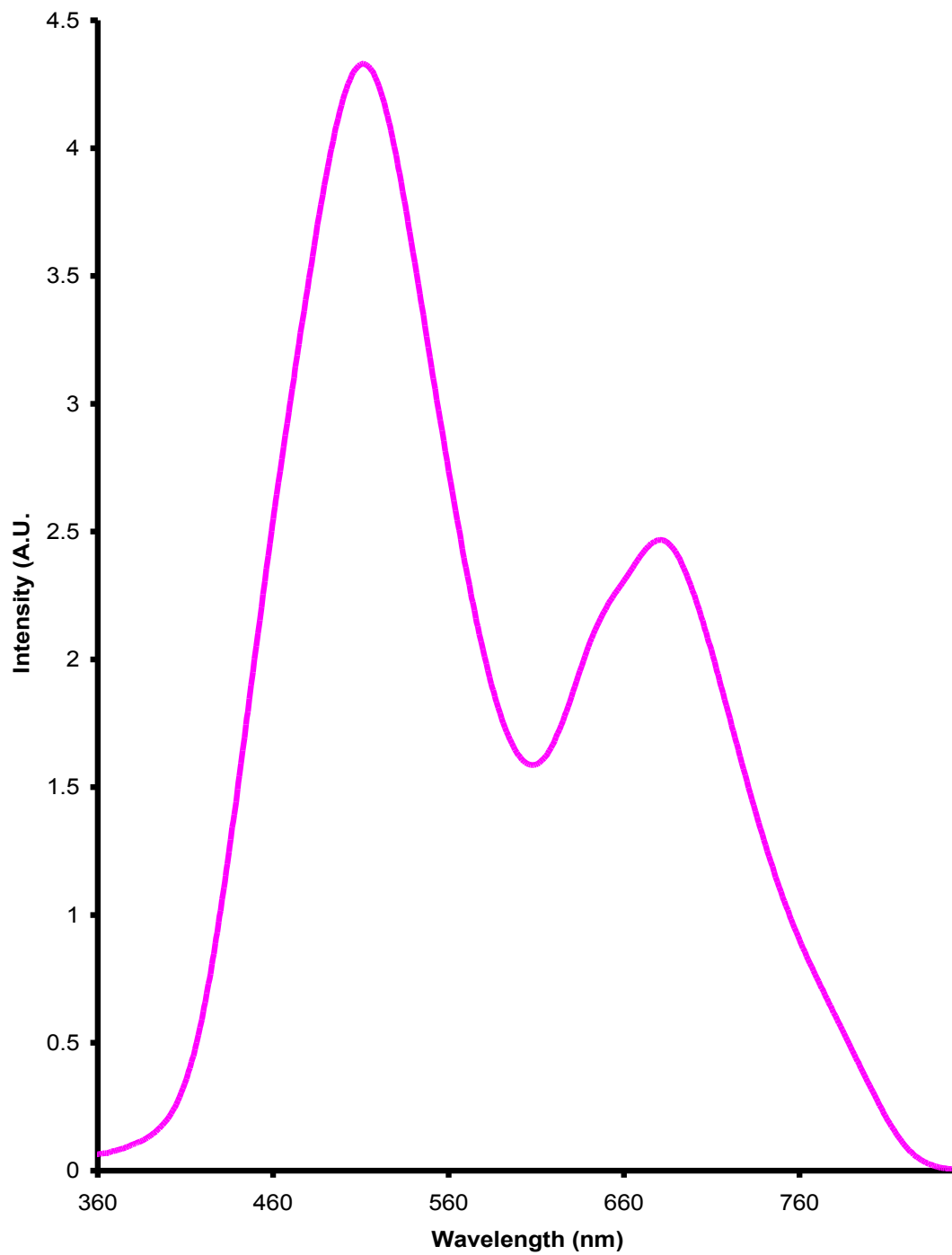


**Figure 2.7:** Emission spectra of  $[Ru(bpy)_2(PPyBBIM)_{10}]^{2+}$  ( $10\mu M$ ) dissolved in acetonitrile.  $\lambda_{ex} = 355\text{ nm}$ . Solutions were deaerated with argon prior to analysis.

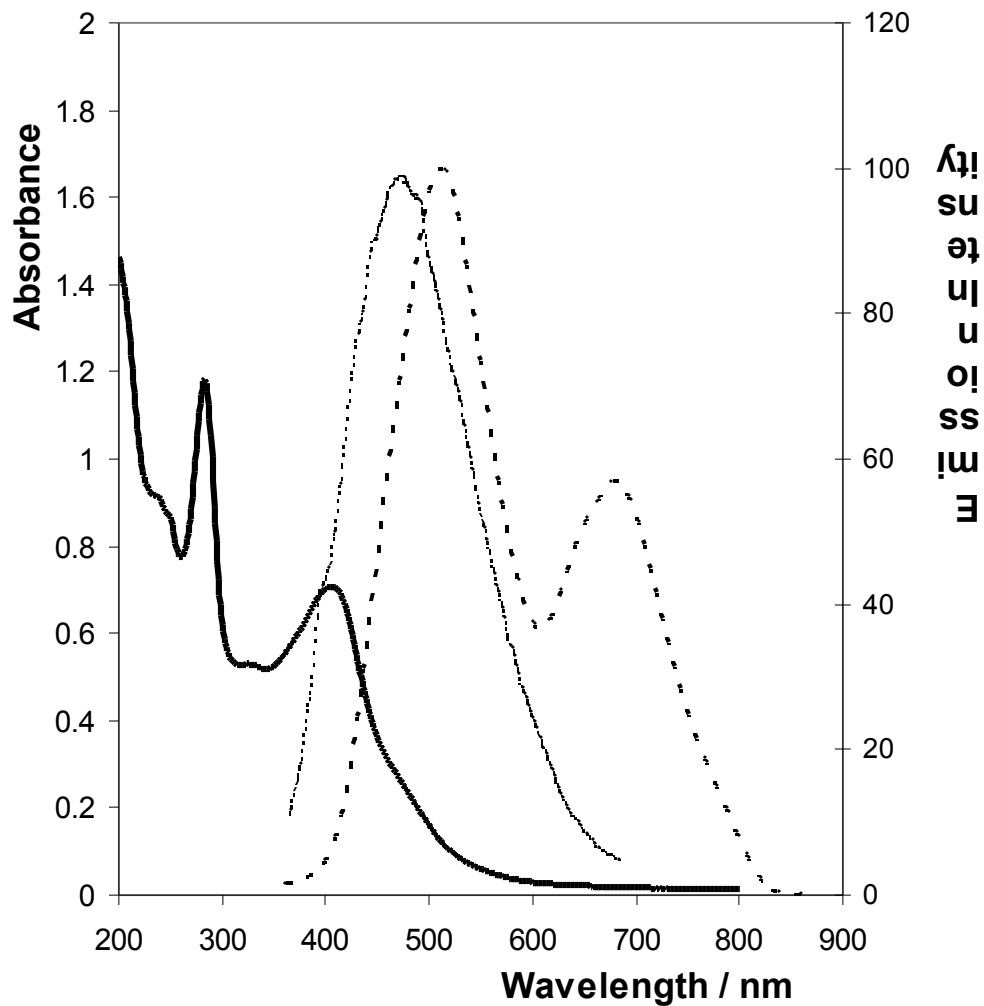


*Figure 2.8: UV-vis spectra of  $[Ru(bpy)_2(PPyBBIM)_{10}]^{2+}$  (heavy line) with  $[PPyBBIM]_{10}$  and  $[Ru(bpy)_2(PPyBBIM)_{10}]^{2+}$  (dashed line) emission spectra.*

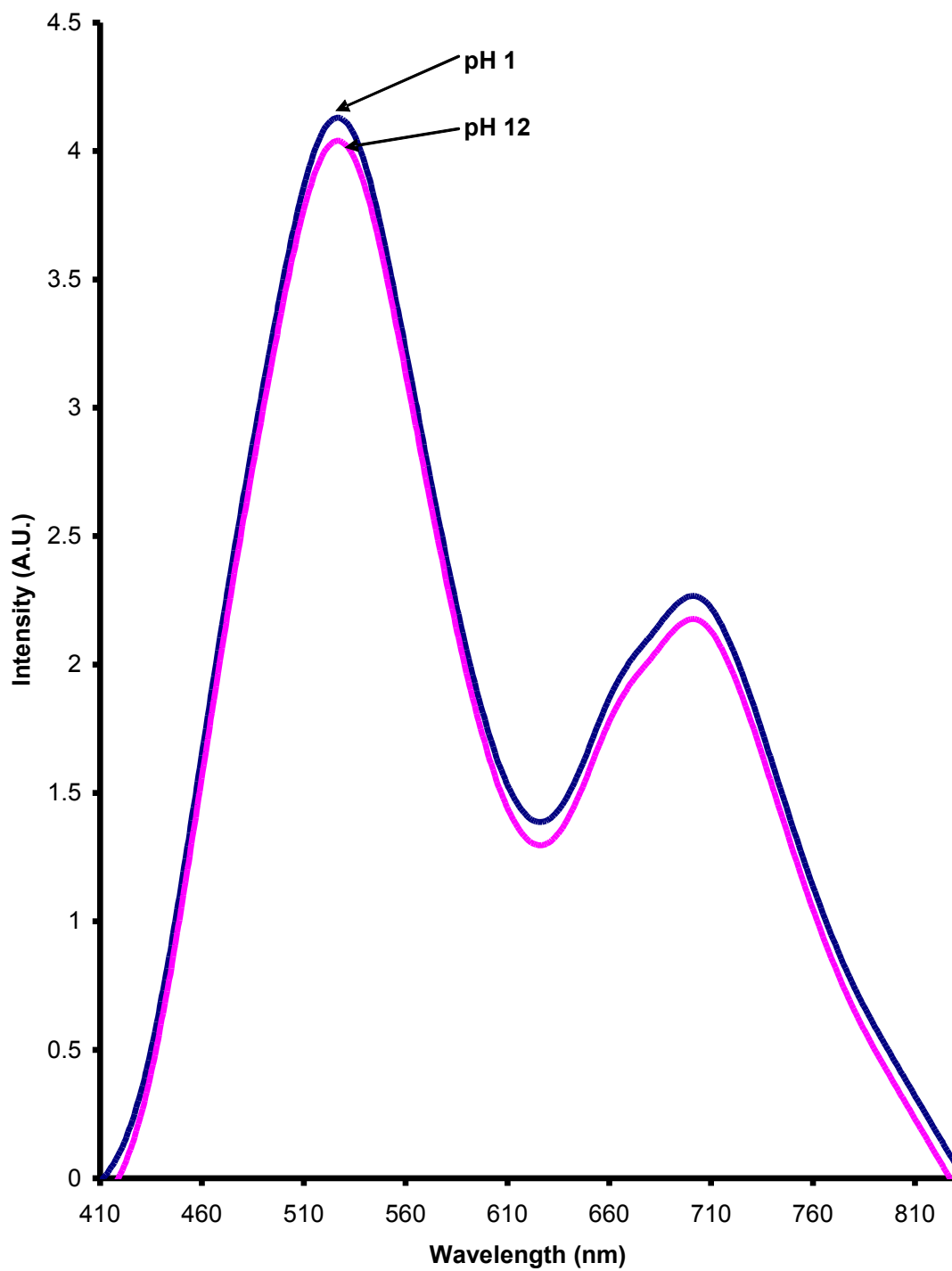


**Figure 2.9:** UV-vis spectra of  $[Ru(bpy)_2(PPyBBIM)_{10}]^{2+}$  (heavy line) with  $[PPyBBIM)_{10}]$  and  $[Ru(bpy)_2(PPyBBIM)_{10}]^{2+}$  (dashed line) emission spectra.

### 2.3.5 Excited State Lifetimes ( $\tau$ )

The Emission lifetime of a substance usually represents the average amount of time the species remains in the excited state prior to its return to the ground state. As previously discussed in Chapter 1 long excited state lifetimes are favourable from an ECL perspective. Fluorescence is usually a unimolecular process and therefore the excited state population established by an impulse of exciting light will generally decay exponentially according to first order kinetics. The impulse response function  $I(t)$  will have the form:

$$I(t) = I_0 e^{-kt} \quad (1)$$

where  $k$  represents the overall relaxation rate and  $I_0$  is simply a scaling factor. Since the Emission lifetime ( $\tau$ ) is by definition the time required for the excited state population to decay to  $1/e$  or  $\sim 37\%$  of its initial intensity, it follows that:

$$\tau = \ln \frac{I_0}{I} / k \quad (2)$$

and  $\tau$  can therefore be determined graphically from the slope of a plot of  $\ln(I)$  versus  $t$ .

The fluorescent lifetime of the metallopolymer in solution phase was measured using transient laser spectroscopy. Due to the dual emission observed, lifetimes were calculated for both the polymer backbone (540 nm) and ruthenium metal centre (700 nm) The decays for the metallopolymer were fitted to the bi-exponential function;

$$I(t) = I_0 e^{-k_1 t} + J_0 e^{-k_2 t} \quad (3)$$

Such a bi-exponential decay is shown in Figure 2.10, ruthenium based transients were typically composed of an early short lived component followed by a longer lived component with a lifetime of  $122 \pm 3$  ns. The luminescent lifetime of the polymer backbone was found to be approximately 30 ns in each case implying that it is independent of the relative metal loading. The luminescent lifetimes of each metallopolymer are presented in Table 2.1.

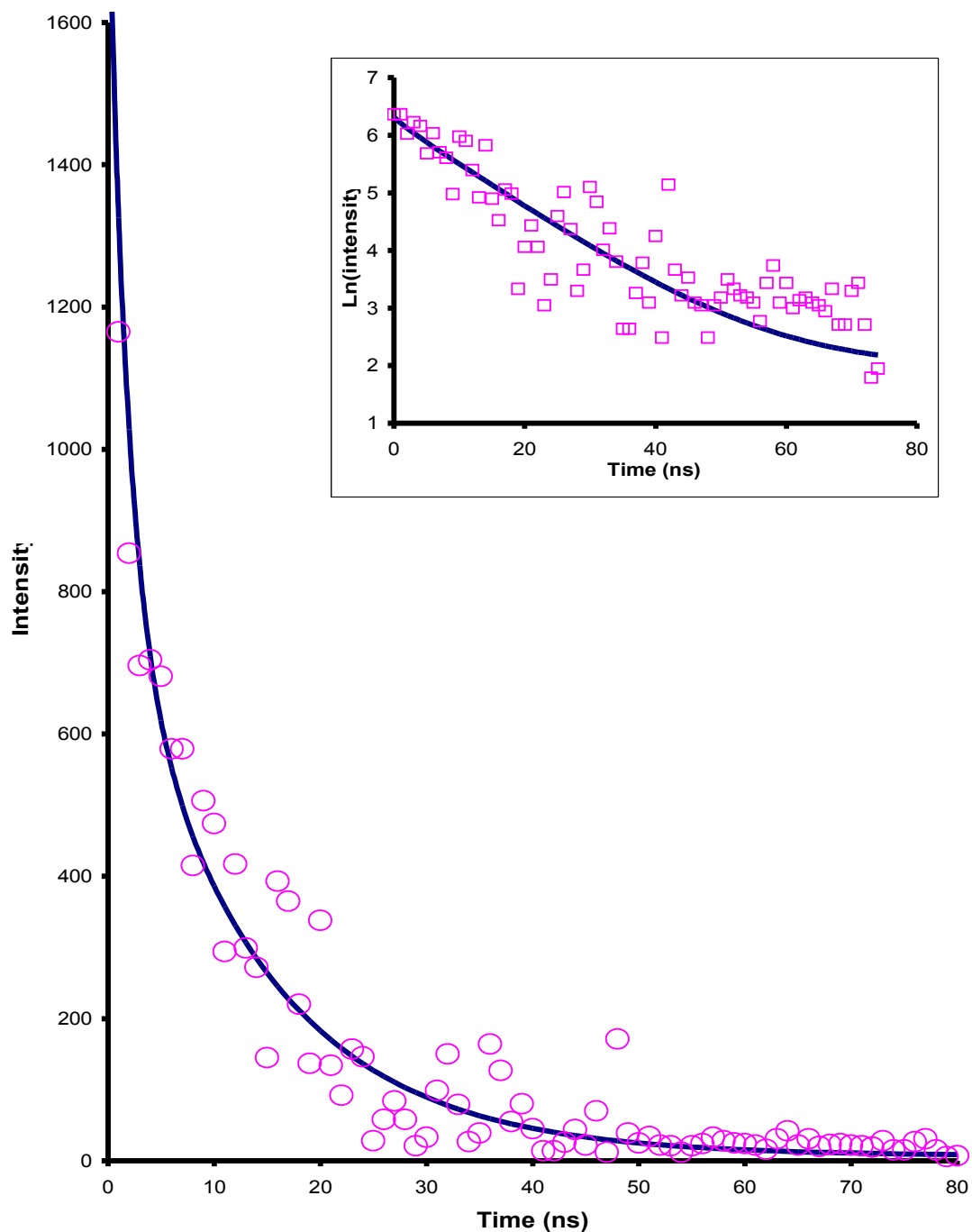


**Figure 2.10:** Emission decay for a  $10^{-4}$  M solution of  $[Ru(bpy)_2(PPyBBIM)_{10}]^{2+}$  in acetonitrile monitored at 680 nm following a 10ns laser pulse of 450 nm light. To prevent lifetime quenching by  $O_2$  solutions were deaerated with argon prior to analysis

**Table 2.1;** Table of lifetime decays values for the respective luminescent components in a  $10^{-4}$  solution of each respective metallopolymer following a 10ns laser pulse of 355 nm light. Emission monitored at 614 nm. All solution were de-aerated with Argon for 30 minutes prior to analysis.

<b>Metallopolymer or Complex</b>	<b>Ruthenium based emission (ns)</b>	<b>PPyBBIM based emission (ns)</b>
$[\text{Ru}(\text{bpy})_2(\text{PPyBBIM})_3]^{2+}$	122±9	33±5
$[\text{Ru}(\text{bpy})_2(\text{PPyBBIM})_{10}]^{2+}$	126±3	36±4
$[\text{Ru}(\text{bpy})_2(\text{PPyBBIM})_{20}]^{2+}$	115±4	32±7
$[\text{Ru}(\text{bpy})_3]^{2+}$	715±27	n/a

### 2.3.6 Cyclic Voltammetry

Cyclic voltammetry (CV) involves monitoring the current response of a small stationary electrode in an unstirred solution that is excited by a triangular potential wave form.<sup>107</sup>

In cyclic voltammetry the potential applied to the working electrode is first swept in a forward direction, “stopped” at a desired potential, then a reverse sweep returns the potential to its initial value. The potential range of these sweeps is chosen to drive redox switching of an analyte and the current ( $I$ ) is recorded as a function of the potential ( $E$ ). A peak in the  $I$  vs.  $E$  output denotes a flow of electrons between the analyte and the electrode associated with a change in the oxidation state of the electroactive analyte. The measured values in this  $I$  vs.  $E$  plot are the anodic and cathodic peak potentials  $E_{p,a}$  and  $E_{p,c}$ ; the anodic and cathodic peak currents  $I_{p,a}$  and  $I_{p,c}$ ; and the half-peak potentials, which are the potentials  $E_{p/2,a}$  and  $E_{p/2,c}$ , at which the cathodic and anodic currents reach half their peak values. A graphic illustration of these parameters can be seen in Figure 2.11.

The advent of polymer-modified electrodes has had a significant impact on sensor development. The modification of electrodes with polymer films was first demonstrated by Murray et al. Polymer modified electrodes allow deliberate control of the electrode catalyst interface. The advantages over solution based electrocatalysis may include (1) a higher effective concentration of catalyst than can be achieved in solution, (2) facilitated transfer of multiple redox equivalents to individual sites, (3) ease of extraction of catalyst from the extraction medium and (4) enhanced cooperative effects between catalyst components owing to small physical separation. These advantages have enabled conducting metallopolymers to be used within many applications.

Figure 2.12 shows the typical theoretical response for a cyclic voltammogram of an electrochemically reversible couple that is confined on the electrode surface at slow

scan rates. The peaks for surface confined species are sharp and symmetrical unlike those for freely diffusing species. This behaviour is due to the presence of a fixed amount of redox active species at the electrode. When a potential is applied to a surface modified electrode the current rises from essentially zero to a peak value and then back to zero during the course of a CV scan. For an ideal system no peak to peak separation is expected. Under the conditions of finite diffusion in which the redox composition of the layer is in thermodynamic equilibrium with the electrode potential, (i.e. the Nernst condition), it will be observed for all electrochemical reversible reactions at sufficiently slow scan rates such that all electroactive centres undergo redox transformations on the time-scale considered.

The model for ideal reversible voltammetric behaviour under such conditions has the following features:

$$i_p = \frac{n^2 F^2 A \Gamma v}{4RT} \quad (4)$$

$$E_{p,c} = E_{p,a} \quad (5)$$

$$FWHM = \frac{90.7}{n} mV \quad (6)$$

$$\frac{i_{p,c}}{i_{p,a}} = 1 \quad (7)$$

where FWHM is the full width at half maximum, n is the number of electrons passed, F is Faraday constant,  $\Gamma$  the surface coverage of the electroactive species, A is the electrode area, v is the scan rate, R the gas constant and T is temperature. These parameters are shown below in Figure 2.12.

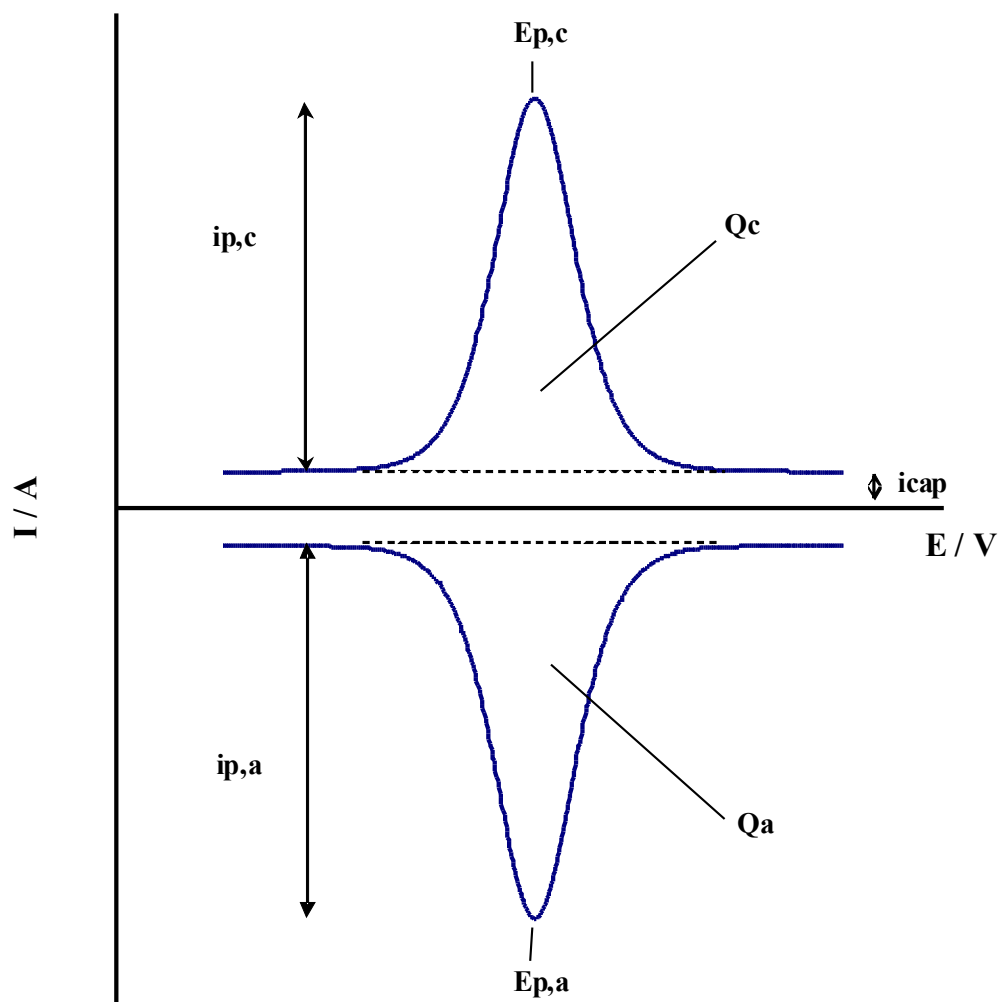


**Figure 2.11:** Cyclic voltammogram of a chemically modified electrode with a monolayer of an electrochemically reversible mediator.

The area under the voltammetric peak, corrected for any background current, represents the charge associated with the reduction or oxidation of the adsorbed species and can be used to calculate the surface coverage ( $\Gamma$ ) according to;

$$\Gamma = \frac{Q}{nFA} \quad (8)$$

For a polymer film under these conditions of finite diffusion, a plot of scan rate versus peak current will be linear. At higher scan rates however, a transition to semi infinite diffusion control occurs and a  $v^{1/2}$  dependence on peak current is observed. Under these semi-infinite diffusion conditions, (in the absence of ohmic effects and slow electron transfer), the following behaviour is ideal.

$$\Delta E_p = \frac{57}{n} mV \quad (9)$$

Figure 2.12 shows a cyclic voltammogram of a the metallopolymer  $[\text{Ru}(\text{bpy})_2(\text{PPyBBIM})_3]^{2+}$  cycled in dried ACN containing 0.1 M TBABF<sub>4</sub> electrolyte. Peak potentials for this and the other metallopolymer investigated are shown in Table 2.2. By analogy with the voltammetric behaviour of  $[\text{Ru}(\text{bpy})_3]^{2+}$  and similar ruthenium complexes, the peaks centred at approximately 1.2 V are attributed to the metal centred  $\text{Ru}^{2+}/\text{Ru}^{3+}$  oxidation/reduction couple and those at -1.6 and -1.8 are bpy based reductions to the +1 and 0 charged species respectively.

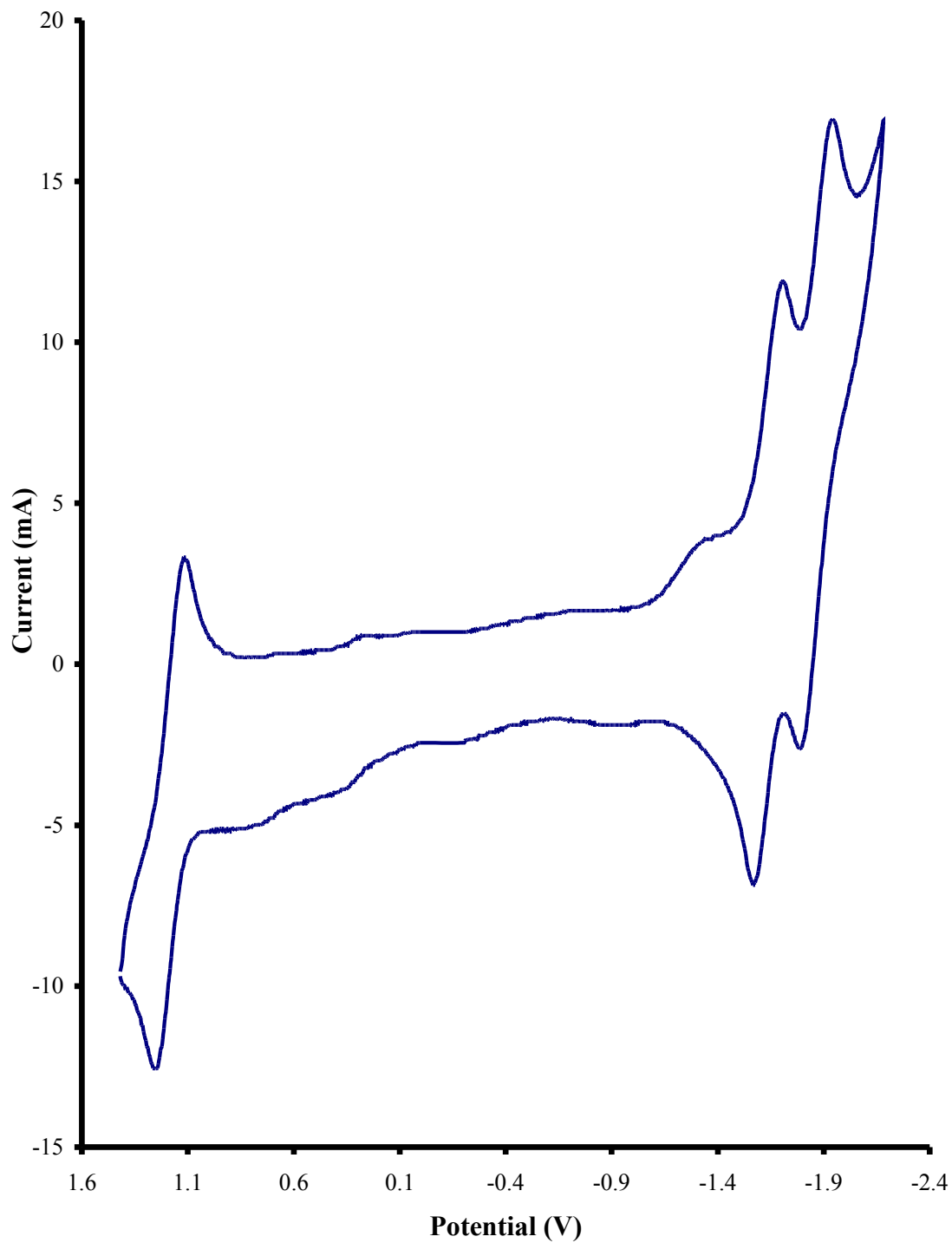


**Figure 2.12:** Typical cyclic voltammetric response of 3 mm diameter platinum electrode to 1 mM  $[\text{Ru}(\text{bpy})_2(\text{PPyBBIM})_3]^{2+}$  in dried ACN containing 0.1M TBABF<sub>4</sub>. Scan rate used was 100  $\text{mV}\text{S}^{-1}$ .

**Table 2.2:** Oxidation and reduction potentials of  $[Ru(bpy)_2(PPyBBIM)_3]^{2+}$  in both solution and thin films. Solutions deaerated with Argon prior to analysis

Metallopolymer	Reduction peaks		Oxidation peak
	E <sup>o</sup> vs. Ag/AgCl		E <sup>o</sup> vs. Ag/AgCl
$[Ru(bpy)_2(PPyBBIM)_3]^{2+}$ (film)	-1.68	-1.82	1.18
$[Ru(bpy)_2(PPyBBIM)_3]^{2+}$ (soln.)	-1.63	-1.85	1.21
$[Ru(bpy)_2(PPyBBIM)_{10}]^{2+}$ (film)	-1.62	-1.78	1.22
$[Ru(bpy)_2(PPyBBIM)_{10}]^{2+}$ (soln.)	-1.58	-1.81	1.26
$[Ru(bpy)_2(PPyBBIM)_{20}]^{2+}$ (film)	-1.68	-1.91	1.22
$[Ru(bpy)_2(PPyBBIM)_{20}]^{2+}$ (soln.)	-1.68	-1.92	1.18

Figure 2.13 shows the voltammetric response of a thin layer of the metallopolymers  $[\text{Ru}(\text{bpy})_2(\text{PPyBBIM})_3]^2$ ,  $[\text{Ru}(\text{bpy})_2(\text{PPyBBIM})_{10}]^2$  and  $[\text{Ru}(\text{bpy})_2(\text{PPyBBIM})_{20}]^2$  polymer film on a glassy carbon electrode at a slow scan rate ( $100\text{mVs}^{-1}$ ) where the supporting electrolyte is  $0.1\text{ M H}_2\text{SO}_4$  adjusted to pH6.0 with  $0.05\text{M KOH}$ . The voltammogram shows a number of the characteristics described above, namely the peak to peak separation between the anodic and cathodic waves is close to unity and shows no variation with scan rate. The full width at half maximum (FWHM) is close to the theoretical value of  $90.6\text{ mV}$  expected for a reaction involving a surface confined reactant and the transfer of a single electron. The metallopolymer showed oxidation and reduction potentials for the Ru(II/III) redox couples at  $\sim 1.15\text{ V vs. Ag/AgCl}$  at pH 6.0 which is typical for a ruthenium oxidation and reduction couple given the protonation state of the polymer backbone at this pH. The peak areas for each of the voltammetric responses correlate to the various concentrations of ruthenium metal centres within the thin film, i.e., the polymer with the highest ruthenium loading produces the highest voltammetric response for a given surface coverage.

These observations are consistent with semi-infinite diffusional charge transport. For all scan rates, the ratio of the anodic to cathodic peak currents is unity indicating that the electron transfer reaction is reversible. These results indicate that the voltammetric behaviour of these metallopolymer films in electrolyte is close to ideal over this range of scan rates.

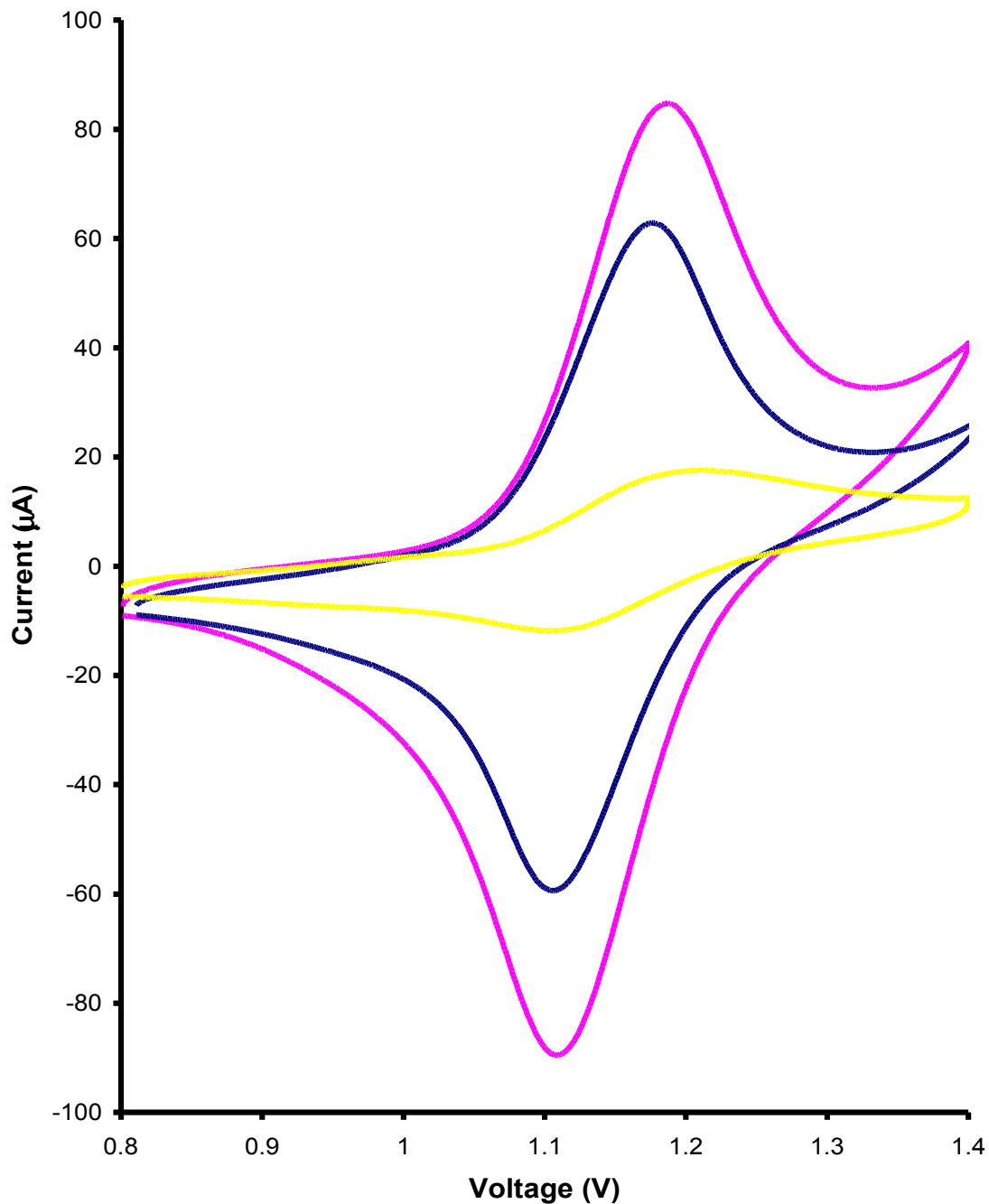


**Figure 2.13:** Cyclic voltammetric response of  $[Ru(bpy)_2(PPyBBIM)_3]^{2+}$  (pink),  $[Ru(bpy)_2(PPyBBIM)_{10}]^{2+}$  (blue) and  $[Ru(bpy)_2(PPyBBIM)_{20}]^{2+}$  (yellow). Respective metallopolymers were confined at the electrode surface in a thin film on glassy carbon electrode, (3 mm diameter). Scan rate used was  $0.1 \text{ Vs}^{-1}$ . The electrolyte is  $0.1 \text{ M LiClO}_4$ .

## ***2.4 Characterisation of Poly(2-methoxyaniline-5-sulfonic acid)***

### ***2.4.1 General.***

As outlined earlier in Chapter one the second approach adopted in this work involves immobilizing a highly luminescent  $[\text{Ru}(\text{bpy})_3]^{2+}$  within a film of the conducting polymer Poly(2-methoxyaniline-5-sulphonic acid) (PMAS). Prior to this however, it is necessary to evaluate the specific electrochemical properties of the polymer itself. PMAS is a water soluble self doped conducting polymer the synthesis of which results in the production of two distinct fractions. The largest of which is a high molecular weight emeraldine salt based polymer (HMWT PMAS) and has a molecular weight of approximately 12kDa. Synthesis of this polymer is accompanied by the formation of low molecular weight oligomers weighing approximately 2kDa (LMWT PMAS). Both fractions display significantly different photophysical and electrochemical properties and are typically characterized based on such differences. Specifically, the conducting HMWT PMAS emeraldine salt is electroactive and does not photoluminesce. In contrast, the non conducting LMWT PMAS oligomers are relatively chemically inert but display good photoluminescence. In recent times the advent of cross flow dialysis tubing has enabled both fractions to be separated more efficiently.<sup>108,97</sup> Both high and low molecular weight PMAS fractions have been probed utilizing UV-visible spectroscopy, Emission spectroscopy, luminescent lifetime measurements and electrochemistry.<sup>94,96,97</sup>

### ***2.4.2 UV- Visible Spectroscopy***

Ultraviolet-visible spectra of conducting polymers provide insights into the electronic transitions within the polymer. Figure 2.14 depicts the UV absorption spectra of both high and low molecular weight fractions of PMAS. aqueous HMWT PMAS exhibited an absorption band at circa 315nm as well as a weak shoulder at 360nm that may be assigned to  $\pi$ -  $\pi^*$  bands. The absorption at 474nm can be assigned to a low wavelength polaron band. Absorption bands observed at wavelengths above 900nm are consistent with a polyaniline emeraldine salt in an extended coil confirmation for the PMAS polymer chains.<sup>109,110,111</sup> In contrast to the HMWT PMAS the LMWT PMAS exhibited no bands in the visible region showing only a single broad peak at ca. 282 nm. These observations are consistent with those previously reported by Wallace et al.<sup>94</sup>

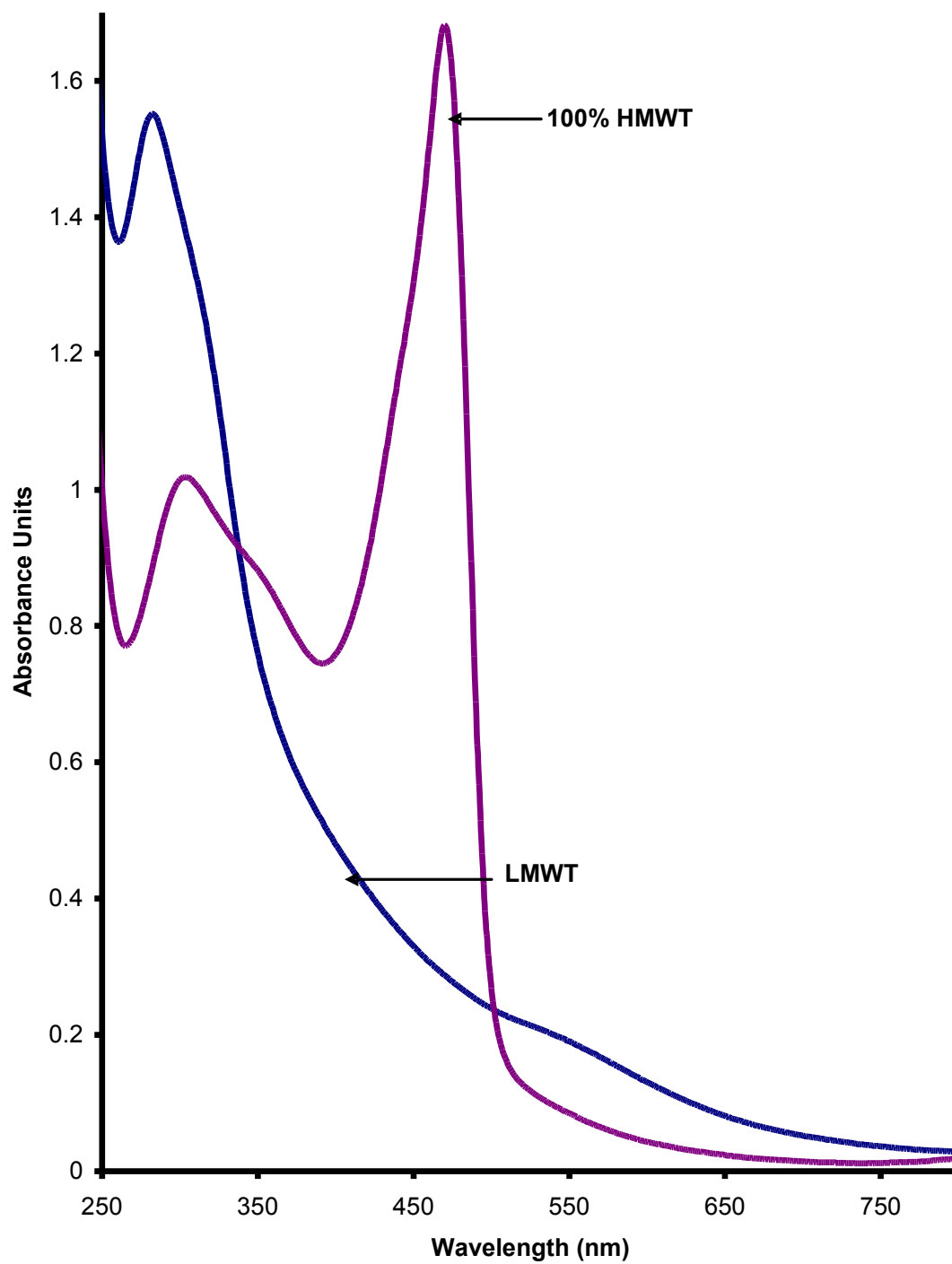


**Figure 2.14:** UV-visible spectra of aqueous LMWT PMAS emeraldine salt and the oligomeric LMWT PMAS in  $dH_2O$

### 2.4.3 Emission Spectroscopy

Previous photoluminescence studies carried out on HMWT PMAS indicated broad and intense emission from what was believed to be the emeraldine salt form of the polymer. This was surprising as the unsubstituted emeraldine form of polyaniline is reported to act as a quencher.<sup>112,113</sup> The observed emission has been attributed to trace impurities of the LMWT PMAS fraction. HMWT PMAS polymers separated using older dialysis techniques were found to contain up to 30% LMWT PMAS.<sup>106</sup> More recent studies carried on High and Low molecular weight samples that had been separated using more efficient cross flow dialysis techniques allowed a more in depth study of the exact photoluminescent processes occurring with each PMAS fraction.

An excitation wavelength of 355 nm was used to excite into the  $\pi$ - $\pi^*$  band transition as this band is relatively independent of the oxidation and protonation levels of the polymer. Emission spectra for each fraction can be seen in Figure 2.15. The spectra obtained were similar to previously reported results for the emission of PMAS.<sup>97</sup> In each case a raman scattering peak was observed at 410 nm. The LWMT PMAS exhibited a strong broad emission with a  $\lambda_{\text{max}}$  at ca. 525 nm. On the other hand the HMWT PMAS sample displayed a very weak photoluminescence emission as expected for an emeraldine salt. The weak photoluminescence from the HMWT PMAS sample can be attributed to trace impurities of the LMWT fraction.<sup>97</sup>

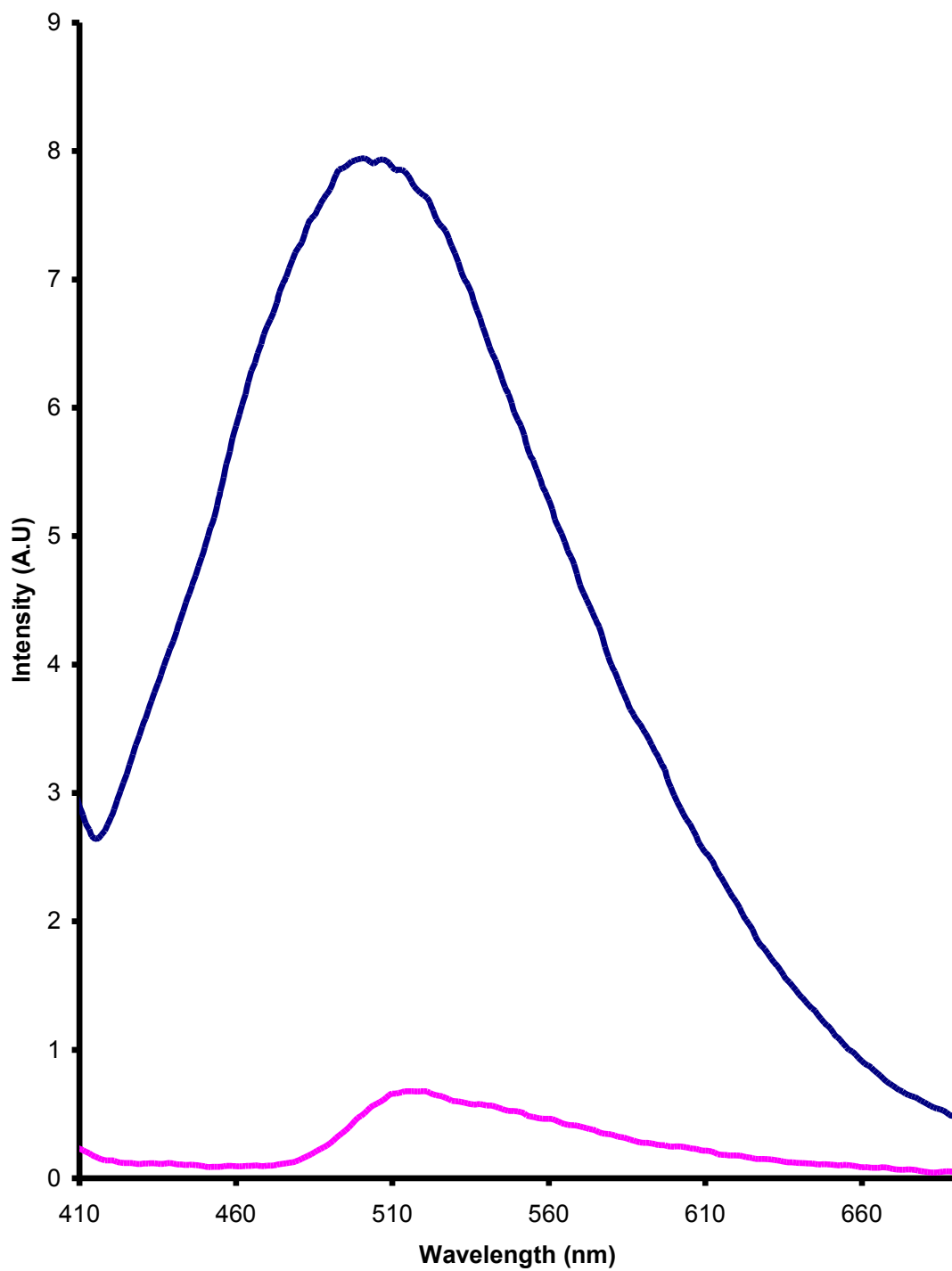


**Figure 2.15:** Emission spectra of 100 $\mu$ M aqueous solutions of LMWT PMAS oligomers (blue) and HMWT PMAS emeraldine salt (pink) in dH<sub>2</sub>O.

#### 2.4.4 Photoluminescent yields and excited state lifetimes

To further elucidate the nature of the LMWT PMAS photoluminescence, emission lifetime studies were carried out on both high and low molecular weight PMAS samples using a TCSPC system with 370 nm and 450 nm laser pulses. In each case the TCSPC responses were collected to the same photon count intensity (10,000 counts). Typical collection times varied from 250 s for LMWT PMAS to over 500 s for HMWT PMAS. Emission responses were analysed using PicoQuant FluoFit software and were fitted using 2 time constants. Luminescent lifetime calculations for both high and low fractions closely corresponded to previously reported results using a similar system.<sup>97</sup> In each case the luminescent lifetimes did not exceed 10 ns. Once again the emission obtained from the HMWT polymer is a result of trace impurities of the LMWT polymer. The precise values are presented in table 2.3.

**Table 2.3:** Photoluminescent lifetimes obtained for (10  $\mu\text{M}$ ) PMAS fractions, solution deaerated with Argon prior to analysis

<b>PMAS Fraction</b>	<b><math>\tau</math> (ns)</b>
LMWT PMAS	$8 \pm 3$
HMWT PMAS	$6 \pm 1$

#### **2.4.5 Cyclic Voltammetry**

Cyclic voltammograms of both HMWT and LWMT PMAS fractions (0.1 mg/ml) cycled between 0 and 1.6 V s<sup>-1</sup> are shown in Figure 2.16. Previous cyclic voltammograms of sulphonated polyanilines typically display two major peaks (each peak corresponding to a two-electron transfer).<sup>114</sup> The HMWT PMAS emeraldine salt displayed typical anodic and cathodic peaks at 0.2 and 0.4 V s<sup>-1</sup>, which can be attributed to leucoemeraldine to emeraldine and emeraldine to pernigraniline redox transitions.<sup>115</sup> In contrast the LMWT PMAS Oligomers are chemically inert as has been reported previously.<sup>94</sup>

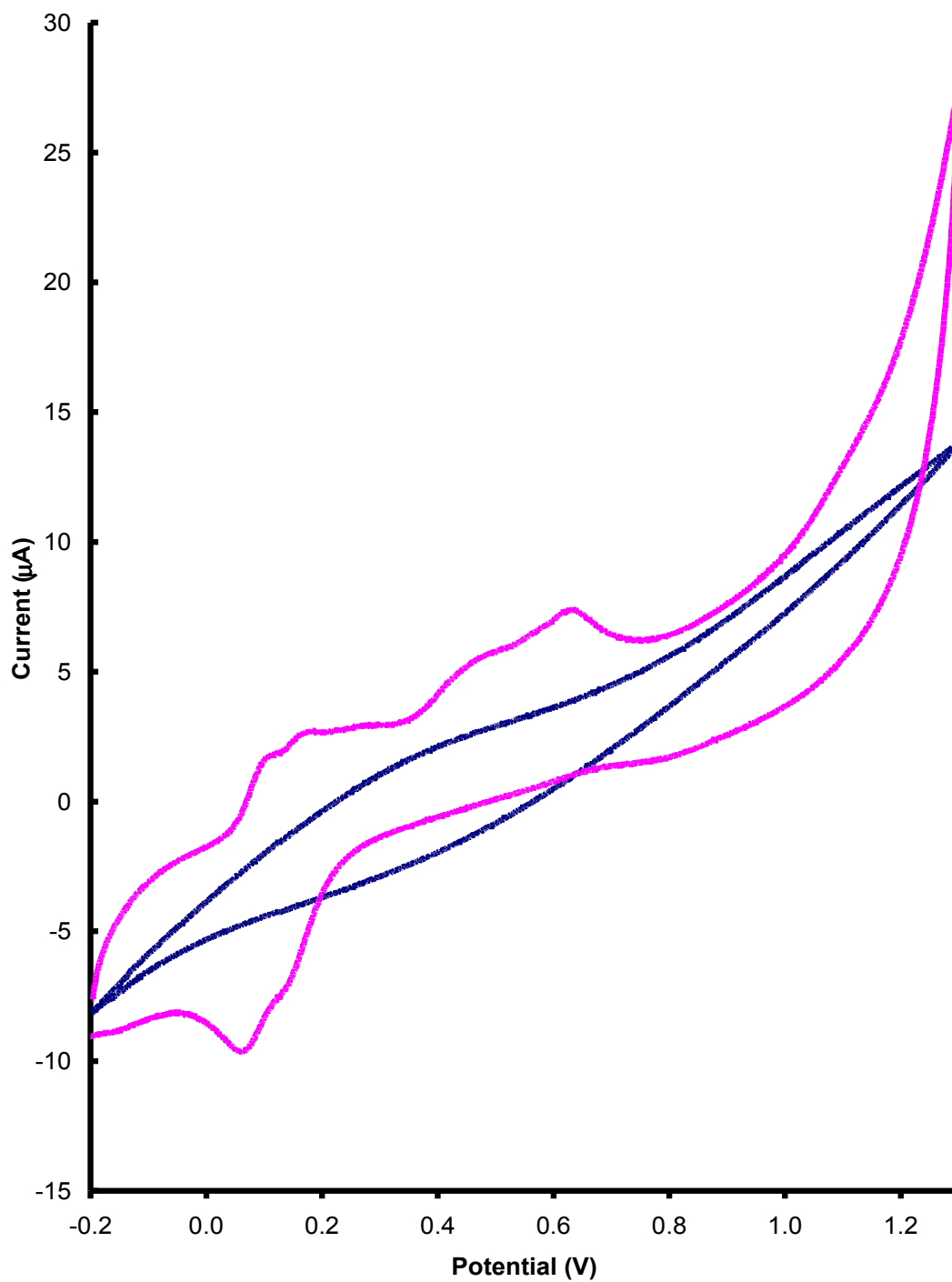


**Figure 2.16:** Cyclic voltammetric response of HMWT PMAS emeraldine salt and LMWT PMAS Oligomers in aqueous solution with 0.1M LiClO<sub>4</sub> electrolyte and 0.1Vs<sup>-1</sup> scan rate. Solutions were deaerated with Argon prior to analysis.

## 2.5 Conclusions

The chapter presented characterisation data for each of the polymers, the results of which were compared to currently published data in the literature. The ruthenium conjugated metallopolymers  $[Ru(bpy)_2(PPyBBIM)_n]^{2+}$  where n corresponds to 3, 10 and 20 respectively were characterised through spectroscopy and electrochemistry. For the most part the spectrochemical and electrochemical properties of the analogous monomeric ruthenium complex,  $[Ru(bpy)_3]^{2+}$ , are carried over to the conjugated polymeric material. Notable exceptions are the excited state lifetimes of the conjugated metallopolymers which are significantly lower than that of  $[Ru(bpy)_3]^{2+}$  (580ns) under similar conditions. Dual emission and a large shift in ruthenium based emission was also observed, however the origins of this shift and its effect on charge transfer within the metallopolymer are further probed in chapter 3. Varying the metal loading of the metallopolymer was found to have little impact on the luminescent lifetime of the ruthenium-based emission of the metallopolymer. In each case the lifetime was calculated to be approximately ~120 ns. Characterisation of thin layers of the conjugated metallopolymer immobilised in an electrode surface showed that they exhibited features typical of surface bound redox sites.

Both high and low molecular weight fractions of PMAS were characterised. Each fraction displayed the identical spectroscopic and electrochemical properties as had been previously reported for sulfonated polyaniline.<sup>97</sup> The high molecular weight polymer displayed reversible electrochemical behaviour and was shown not to photoluminesce with the exception of trace impurities of LMWT PMAS. The low molecular weight fraction displayed significant luminescence accompanied by little or no electroactivity.

## *Chapter 3*

### *Ground vs. Excited State electron transfer in [Ru(bpy)<sub>2</sub>(PPyBBIM)<sub>n</sub>]<sup>2+</sup> Films*

### ***3.1 Introduction***

Electron and energy transfer processes play a vital role in defining the physical and chemical characteristics of new and existing materials.<sup>116,117,118,119,120</sup> As such the full benefits of such materials may only be exploited after these characteristics have been fully investigated and are well understood. Much work has been carried out on investigating the electron transfer properties of conjugated metallopolymers in the ground state, however it is less common to also investigate the electron or energy transfer in the excited state. Electronically excited states play an important role in areas as diverse as semiconductors to photosynthesis, since upon absorption of a photon they are simultaneously better electron donors and acceptors than their ground state precursors.<sup>121,122,123</sup>

Electron transfer rates in polymers have been ever increasing since the first polymer capable of conducting electricity was first discovered in the mid 1970s. The goal of producing a material that could combine the processibility, environmental stability and weight advantages of a fully organic polymer with the useful electrical properties of a metal has become increasingly more likely. To achieve these aims various novel approaches have been adopted. Pickup and co-workers<sup>124,125,126,127,128</sup> extensive use of impedance spectroscopy, rotating disk voltammetry, and dual sandwich electrode voltammetry to elucidate charge transport mechanisms in several ruthenium and osmium containing conducting metallopolymers. They outlined how different conductivity mechanisms depend upon the nature of the interaction between the metal centres and the ligand backbone. Previous investigations using electrochemistry on ruthenium containing benzimidazole metallopolymers have shown promising results indicating an electronic communication between the metal centers through the conjugated backbone in the ground state.<sup>124</sup> This enhanced communication could be advantageous not only from a “synthetic metal” standpoint but also for sensing applications. For example, the light intensity of electrochemiluminescent based sensors depends on the rate at which  $\text{Ru}^{3+}$  is regenerated electrochemically.<sup>129,130</sup>

While enhanced rates of charge transport are without doubt highly advantageous from an electrochemical viewpoint, the effect on the polymer's photophysical properties should not be overlooked. Moreover, from the perspective of excited state interactions, the extent of electronic communication between the luminescent polymer backbone and metal complexes will influence the emission properties. For example, where strong coupling occurs only a single emission would be expected from the lowest energy state but the intensity could be enhanced due to the greater quantum efficiency across a wider wavelength range. These effects could produce sensors with lower limits of detection and increased analyte specificity.<sup>131</sup>

This chapter focuses on examining the ground and excited state properties of  $[\text{Ru}(\text{bpy})_2(\text{PPyBBIM})_n]^{2+}$  series of conjugated metallopolymers. In contrast to the metallopolymers investigated by Pickup et al<sup>124</sup>, the average separation of the metallopolymer metal centers in this study is systematically varied to reveal the distance dependence of their electronic interaction in the ground state. The interactions of the polymer backbone with the ruthenium metal centres in the excited state is also fully probed along with driving forces responsible for the observed results.

### ***3.2 Apparatus and Reagents***

Electrochemical experiments were performed in a standard electrochemical cell using a CH instruments (Memphis TN) model 440 potentiostat. With the exception of electrochemical studies performed on IDA electrodes all other voltammetry experiments were carried out using a 3 mm diameter glassy carbon working electrode in a conventional three electrode assembly using a platinum flag as the counter electrode. Working electrodes were cleaned by polishing with alumina on felt pad, followed by sonication in distilled deionized water for 30 min. Where appropriate, working electrodes were modified by applying a drop ( $\approx 15 \mu\text{L}$ ) of an ethanolic solution of the metallopolymer to the electrode surface (0.1 - 1.0 % depending on desired surface coverage). Modified electrodes were then allowed to dry in the dark for 10 to 12 hours. Surface coverage  $\Gamma$  was determined by graphical integration of background corrected cyclic voltammograms ( $< 5 \text{ mV s}^{-1}$ ). The surface coverage ranged from  $2\text{-}5 \times 10^{-8} \text{ mol cm}^{-2}$ , specific values however are stated in the respective figure legends. Potentials were measured versus a Ag/AgCl reference electrode. Interdigitated Array Electrodes (IDA) were purchased from Abtech (Richmond, VN) and modified by drop casting polymer films as described above. All electrochemical measurements were performed in  $\text{CH}_3\text{CN}$  containing 0.1M  $\text{Bu}_4\text{NOH}$ , which had been acidified with a few drops of  $\text{HClO}_4$  and were carried out at room temperature. All solutions were deoxygenated using nitrogen or argon prior to measurement.

Photoluminescence was recorded using a Perkin Elmer LS-50 luminescence spectrometer. Samples were prepared at concentrations of  $10^{-4}$  to  $10^{-5}$  M in spectroscopic grade acetonitrile and all spectroscopic measurements were carried out using 1 cm quartz cuvettes. Luminescent lifetimes were measured using the

third harmonic (355 nm) of a Spectron Q-switched Na-Yag laser for excitation. Emission was detected in a right-angled configuration to the laser using an Oriel model IS520 gated intensified CCD coupled to an Oriel model MS125 spectrograph. With suitable signal averaging, this configuration allows a complete spectrum (spectral range 250 nm) to be obtained within times as short as 10 ns. The emission spectra were typically recorded using the average of twenty laser shots. The gate width, i.e., the exposure time of the CCD, was never more than 5% of the excited state lifetime. The step size, i.e., the time between the acquisitions of discrete spectra, was typically 5% of the excited state half-life.

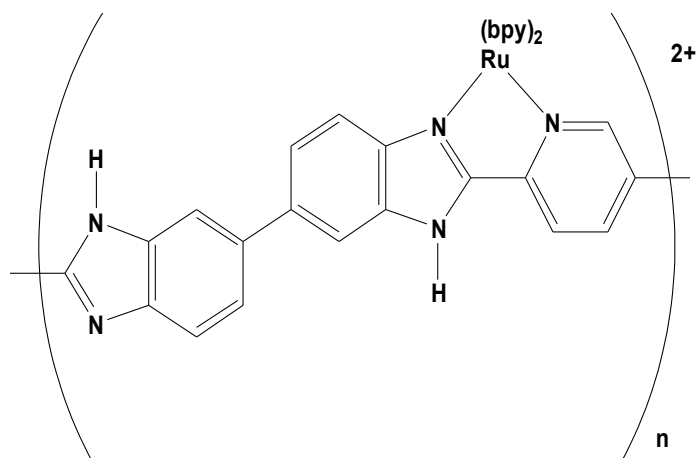


**Figure 3.1:** Structure of  $\text{Ru}(\text{bpy})_2(\text{PPyBBIM})^{2+}$

### ***3.3 Results and Discussion***

#### ***3.3.1 Ground State Electron Transfer***

Pickup et. al.<sup>124</sup> first reported on the electrochemical properties of these metallopolymers. However his work focused on metallopolymers where the ratio of metal ligand to monomeric polymer backbone unit was 1:1. A key advantage of the metallopolymers in this study is that the average separation of the metal centers can be systematically varied to reveal the distance dependence of their electronic interaction in both the ground and excited states.

The effect of electrochemical cycling of the metallopolymers can be seen in Figure 3.2. This figure shows an electrochemically reversible response centered at approximately +1.1 V associated with the Ru<sup>2+/3+</sup> couple. The supporting electrolyte in each case is LiClO<sub>4</sub>. The observed voltammograms are consistent with one another given the different metal loadings and can be seen in Figure 3.2. The oxidation and reduction potentials for each metallopolymer can be seen in Table 3.1. In common with the behavior reported by Pickup et. al. for the metallopolymers where the metal to monomer unit was not altered, the redox couple ranges from 0.8 to 1.2 V depending on the pH of the contacting electrolyte solution.<sup>124</sup> This dependence arises from protonation induced changes in the electron density of the polymer backbone suggesting that significant electronic communication between the metal centers can occur through the conjugated backbone.<sup>132</sup> The lower limit on the range of useful scan rates in cyclic voltammetry is dictated by the requirement that the depletion layer thickness be significantly less than the overall film thickness, while the upper scan rate is limited by the rate of heterogeneous electron transfer across the electrode layer interface. In this study, these conditions are met for  $100 \geq v \geq 500 \text{ mVs}^{-1}$  and plots of the peak current varied linearly with the square root of scan rate over this

range. The voltammetric response for each metallopolymer can be seen in Figure 3.2.

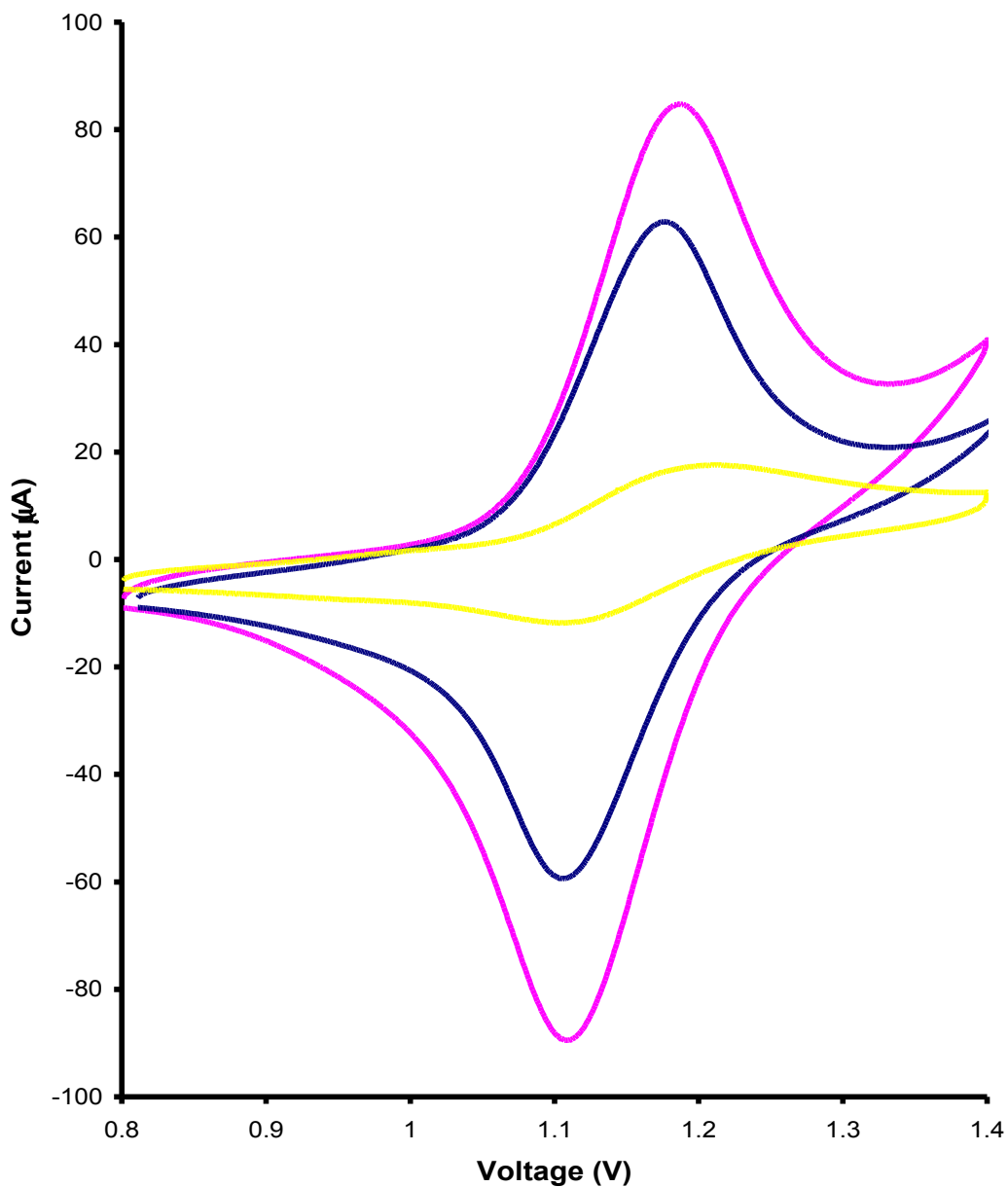


**Figure 3.2:** Cyclic voltammetry of  $[Ru(bpy)_2(PPyBBIM)_3]^{2+}$  (pink),  $[Ru(bpy)_2(PPyBBIM)_{10}]^{2+}$  (blue) and  $[Ru(bpy)_2(PPyBBIM)_{20}]^{2+}$  (yellow). Respective metallopolymer were confined at the electrode surface in a thin film on glassy carbon electrode, (3 mm diameter). Scan rate used was  $0.1 \text{ Vs}^{-1}$  and

293K. The electrolyte is 0.1 M LiClO<sub>4</sub>.  $\Gamma = 5 \times 10^{-8} \text{ mol cm}^{-2}$   $4 \times 10^{-8} \text{ mol cm}^{-2}$  and  $2 \times 10^{-8} \text{ mol cm}^{-2}$  respectively. Analysis performed at pH (6.0)

**Table 3.1.** Oxidation and Reduction potentials for [Ru(bpy)<sub>2</sub>(PPyBBIM)<sub>n</sub>]<sup>2+</sup> in both solution and thin film. Solution were degassed with Argon prior to analysis.

Metallopolymer	Reduction peaks		Oxidation peak
	E <sup>o</sup> vs. Ag/AgCl		E <sup>o</sup> vs. Ag/AgCl
[Ru(bpy) <sub>2</sub> (PPyBBIM) <sub>3</sub> ] <sup>2+</sup> (film)	-1.68	-1.82	1.18
[Ru(bpy) <sub>2</sub> (PPyBBIM) <sub>3</sub> ] <sup>2+</sup> (soln.)	-1.63	-1.85	1.21
[Ru(bpy) <sub>2</sub> (PPyBBIM) <sub>10</sub> ] <sup>2+</sup> (film)	-1.62	-1.78	1.22
[Ru(bpy) <sub>2</sub> (PPyBBIM) <sub>10</sub> ] <sup>2+</sup> (soln.)	-1.58	-1.81	1.26
[Ru(bpy) <sub>2</sub> (PPyBBIM) <sub>20</sub> ] <sup>2+</sup> (film)	-1.68	-1.91	1.22
[Ru(bpy) <sub>2</sub> (PPyBBIM) <sub>20</sub> ] <sup>2+</sup> (soln.)	-1.68	-1.92	1.18

### 3.3.1.1 Effect of Scan Rate

The evaluation of charge transport is an important parameter from an ECL perspective, as the sensitivity of the sensor will ultimately be dictated by the rate at which the  $\text{Ru}^{3+}$  sites can be regenerated. Therefore, it is important to determine the rate of charge transport through the solution leading to the conversion of the ECL inactive  $\text{Ru}^{2+}$  centres into the mediating  $\text{Ru}^{3+}$  centres. The rate of charge transfer through the metallopolymer layer can be quantified by measuring the homogeneous charge transfer diffusion coefficient ( $D_{\text{CT}}$ ). This parameter can be obtained from a plot of  $i_p$  vs.  $v^{1/2}$  under diffusion controlled conditions. If ion charge transport is not rate limiting this value represents so called “electron-hopping” between the ruthenium redox sites in the film.  $D_{\text{CT}}$  is commonly measured by cyclic voltammetry, however the use of chronoamperometry is also common. As one of the aims of this work is to produce metallopolymer systems for use in an ECL based sensing device for the detection of biological analytes, the pH of which needs to be close to neutral therefore the  $D_{\text{CT}}$  was measured at pH 6.0 to evaluate the metallopolymer performance at near neutral pH. Pick up *et al* reported extremely fast electron transfer rates ( $10^{-9}\text{cm}^2\text{s}^{-1}$ ) for the  $[\text{Ru}(\text{bpy})_2(\text{PPyBBIM})]^{2+}$  metallopolymer at basic pH values.<sup>124</sup> To compare the rate of charge transport for these metallopolymer at basic pHs values the  $D_{\text{CT}}$  was also evaluated at pH 10.

*Figure 3.3 shows the effect of changing the scan rate,  $v$ , for  $0.1 \leq v \leq 0.5 \text{ Vs}^{-1}$  on the cyclic voltammetry of a thin film of  $[\text{Ru}(\text{bpy})_2(\text{PPyBBIM})_{10}]^{2+}$ , deposited on a glassy carbon electrode in  $0.1\text{M LiClO}_4$  at pH 6.0. Similar responses are observed for each loading of metal complexes investigated as can be seen in Figures 3.4 and 3.5 respectively. Figure 3.3 shows an electrochemically reversible response centered at approximately  $+1.1 \text{ eV}$  associated with the  $\text{Ru}^{2+/3+}$  couple. The rate of homogeneous charge transport can be determined from the slope of a plot of  $i_p$  vs  $v^{1/2}$  for each metallopolymer. For  $0.1 \leq v \leq 0.5 \text{ Vs}^{-1}$ , the inset of Figure 3.3 shows that the voltammetric peak currents,  $i_p$ , increase as  $v^{1/2}$ . This*

*behavior is consistent with semi-infinite linear diffusion and under these conditions, the response can be described by the Randles-Sevcik Equation;*

$$i_p = 2.69 \times 10^5 n^{3/2} A D_{ct}^{1/2} C \nu^{1/2} \quad (3.1)$$

where  $n$  is the number of electrons transferred,  $A$  is the area of the working electrode,  $D_{CT}$  is the diffusion coefficient, and  $C$  is the concentration of the redox centers. The concentration of ruthenium centers within the metallopolymer has been determined from density measurements in non-swelling solvents as **0.8M**. Thus, Equation 3.1 allows  $D_{CT}$  to be estimated for both the oxidation and reduction processes as  $3.9 \pm 0.2 \times 10^{-10} \text{ cm}^2 \text{ s}^{-1}$ .

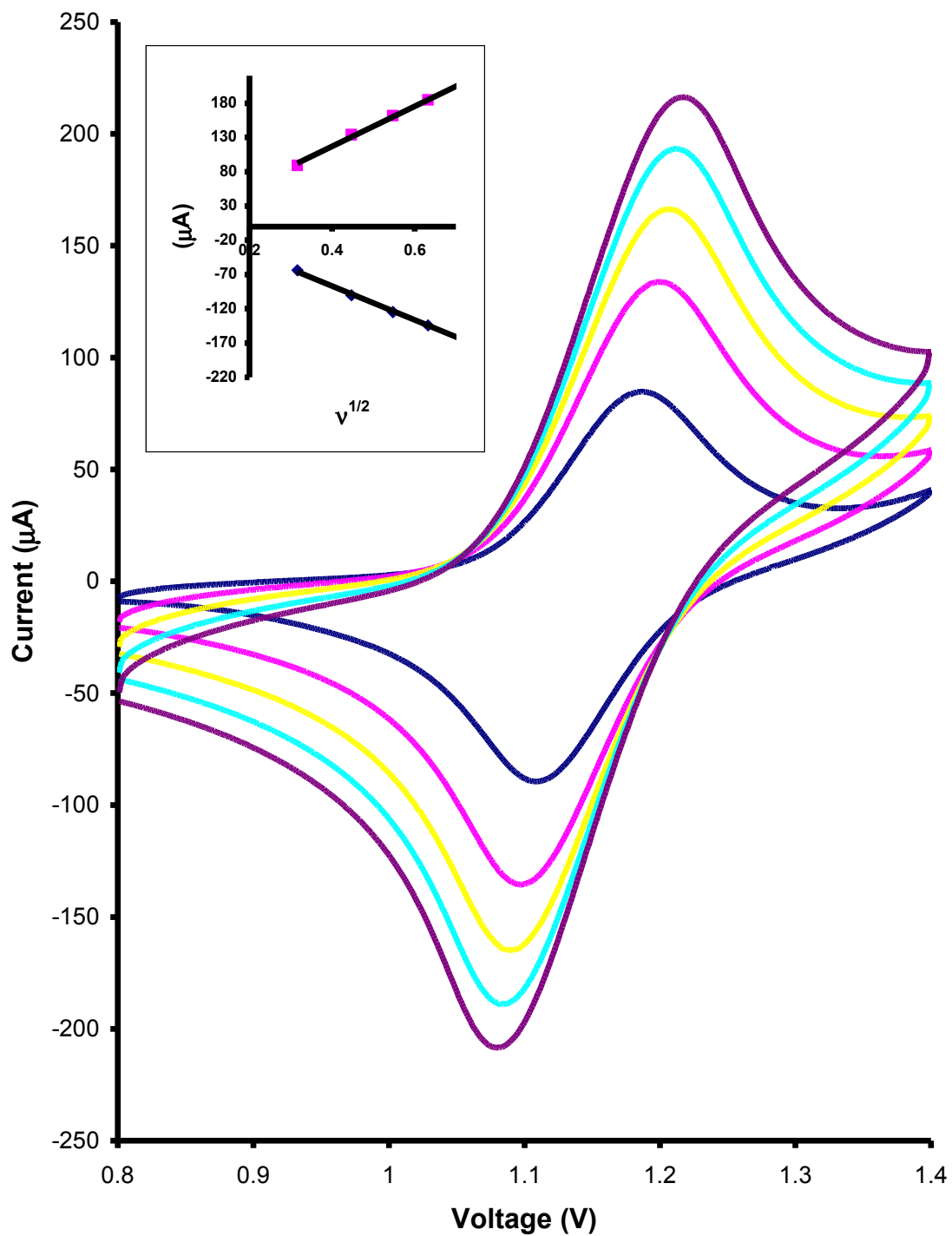


**Figure 3.3:** Effect of scan rate on cyclic voltammetry of thin films of  $[Ru(bpy)_2(PPyBBIM)_3]^{2+}$  in  $0.1\text{ M LiClO}_4$  (pH 6.0 @ 293K). Insert shows plot of peak current (cathodic and anodic branches) versus  $v^{1/2}$  for this data.

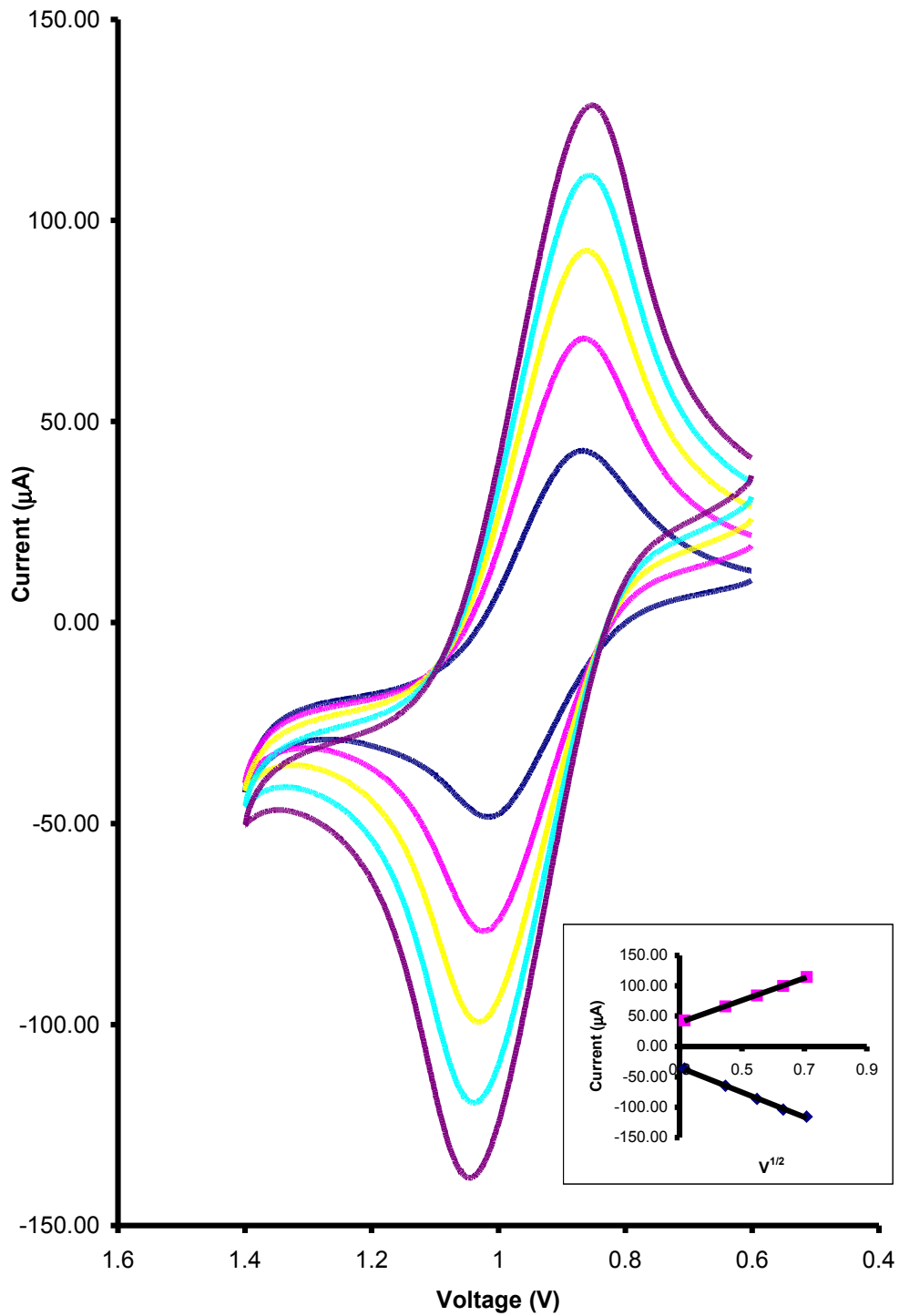


**Figure 3.4:** Effect of scan rate on cyclic voltammetry of thin films of  $[Ru(bpy)_2(PPyBBIM)_{10}]^{2+}$  in  $0.1\text{ M LiClO}_4$  (pH 6.0 @ 293K) Insert shows plot of peak current (cathodic and anodic branches) versus  $v^{1/2}$  of this data.

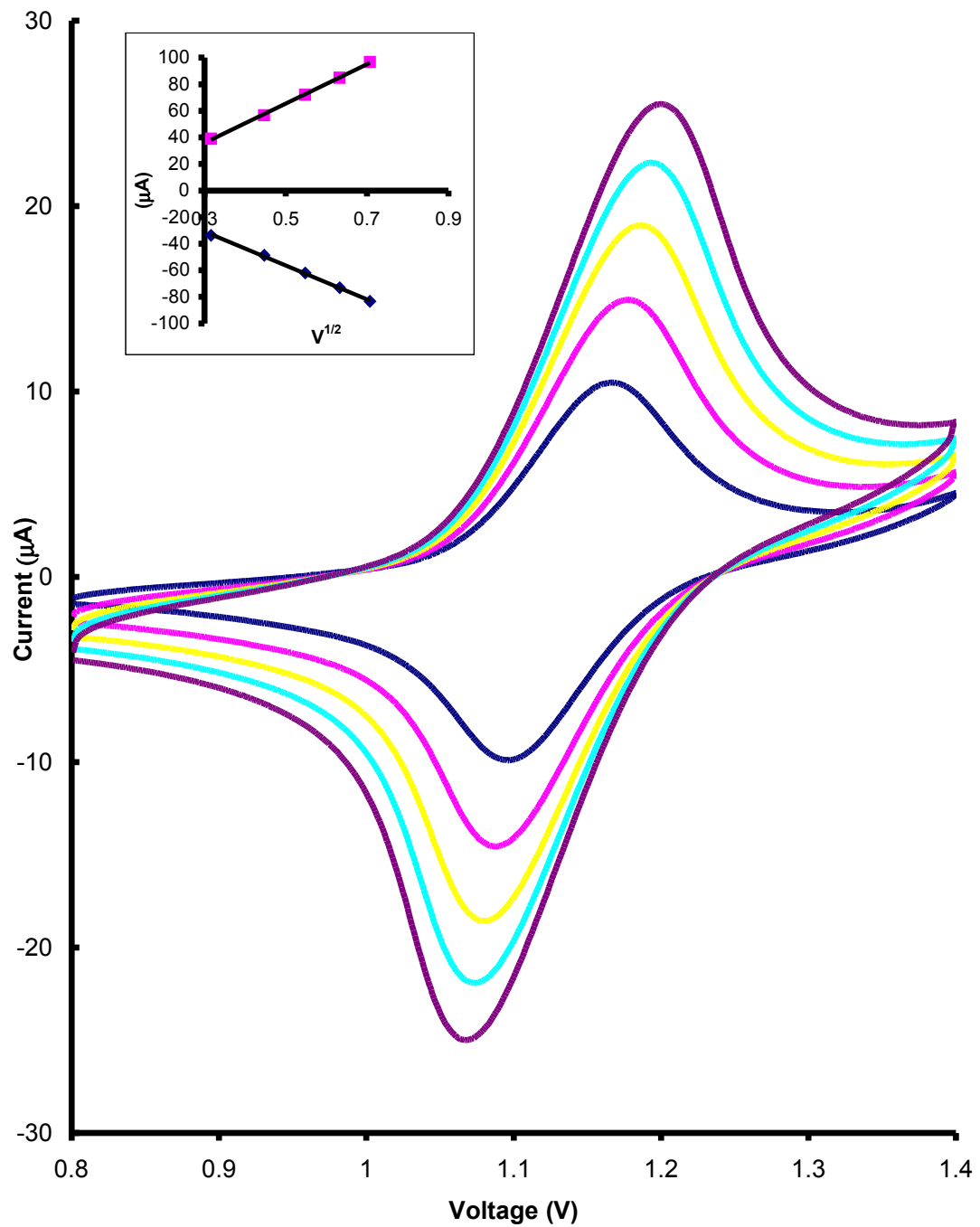


**Figure 3.5:** Effect of scan rate on cyclic voltammetry of thin films of  $[Ru(bpy)_2(PPyBBIM)_{20}]^{2+}$  in  $0.1\text{ M LiClO}_4$  (pH 6.0 @293K). Insert shows plot of peak current (cathodic and anodic branches) versus  $v^{1/2}$  of this data.

**Table 3.2:**  $D_{CT}$  values recorded for each metallopolymer at both pH 5.5 and pH10.

Metallopolymer	$D_{CT}$ ( $\text{cm}^2\text{s}^{-1}$ ) pH 6.0		$D_{CT}$ ( $\text{cm}^2\text{s}^{-1}$ ) pH 10	
	Anodic	Cathodic	Anodic	Cathodic
$[\text{Ru}(\text{bpy})_2(\text{PPyBBIM})_3]^{2+}$	$3.9 \times 10^{-10}$	$1.7 \times 10^{-10}$	$2.3 \times 10^{-10}$	$2.3 \times 10^{-10}$
$[\text{Ru}(\text{bpy})_2(\text{PPyBBIM})_{10}]^{2+}$	$4.7 \times 10^{-10}$	$4.1 \times 10^{-10}$	$4.1 \times 10^{-10}$	$3.0 \times 10^{-10}$
$[\text{Ru}(\text{bpy})_2(\text{PPyBBIM})_{20}]^{2+}$	$7.0 \times 10^{-12}$	$1.7 \times 10^{-12}$	$3.0 \times 10^{-10}$	$2.6 \times 10^{-10}$

### 3.3.1.2 Contribution of the metallopolymer backbone to charge transport.

There are a number of processes that could contribute to homogeneous charge transport through films of this kind, including electron hopping, counterion diffusion/migration or movement of polymer chains or segments to bring adjacent redox centers sufficiently close to allow electron transfer to occur.<sup>133</sup> Table 3.2 shows that increasing the number of metal centers within the metallopolymer structure increases the rate of homogeneous charge transport through the film. To address the issue of the rate limiting step the electronic conductivity has been determined using interdigitated array electrodes (IDAs) coated with the metallopolymer. As originally demonstrated by Wrighton and co-workers<sup>134,135,136</sup> the film conductivity is obtained from the slope  $\partial i / \partial E$ .

Figure 3.6 shows that the current varies approximately linearly with potential between 0.040 V and +0.200 V and the slopes can be used in conjunction with Equation 3.2 below to determine the conductivity,  $\sigma$ , where  $(d_G / A_{total})$  is the Zaretsky cell constant. The constant of the IDAs used in this experiment is 0.04 cm<sup>-1</sup>.

$$\sigma = d_G \partial i / A_{total} \partial E \quad (3.2)$$

The change of film conductivity has been measured in the presence of dry N<sub>2</sub> at room temperature and pressure. The slopes of the best fit line to the data in Figure 3.6 yield conductivities between 4.4x10<sup>-9</sup> and 2.3x10<sup>-8</sup> S cm<sup>-1</sup> depending on the ruthenium loading.

When electron hopping represents the overall charge transport rate through the metallopolymer film, the Dahms-Ruff equation<sup>137,138</sup> can be used to calculate the electron self-exchange rate constant,  $k_{SE}$ , from the  $D_{CT}$  according to Equation 3:

$$D_{CT} = D_{phys} + \frac{1}{\gamma} k_{SE} \delta^2 C \quad (3.3)$$

where  $C$  is the concentration of Ru redox centers within the film,  $\delta$  is the intersite separation between adjacent Ru redox centers, and  $D_{phys}$  describes physical diffusion in the absence of electron hopping. In this situation,  $D_{phys}$  is assumed to be zero, because the ruthenium centers are bound to the polymer chains. Therefore, Equation 3.3 reduces to:

$$D_{CT} = \frac{1}{6} k_{SE} \delta^2 C \quad (3.4)$$

For a hypothetical cubic lattice model<sup>139,140</sup> applied to electron transport in redox polymers, the electron self-exchange rate constant,  $k_{SE}$ , also can be calculated according to Equation 3.5:

$$k_{SE} = \frac{6RT\sigma}{10^{-3} F^2 \delta^2 [Ru]^{2+} [Ru]^{3+}} \quad (3.5)$$

where  $k_{SE}$  is the electron self-exchange rate constant,  $R$  is the gas constant,  $\sigma$  is the conductivity at temperature  $T$  (K),  $F$  is the Faraday constant, and  $\delta$  is the intersite separation between adjacent Ru redox centers. When Equations 3.4 and 3.5 are combined and the concentration ratio  $[Ru]^{2+} / [Ru]^{3+}$  is taken as 1,  $D_{CT}$  is given by Equation 3.6:

$$D_{CT} = \frac{\epsilon RT \sigma}{\nu \cdot \tau F^2 C} \quad (3.6)$$

As shown in Table 3.3, the  $D_{CT}$  values obtained using the IDAs and cyclic voltammetry are consistent with one another to within a factor of three in the worst case. Therefore, these IDA measurements confirm that the movement of charge compensating counterions does not represent the rate determining step for homogeneous charge transport through these films. This result, coupled to the

relatively large  $D_{CT}$  values obtained, suggests that electron transfer, most likely mediated by the conjugated polymer backbone, limits the overall rate of charge transport. It is important to note that the  $D_{CT}$  values reported here are approximately an order of magnitude smaller than those previously reported for the  $n=10$  polymer at pH 12. This pH dependence is expected since the electron density of the polymer backbone ought to be higher in the deprotonated state thus increasing the efficiency of electron transfer.

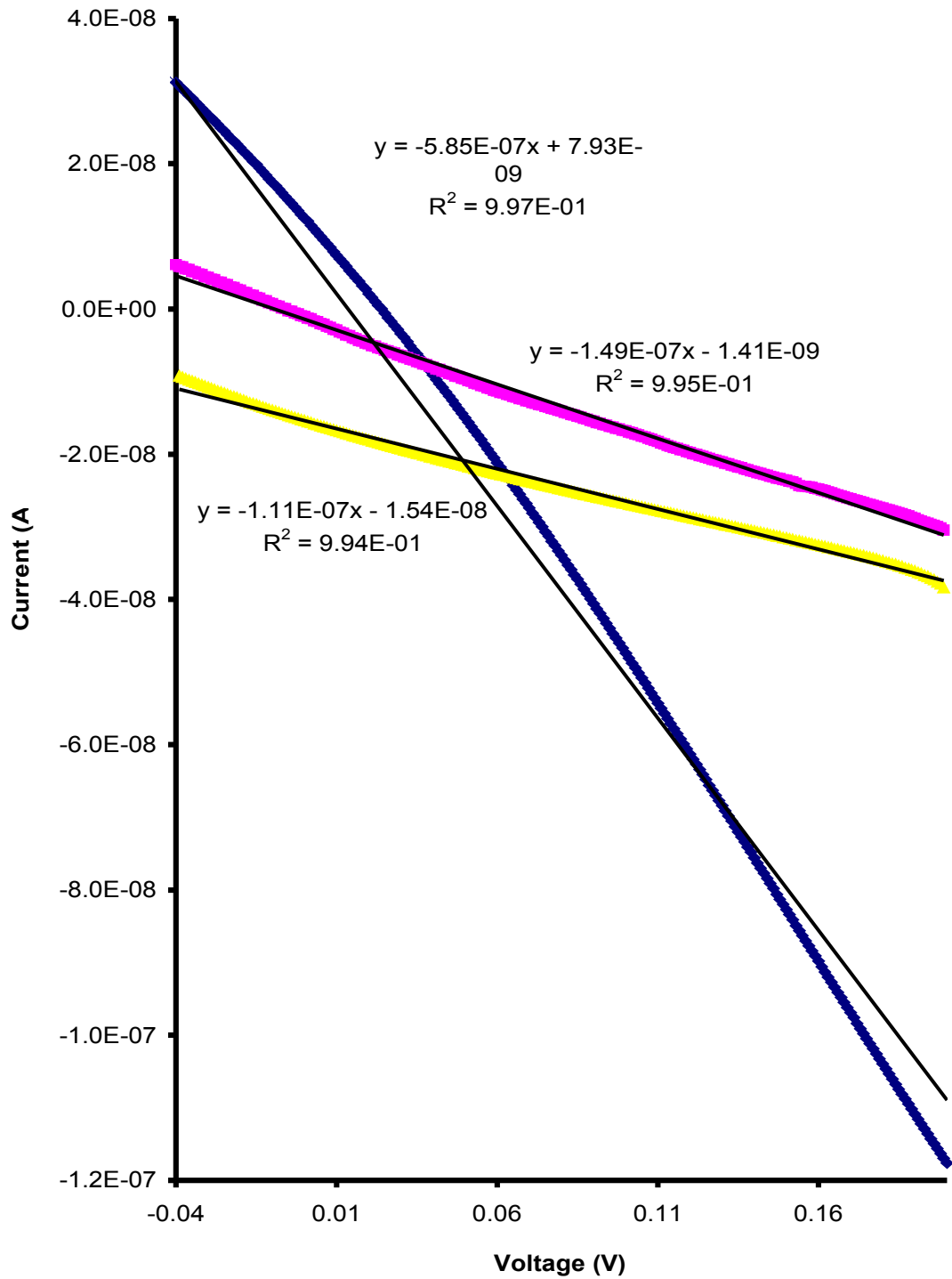


**Figure: 3.6.** Voltammetric response of  $[Ru(bpy)_2(PPyBBIM)_3]^{2+}$  (blue),  $[Ru(bpy)_2(PPyBBIM)_{10}]^{2+}$  (pink) and  $[Ru(bpy)_2(PPyBBIM)_{20}]^{2+}$  (yellow) cycled between  $-0.04$  and  $0.2$   $Vs^{-1}$  on Interdigitated Array Electrodes (IDA).

**Table 3.3:**  $D_{CT}$ ,  $D_e$  and Conductivity values for each metallopolymer. Scans performed in 0.1M LiClO<sub>4</sub> at 293 K

<b>Polymer Loading</b>	<b><math>D_{CT}</math> (cm<sup>2</sup>S<sup>-1</sup>)</b>	<b><math>D_e</math>(cm<sup>2</sup>S<sup>-1</sup>)</b>	<b>Conductivity (S cm<sup>-1</sup>)</b>
1/3	3.96±0.8 x 10 <sup>-10</sup>	1.53±0.5 x 10 <sup>-10</sup>	2.34 x 10 <sup>-8</sup>
1/10	4.79±1.1 x 10 <sup>-10</sup>	9.09±1.5. x 10 <sup>-10</sup>	5.96 x 10 <sup>-9</sup>
1/20	7.05±1.2 x 10 <sup>-12</sup>	4.79±1.3 x 10 <sup>-11</sup>	6.44 x 10 <sup>-9</sup>

### 3.3.2 Excited State Electron Transfer

### 3.3.2.1 UV-Vis Spectroscopy.

Ultraviolet-visible spectra of transition metal complexes can provide insights into the electronic transitions within a metallopolymer complex. Figure 3.7 depicts the absorption spectra of the  $[\text{Ru}(\text{bpy})_2(\text{PPyBBIM})_n]^{2+}$  metallopolymer complexes. The  $[\text{Ru}(\text{bpy})_2(\text{PPyBBIM})_{10}]^{2+}$  metallopolymer exhibits an intense absorption at 410 nm due to the  $\pi$ - $\pi^*$  transition of the polymer backbone. This absorption is slightly red shifted by  $\sim 10$  nm compared to the UV-Vis spectrum of the uncomplexed polymer reported by Pickup.<sup>125</sup> Absorptions at 245 and 280 nm can be attributed to bipyridine transitions.

Spin allowed metal to ligand charge transfer ( $^1\text{MLCT}$ ) absorptions are visible at 345 and 470 nm and are indicative of the  $[\text{Ru}(\text{N})_6]^{2+}$  coordination-sphere. The MLCT absorption at 470 nm appears as a shoulder on the polymer  $\pi$ - $\pi^*$  peak. Figure 3.5 shows the UV-visible spectra of the metallopolymer complexes with various metal loadings. As the  $[\text{Ru}(\text{bpy})_2(\text{PPyBBIM})_3]^{2+}$  metallopolymer has the largest amount of ruthenium present it generates the largest absorption intensity. This is closely followed by that of the  $[\text{Ru}(\text{bpy})_2(\text{PPyBBIM})_{10}]^{2+}$  and  $[\text{Ru}(\text{bpy})_2(\text{PPyBBIM})_{20}]^{2+}$  metallopolymer complexes respectively.

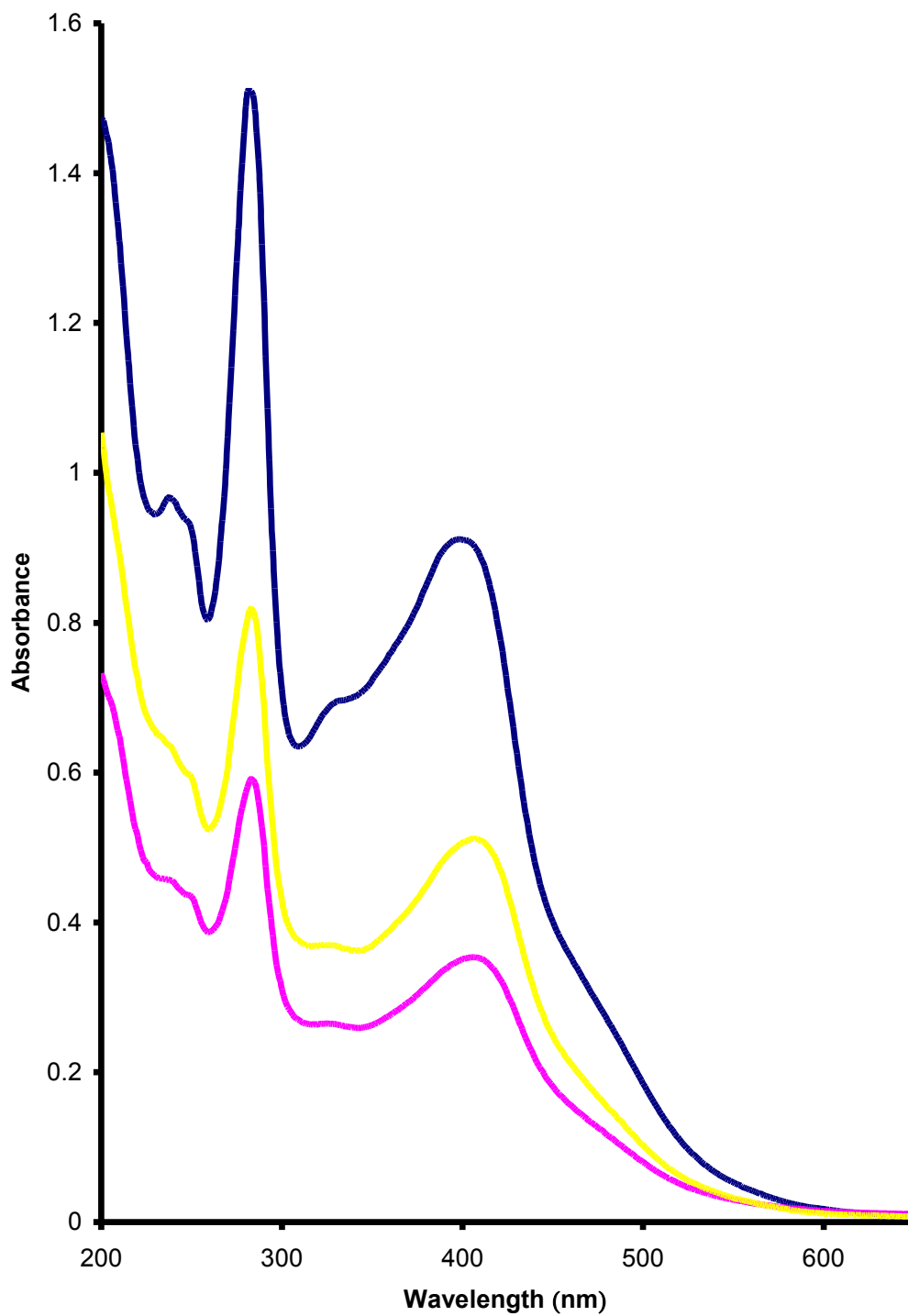


**Figure 3.7:** UV-visible absorption spectra of  $[\text{Ru}(\text{bpy})_2\text{PPyBBIM}]_3^{2+}$  (blue),  $[\text{Ru}(\text{bpy})_2\text{PPyBBIM}]_{10}^{2+}$  (pink) and  $[\text{Ru}(\text{bpy})_2\text{PPyBBIM}]_{20}^{2+}$  (yellow) dissolved in acetonitrile. Solution concentrations of  $100\mu\text{M}$  were used.

### 3.3.2.2 Emission Spectroscopy

As previously discussed in Chapter 2 the luminescence spectra for these metallopolymers displays the phenomenon of dual emission. Figure 3.8 shows the emission spectrum obtained for the each of the metallopolymers. The intensities of the polymer backbone emission have been normalised in order to accurately compare the metal emission intensities. It can be seen that the highest ruthenium emission is observed from the  $[\text{Ru}(\text{bpy})_2(\text{PPyBBIM})_{10}]^{2+}$  metallopolymer closely followed by the  $[\text{Ru}(\text{bpy})_2(\text{PPyBBIM})_{20}]^{2+}$  and  $[\text{Ru}(\text{bpy})_2(\text{PPyBBIM})_3]^{2+}$  respectively. In each case the metallopolymer shows two peaks at approximately 520 and 670 nm. The emission observed at 500 nm is assigned to the poly[2-(2-pyridyl)-bibenzimidazole] polymer backbone while the 670 nm emission is attributed to the ruthenium metal centre. This observation of dual emission is important since according to Kasha's Rule<sup>141</sup> an emission should only be observed from the lower energy ruthenium based excited state if energy or excited state electron transfer is possible.<sup>142,143</sup>

Figure 3.10 shows UV-Visible absorption and luminescence spectra for the polymer backbone overlaid with the emission spectra of the metallopolymer. This figure shows that the polymer emits at approximately 480 nm and has a Stokes shift of approximately 70 nm. Figure 3.10 also shows that while there is overlap between the emission spectrum of the benzimidazole polymer backbone and the ruthenium based absorbance this does not lead to emission exclusively from the ruthenium centers. The electrochemical investigations discussed above reveal that there is significant electronic communication between the ruthenium centers in the ground state. A key issue is the extent to which excited state electron transfer can occur in this metallopolymer.

A key advantage of these metallopolymers is that the loading of ruthenium centers can be systematically varied. Figures 3.8 and 3.9 illustrate the dependence of the emission spectra on the ruthenium loading following excitation at 355 and 450

nm, respectively. Significantly, irrespective of the excitation wavelength, this figure shows that the metallopolymer with the highest loading of ruthenium centers *does not* produce the most intense emission. Moreover, the relative intensities of the polymer and ruthenium based emission processes depends on the excitation wavelength. This behavior is expected given the differences in absorption spectra for the polymer backbone (Figure 3.9) and ruthenium centers which exhibit a strong MLCT absorption at 450nm. However, for both excitation wavelengths, the maximum ruthenium emission intensity is reached at intermediate metal loadings. There are at least two possible explanations of this behavior. Firstly, excited state electron transfer from the ruthenium excited state, e.g., to the polymer backbone, which would be favoured by a high metal loading. Secondly, trivial energy transfer, i.e., re-absorption of the 620 nm emitted photon by a ground state ruthenium. To provide further insight into both this phenomena and the nature of the dual emission occurring it is necessary to examine the driving force required for photo-induced charge transfer to occur.

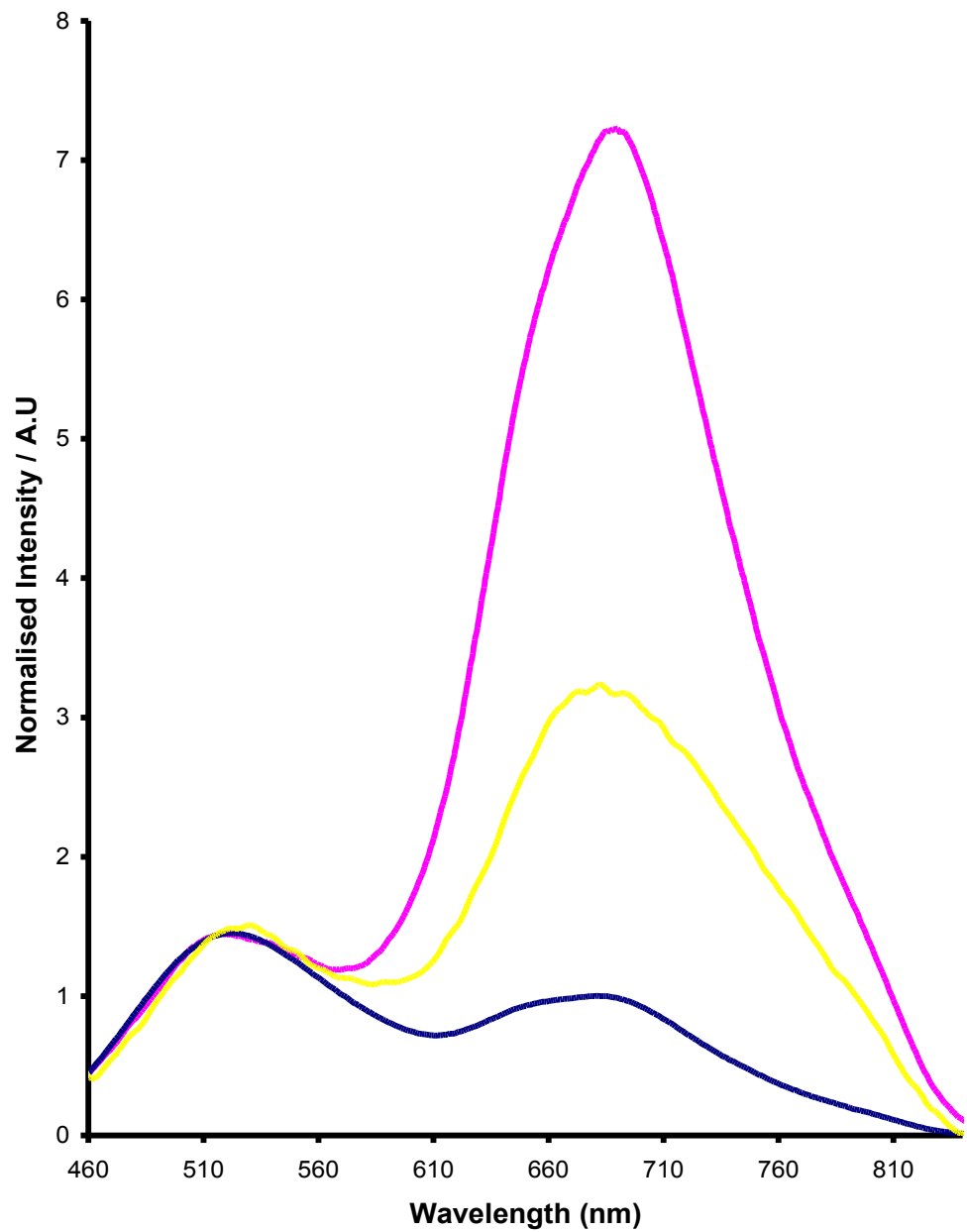


**Figure 3.8:** Emission spectra of  $[Ru(bpy)_2(PPyBBIM)_3]^{2+}$  (blue),  $[Ru(bpy)_2(PPyBBIM)_{10}]^{2+}$  (pink) and  $[Ru(bpy)_2(PPyBBIM)_{20}]^{2+}$  (yellow) dissolved in acetonitrile ( $100\mu M$ ).  $\lambda_{ex} = 450$  nm.

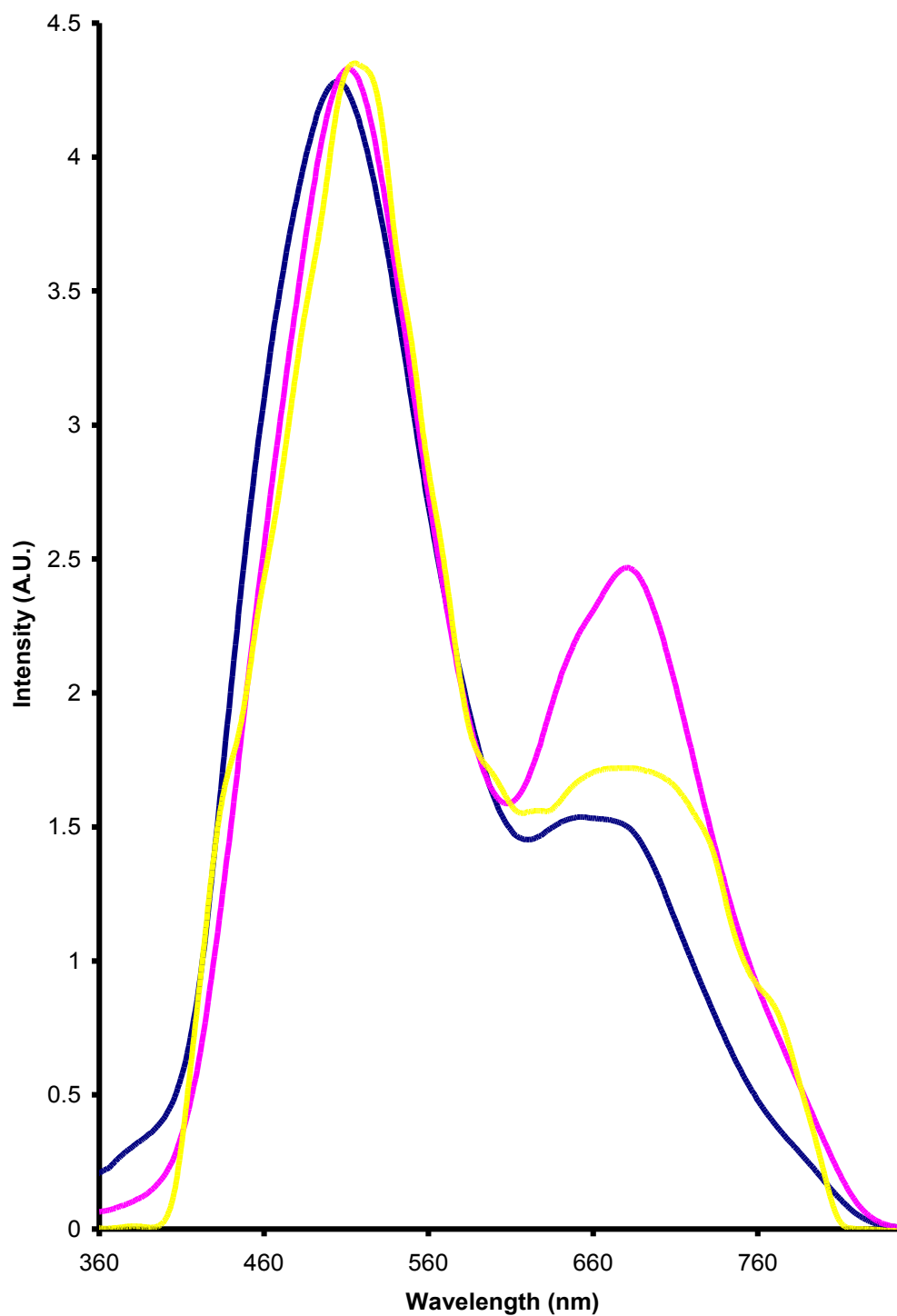


**Figure 3.9:** Emission spectra of  $[Ru(bpy)_2(PPyBBIM)_3]^{2+}$  (blue),  $[Ru(bpy)_2(PPyBBIM)_{10}]^{2+}$  (pink) and  $[Ru(bpy)_2(PPyBBIM)_{20}]^{2+}$  (yellow) dissolved in acetonitrile.  $\lambda_{ex} = 355$  nm.

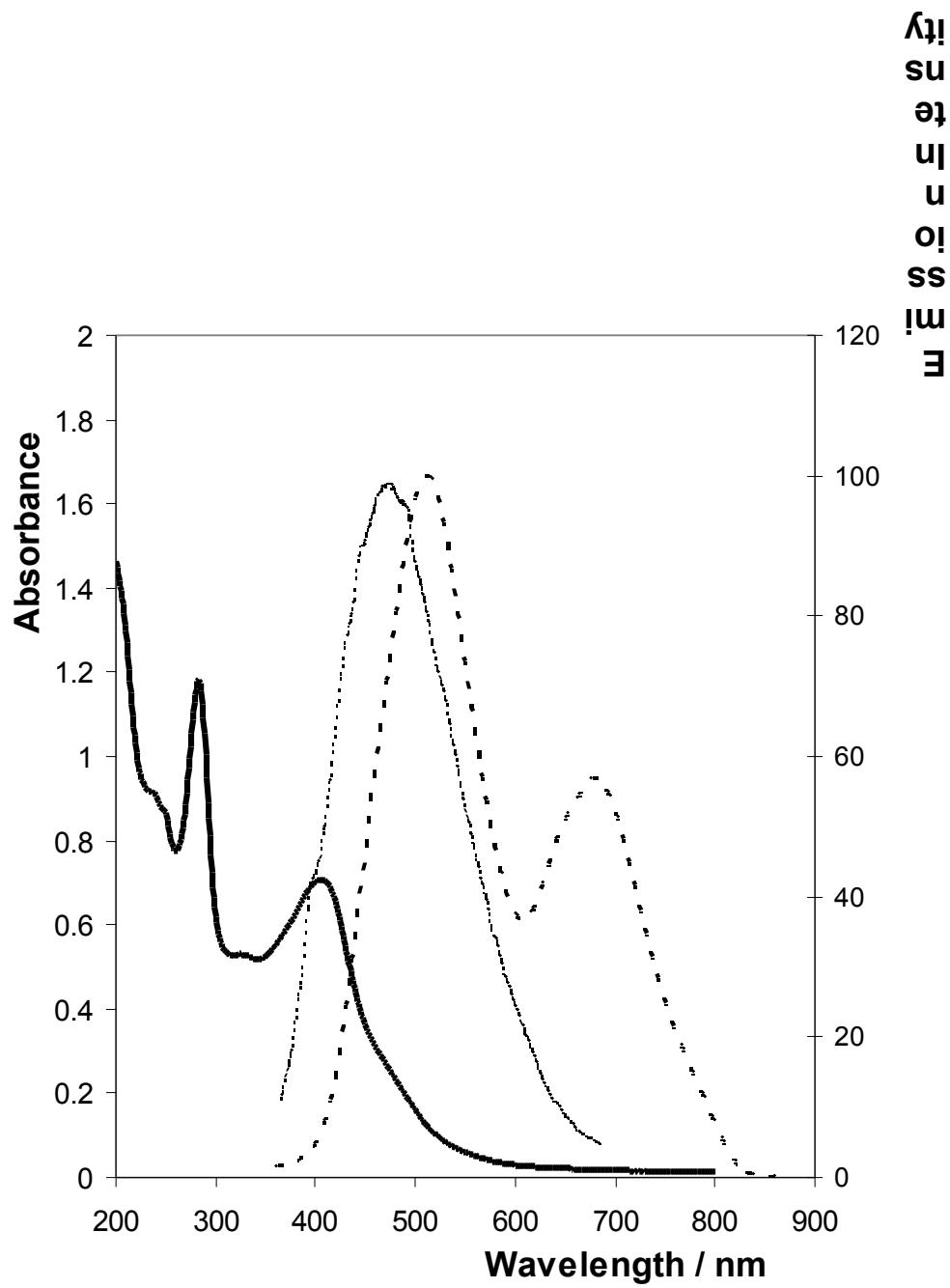


**Figure 3.10:** UV-vis spectra of  $[Ru(bpy)_2(PPyBBIM)_{10}]^{2+}$  (heavy line) with  $[(PPyBBIM)_{10}]$  and  $[Ru(bpy)_2(PPyBBIM)_{10}]^{2+}$  (dashed line) emission spectra.

### 3.3.2.3 Driving force for Photoinduced Electron Transfer

An estimation of the thermodynamic driving force for the respective electron transfer allows the most energetically favourable electron transfer process to be identified. If the coulombic stabilization energy of the products is negligible (typically less than 0.1eV in polar solvents) then the thermodynamic driving force for electron transfer,  $\Delta G^0$  can be estimated from the Rehm-Weller equation<sup>144</sup> and the relevant reduction and oxidation potentials

$$\Delta G^0 = [E^0(\text{Donor}) - E^0(\text{Acceptor})] - E^{00} - e^2/\epsilon r_{DA} \quad (3.7)$$

$E^{00}$  is the energy difference between the lowest vibrational levels of the ground and excited states and has been estimated from the wavelength of maximum emission at 77K. The final term in the expression is referred to as the Coulombic stabilization energy of the charge separated state, where  $e$  is electronic charge,  $\epsilon$  solvent dielectric constant, and  $r$  is the distance separating donor and acceptor centers. In polar media, the Coulombic stabilization energy is typically less than 0.1 eV and is therefore usually neglected.

The Rehm-Weller equation<sup>144</sup> can be adapted to estimate the excited state oxidation and reduction potentials ( $E_{ox}^{0*}$  and  $E_{Red}^{0*}$ ):

$$E_{ox}^{0*} = E_{ox}^0 - E^{00} \quad (3.8)$$

$$E_{\text{Red}}^{0*} = E_{\text{Red}}^0 + E^{00} \quad (3.9)$$

where  $E^{\circ}_{\text{Ox}}$  and  $E^{\circ}_{\text{Red}}$  are the potentials associated with the first oxidation and reduction of the metal centre or polymer in the ground state. For the imidazole based polymer backbone the  $E^{00}$  value is 2.4 eV. As previously reported no polymer based oxidation process can be observed for potentials up to +1.400 V while the  $E^{\circ}_{\text{Red}}$  of the backbone has been shown to be -0.7 V. Therefore using Equation 3.7 the  $E^{\circ}_{\text{Ox}}$  for the polymer is estimated to be -1.0 V, ( $E^{\circ}_{\text{Ox}} = 1.4 - 2.4$  eV). For the ruthenium centers, solution phase cyclic voltammetry indicates that  $E^{\circ*}_{\text{Ox}}$  and  $E^{\circ*}_{\text{Red}}$  (metal based  $\text{Ru}^{2+/3+}$ ) are -0.8 and +0.8 respectively.

The thermodynamic driving force for electron transfer to the ruthenium centers can be estimated from:

$$\Delta G = E_{\text{Donor}} - E_{\text{Acceptor}} \quad (3.10)$$

Equation 3.10 reveals that electron transfer from the polymer excited state to the ruthenium is endergonic by at least 0.2 eV, ( $\Delta E = (-1.0 \text{ eV} - (-1.2 \text{ eV}))$ ). While electron transfer from the ruthenium metal to the polymer is exergonic by approximately 0.1V eV ( $\Delta E = (-0.8 \text{ eV} - (-0.7 \text{ eV}))$ ). Therefore, in contrast to the relatively efficient electron transfer that occurs in the ground state, excited state electron transfer from the polymer to the ruthenium centers is thermodynamically uphill, preventing energy transfer from occurring and resulting in the phenomena of dual emission.



#### ***3.3.2.4 Luminescence Lifetime Measurements.***

The luminescent lifetime can provide useful insights into the excited state interactions between the metal centre of the metallopolymer and the PPyBBIM backbone. The metallopolymer dissolved in solution exhibits a complex decay characterized by at least two time constants. This was expected due to the dual emission observed from the emission spectra, namely the PPyBBIM backbone and the ruthenium centre. Varying the metal loading of the metallopolymer was found to have little impact on the luminescent lifetime of the ruthenium-based emission of the metallopolymer. In each case the lifetime was calculated to be approximately ~210 ns, as shown in Table 3.4. Similarly the luminescent lifetime of the polymer backbone is also unaffected by the different metal loadings, remaining at ~35 ns for all 3 metallopolymer structures.

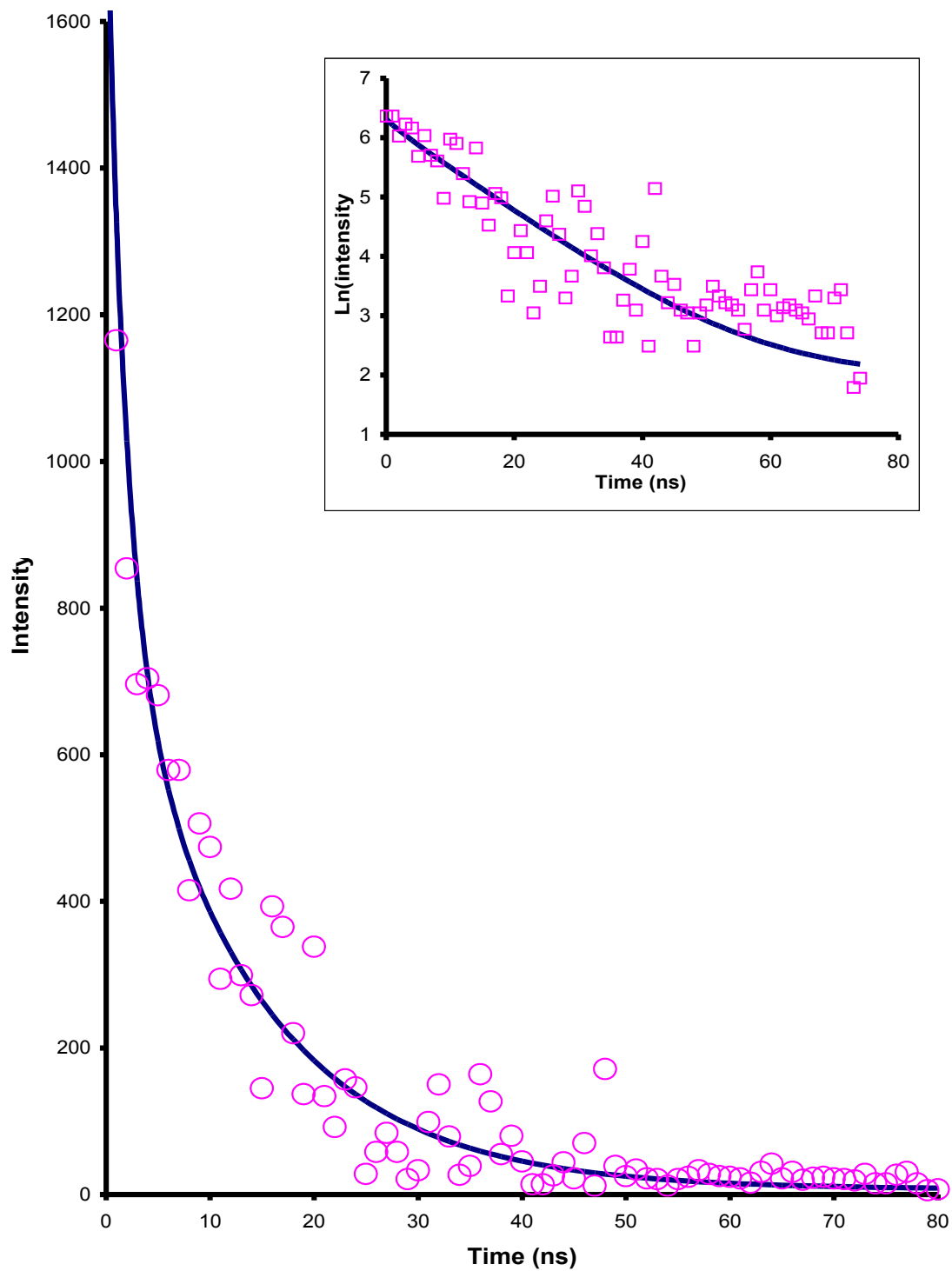


**Figure 3.11:** Emission decay for a 100 μM solution of [Ru(bpy)<sub>2</sub>(PPyBBIM)<sub>10</sub>]<sup>2+</sup> in acetonitrile following the application of a 10 ns laser pulse of 355 nm light.

**Table 3.4:** Metallopolymer luminescent lifetimes, 100 $\mu$ M solutions in MeCN

<b>Metal Loading</b>	<b>Ruthenium based emission (ns)</b>	<b>PPyBBIM based emission (ns)</b>
1/3	122 $\pm$ 11	33 $\pm$ 6
1/10	126 $\pm$ 21	36 $\pm$ 5
1/20	115 $\pm$ 13	32 $\pm$ 7

### 3.4 Conclusions

Poly[2-(2-pyridyl)-bibenzimidazole] containing ruthenium bis-bipyridyl complexes at controlled intersite separations offer the possibility of combining an electronic  $\pi$  conjugated polymer with highly luminescent metal centre. Photophysical and electrochemical measurements reveal significant differences in the extent of electronic communication in the ground and electronic excited states. Significantly, cyclic voltammetry reveals that the rate of homogeneous charge transport,  $D_{CT}$ , is approximately an order of magnitude higher than that previously reported for a non conjugated backbone. Significantly, electron transfer rather than ion or polymer chain movement appears to represent the rate determining step. Also, the magnitude of  $D_{CT}$  is directly related to the relative concentration of ruthenium metal centers within the film. This data suggests that the enhanced rates of charge transfer obtained by combining a PPyBBIM based conducting polymer with ruthenium is maximized if there is one metal unit per polymer monomer.

Significantly, the metallopolymers exhibit poor excited state communication with emission being observed from *both* the polymer backbone *and* the ruthenium centers. Given the extent of spectral overlap between the absorbance spectrum of the ruthenium centers and the polymer based emission it is surprising that dual emission is observed. This can be attributed to unfavourable thermodynamics as electron transfer from the polymer backbone to the ruthenium metal centres is thermodynamically uphill by at least 0.2 eV. In contrast electron transfer from the ruthenium excited state to the polymer backbone is possible. This would be favoured by high metal loadings and as such may be the reason why the maximum emission is observed at intermediate metal loadings. It is possible to exploit the differences in absorbance spectra of the polymer backbone and the ruthenium centers to selectively pump emission from the polymer backbone and the ruthenium centers. In conclusion, this work demonstrates that there is an

effective trade off between maximum charge transfer rates and maximum luminescence which must be considered if these metallopolymers are to be applied to electrochemiluminescent sensor design.

## *Chapter 4*

### *Electrochemical and Photophysical Studies of Ru-PMAS Composite Films.*

## 4.1 Introduction

As previously mentioned in Chapter 1 ruthenium bipyridyl complexes have many possible applications in areas such as solar energy conversion, photosynthesis, high speed display devices and DNA sensors.<sup>145,146,147,148,149</sup> The subsequent interaction of an inherently conducting polymer and a luminescent metal centre to produce novel materials has been an attractive approach to forming interfacial metallopolymer films. This approach is attractive since the  $\pi$  conjugated backbone can provide a rapid electron transfer pathway between the metal complex and the electrode. The ability of conjugated linkages to provide an effective pathway for the electron transfer between metal centers has been demonstrated in a number of polymeric systems. Zotti *et. al.* have shown that electron transfer rates between metal centers in polythiophenes with pendant ferrocene moieties are enhanced by up to an order of magnitude when a conjugated linkage is used.<sup>150</sup> Cameron *et. al.* have also shown that coordination of ruthenium moieties to a conjugated polybenzimidazole provides a rapid electron-transfer pathway by superexchange interactions between metal centers.<sup>151,152</sup> However, in Chapter 3 of this thesis it was demonstrated that this increased electron-transfer did not translate into enhanced luminescence of the ruthenium moiety.

Various synthetic approaches have been adopted to covalently attach various metal centres or complexes to conducting polymer backbones, the results of which have been widely reported. One approach to overcome many of the synthetic difficulties associated with covalent binding is to electrostatically isolate the luminescent metal within the conducting polymeric in a similar way to that used with Nafion. For example, this group have explored the electrochemical incorporation of a ruthenium metal centre by ion pairing with sulfonate groups of PMAS, poly(2-methoxyaniline-5-sulfonic acid).<sup>153</sup> These novel composites exhibited enhanced electronic communication between adjacent metal centres as well as modulated photophysical properties. The immobilisation of the positively charged ruthenium metal complex on an electrode surface revealed charge transfer diffusion coefficients an order of magnitude larger than that previously reported for metal centres covalently bound to non conjugated metallopolymers. This enhancement is most

likely due to mediated electron transport through the PMAS conjugated structure contrasting with the site to site electron hopping processes typically observed in non-conducting metallopolymers.

Sulfonated, self-doped, polyaniline has been extensively studied due to its unique electrochemical properties, water solubility, improved processability and potential industrial applications. PMAS is a fully sulfonated conducting polymer that has been synthesised by chemical and electrochemical polymerisation of 2-methoxyaniline 5-sulfonic acid, MAS. To date, these studies have focused on the electrochemical synthesis of PMAS in aqueous media. However, this type of synthesis has been found to produce a combination of two distinct polymer fractions with molecular weights of approximately 8 – 10 and 2 kDa respectively. By isolating these polymer fractions, their individual interactions with a ruthenium metal centre can be investigated.<sup>154</sup> The two fractions of PMAS show very distinct electrochemical and photochemical properties. The high molecular weight, HMWT PMAS, has a  $M_w$  of 8 – 10 kDa and was confirmed to be an emeraldine salt by its characteristic redox and pH switching behaviour. In contrast, the low molecular weight, LMWT PMAS, fraction is an oligomer with  $M_w$  of ca. 2 kDa and was shown to be electrochemically inert, but to exhibit intense photoluminescence. Previous studies have examined the differences between these two fractions in detail.<sup>154</sup>

In this chapter, we report on the individual influences of the two fractions of PMAS on the electrochemical and photophysical properties of a luminescent metal centre. Electrochemical measurements, charge transfer studies, steady state luminescence and measurements of luminescent lifetimes have been utilised to elucidate the influence of these fractions.

## ***4.2 Apparatus and Reagents***

### ***4.2.1 Apparatus***

Electrochemical measurements were performed using a CH Instruments Model 660 electrochemical analyzer. All electrochemical experiments were carried out using a 2 or 3 mm diameter platinum or glassy carbon working electrode in a conventional three-electrode assembly. Potentials are quoted versus Ag/AgCl and all measurements were made at room temperature. Absorbance and photo-luminescence were recorded using a Shimadzu UV-240 spectrophotometer and a JY Spex fluorescence spectrophotometer. Emission lifetime studies were made on a PicoQuant PDL-800B pulsed diode laser controller and FluoTime 100 time-correlated single photon counting system (TCSPC) with 280, 370 and 450nm pulsed laser sources with cut-on filters of 400, 475 and 530nm respectively. TCSPC analysis was performed using PicoQuant FluoFit software. Samples were deoxygenated for approximately 20 min with nitrogen prior to analysis. FTO conductive glass was obtained from Hartford Glass Co. Inc. (Hartford City, Indiana, USA) and was cut into 0.8 x 0.2 cm working electrodes. These electrodes were utilised for all spectrochemical analysis. Prior to use the working electrodes were rinsed with ethanol, and gradually heated to 400°C for 15 mins, then cleaned with household detergent in water, then deionised water, followed by acetone and finally deionised water. The electrodes were then dried completely under a flow of nitrogen gas and modified with the Ru-PMAS composite prior to use. Fluorescent Lifetime Imaging Microscopy was performed using a Carl Zeiss LSM 510 and PicoQuant fitting software. For LSM studies an excitation wavelength of 457 nm was used and for Lifetime calculations the excitation wavelength was 458 nm.

#### **4.2.2 Materials and Reagents**

$[\text{Ru}(\text{bpy})_3]^{2+}$  was purchased from Sigma Aldrich as its chloride salt and used as received. PMAS emeraldine salt was prepared via the chemical synthesis method.<sup>155</sup> 2-Methoxyaniline-5-sulfonic acid (MAS) was provided by Mitsubishi Rayon, Japan and purified by acid base crystallization before polymerisation. It was then fractionated by cross-flow dialysis.<sup>154</sup> The two pure fractions are labelled high molecular weight (HMWT) PMAS (8-10 kDa) and low molecular weight (LMWT) PMAS of (2kDa). MAS was provided by Mitsubishi Rayon, Japan and purified by acid base crystallisation before polymerisation. All other reagents used were of analytical grade and all solutions were prepared in milli-Q water.

#### **4.2.3 Composite Formation.**

Composite solutions containing equal amounts of  $[\text{Ru}(\text{bpy})_3]^{2+}$  (w/w) and either HMWT or LMWT PMAS in ethanol were prepared. Where appropriate, working electrodes were modified by applying a drop ( $\approx 15 \mu\text{L}$ ) of an aqueous solution of the composite to the electrode surface (0.1 - 1.0 % depending on desired surface coverage) that was allowed to dry in the dark for 24 to 36 hours. Films were deposited onto glassy carbon working electrodes. These modified electrodes were then washed (Milli-Q water) and allowed to dry overnight prior to analysis. Good film coverage was achieved for each composite with the Ru-LMWT composite displaying slightly better uniform coverage. An optical image of each of the composites can be seen in Figure 4.2. Post synthesis characterisation was performed in ACN containing 0.1 M TBABF<sub>4</sub> electrolyte unless otherwise stated. Surface coverage of the composite films,  $\Gamma$ , were determined by graphical integration of background corrected cyclic voltammograms ( $< 5 \text{ mV s}^{-1}$ ). The ruthenium surface coverage's were approximately  $7 \pm 2 \times 10^{-8} \text{ mol cm}^{-2}$  unless otherwise stated.

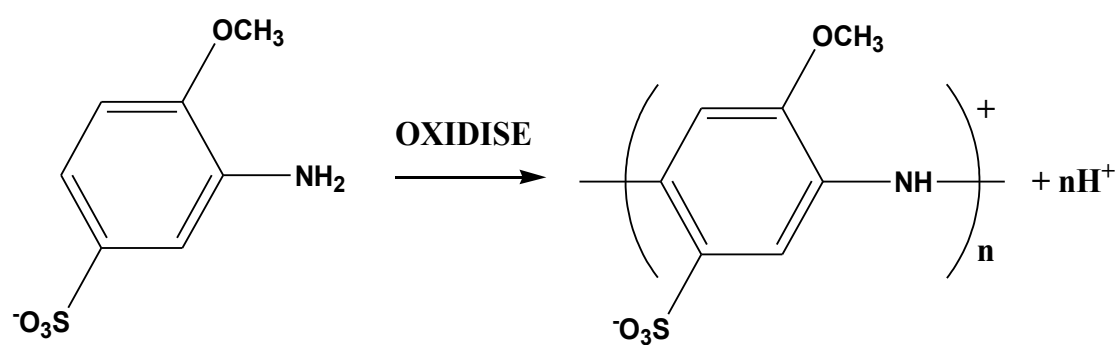


*Figure 4.1* Polymerisation of poly 2-Methoxyaniline-5-sulfonic acid (MAS)

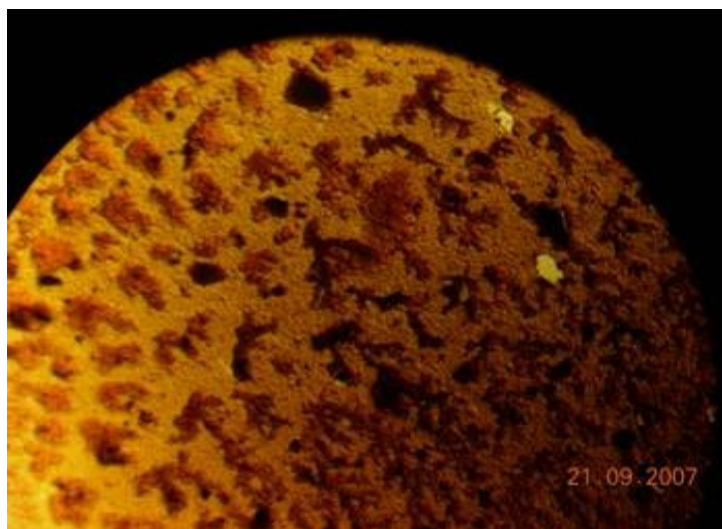


**Figure 4.2:** *Optical image of Ru-LMWT PMAS (top) and Ru-HMWT PMAS composite films.*

### ***4.3 Results and Discussion***

#### ***4.3.1 Electrochemical properties of the novel [Ru(bpy)<sub>3</sub>]<sup>2+</sup>-PMAS Composite films.***

We have previously reported on the voltammetric behavior of all fractions of PMAS, used within this investigation, and on thin films containing ruthenium moieties. The electrochemical behavior of the composite films was investigated and showed numerous similarities. Figure 4.3 illustrates the typical background corrected cyclic voltammograms obtained for composite films containing Ru-HMWT PMAS and Ru-LMWT PMAS composite films vs. Ag/AgCl. Surface coverages were calculated by graphical integration of background corrected cyclic voltammograms ( $< 5 \text{ mV s}^{-1}$ ) and were typically varied from  $4.1 \pm 1.0 \times 10^{-8}$  to  $6.9 \pm 1.2 \times 10^{-8} \text{ mol cm}^{-2}$ . The voltammograms exhibit a number of features characteristics of surface bound redox sites;<sup>156</sup> namely, the peak to peak separation between the anodic and cathodic waves is close to zero, also, the full width at half-maximum (FWHM) is close to the theoretical value of 90.6 mV expected for a reaction involving the transfer of a single electron. This also suggests that the system is chemically reversible for the ruthenium moiety. The anodic and cathodic peaks corresponding typical of a  $\text{Ru}^{2+/3+}$  couple are visible in all the voltammograms at approximately 1050 mV.<sup>157</sup> The Ru-HMWT PMAS composite shows anodic and cathodic peaks, which are attributed to different oxidation states of PMAS. The anodic peaks and the corresponding cathodic peaks can be attributed to leucoemeraldine, emeraldine and pernigraniline respectively.<sup>158</sup> The impact of doping the films with ruthenium moieties did not seem to impact on these peaks. The LMWT PMAS is electrochemically inactive, however upon addition of the ruthenium metal centers, there does seem to be a slight pre-peak at  $\sim 850\text{mV}$ .

Surface coverages for the RuLMWT film were very good, however, as can be seen from Figure 4.2 shows that the RuHMWT film did not produce a homogeneous film on the electrode surface and the resultant film was not as stable as the others investigated.

The ruthenium peak current of these composite films varies linearly with scan rate,  $v$ , up to  $30 \text{ mVs}^{-1}$  indicating that the response is controlled by finite charge transport diffusion on these long timescales. At shorter experimental timescales, i.e., at scan rates above  $100 \text{ mVs}^{-1}$ , the thickness of the depletion layer is smaller than the film thickness and the peak current varies linearly with the square root of scan rate. This observation is similar to the electron transport of a  $[\text{Ru}(\text{bpy})_2(\text{PVP})_{10}]^{2+}$  film we have previously investigated suggesting semi-infinite diffusional charge transport through the film.<sup>159</sup> For all scan rates, the ratio of the anodic to cathodic ruthenium peak currents is unity indicative of reversible electron transfer. Taken together, these results indicate that the voltammetric behavior of these composite films is close to ideal over a wide range of scan rates.

Given the conducting nature of the HMWT PMAS the possibility of excited state electron transfer from the ruthenium excited state to acceptor states on the HMWT PMAS polymer exists. As can be seen from Figure 4.3 the HMWT PMAS displays ground state oxidation and reduction peaks at approximately  $0.5\text{V}$  and  $0.4 \text{ V}$  respectively. Given that the  $E^{o*}_{\text{ox}}$  for ruthenium is  $-0.8 \text{ V}$  as demonstrated in Chapter 3 allows the driving force to be calculated. Using Equation 4.1 the driving force for excited state electron transfer from the ruthenium to the HMWT polymer can be calculated as  $-0.4 \text{ V}$  ( $\Delta E = -0.8 - (-0.4)$ ). Therefore deactivation of the ruthenium excited state via electron transfer to acceptor states on the HMWT PMAS polymer is thermodynamically feasible. The effect of this on the excited state luminescence of the composites is examined in section 4.3.2.

$$\Delta G = E_{\text{Donor}} - E_{\text{Acceptor}} \quad (4.1)$$

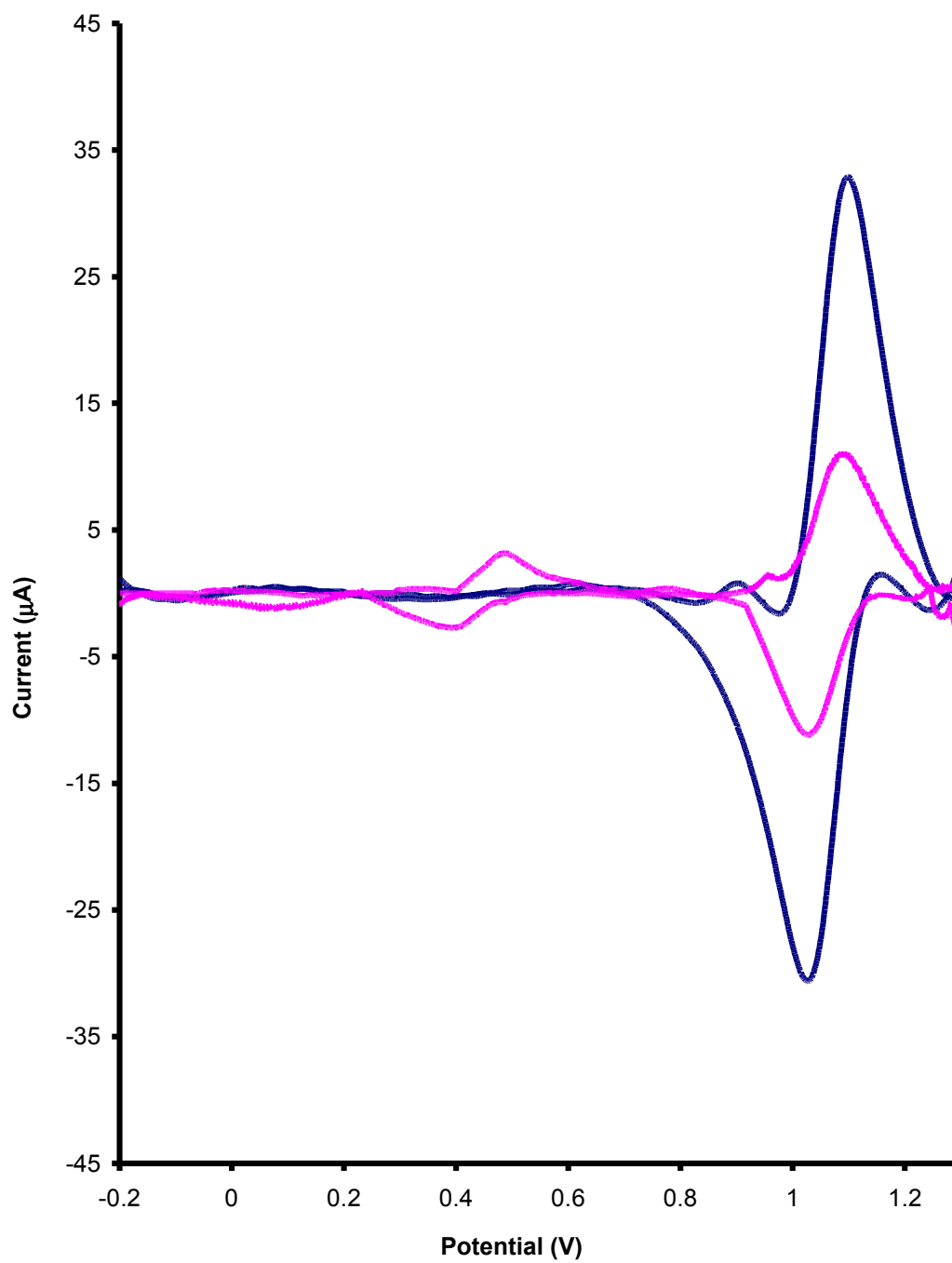


**Figure 4.3:** Cyclic voltammetric response of Ru-HMWT (pink) and Ru-LMWT (blue) PMAS composite films in ACN with 0.1M TBABF<sub>4</sub> electrolyte. Scan rate 0.1Vs<sup>-1</sup>.

$\Gamma = 3.1 \times 10^{-9}$  and  $6.9 \times 10^{-9}$  mol cm<sup>-2</sup> respectively.

#### ***4.3.2 Effect of Scan rate on Electron Transfer***

The sensitivity of an ECL sensor is ultimately dictated by the rate at which the Ru<sup>3+</sup> sites can be regenerated within the film. Therefore, the electronic communication between the ruthenium centers in these composites is of major importance. For example the ruthenium metal centers may communicate through the conducting polymer, which in turn would enhance electron transport in the film.

Electron transport in redox polymers has been shown to occur by at least three mechanisms.<sup>160</sup> Where the polymer backbone is non conducting, outer-sphere electron exchange between redox sites (outer-sphere mechanism) provides the only significant contribution to electron transport.<sup>161,162</sup> In unsaturated systems, and particularly in highly conjugated systems, electron transport can also occur through the polymer backbone by mediated and/or superexchange mechanisms.<sup>163</sup> These are distinguished by the availability of redox states of suitable energy on the polymer to mediate electron transport. If such states are available, the electron can hop between a localized metal-based redox site, a polymer-based site, and a second metal site in two steps (mediated mechanism). If these states are not accessible, then electron transfer through the backbone must result from a mixing of appropriate orbitals of both metals with the HOMO and/or LUMO of the backbone (superexchange). Although in these systems the ruthenium complex is not covalently bound to the PMAS polymer the composite films may show similarities with these electron transfer mechanisms.

As reported previously, the rate of charge transport through a film can be quantified by measuring the charge transfer diffusion coefficient ( $D_{CT}$ ), for the film, using cyclic voltammetry.<sup>164,165</sup> When compared to non conjugated metallopolymers the diffusion coefficient calculated for the ruthenium redox couple for the Ru-PMAS composites

was faster an order of magnitude. As can be seen from Table 4.1 the Ru-HMWT composite films displayed the fastest  $D_{CT}$ . Consistent with an electrochemically reversible reaction involving a surface confined reactant; the  $i_p$  values varied linearly with the square root of scan rate over the  $100 \leq v \leq 500 \text{ mVs}^{-1}$ , as can be seen for the Ru-HMWT composite film in Figure 4.4. This suggests enhanced long-range electronic communication between the ruthenium centers through the PMAS. Such long-range interactions between metal centers will certainly be a crucial feature of future electrocatalytic and electronic materials.

*Table 4.1: Diffusion Coefficients and  $E^0$  values for Ru-PMAS composite films*

<b>Composite Film</b>	<b><math>D_{CT}</math> (<math>\text{cm}^2\text{s}^{-1}</math>)</b>	<b><math>E^0</math> <math>\text{Ru}^{2+}/\text{Ru}^{3+}</math> (V)</b>
<b>Ru-HMWT</b>	$1.44 \pm 0.2 \times 10^{-10}$	1.145
<b>Ru-LMWT</b>	$3.59 \pm 0.5 \times 10^{-10}$	1.161

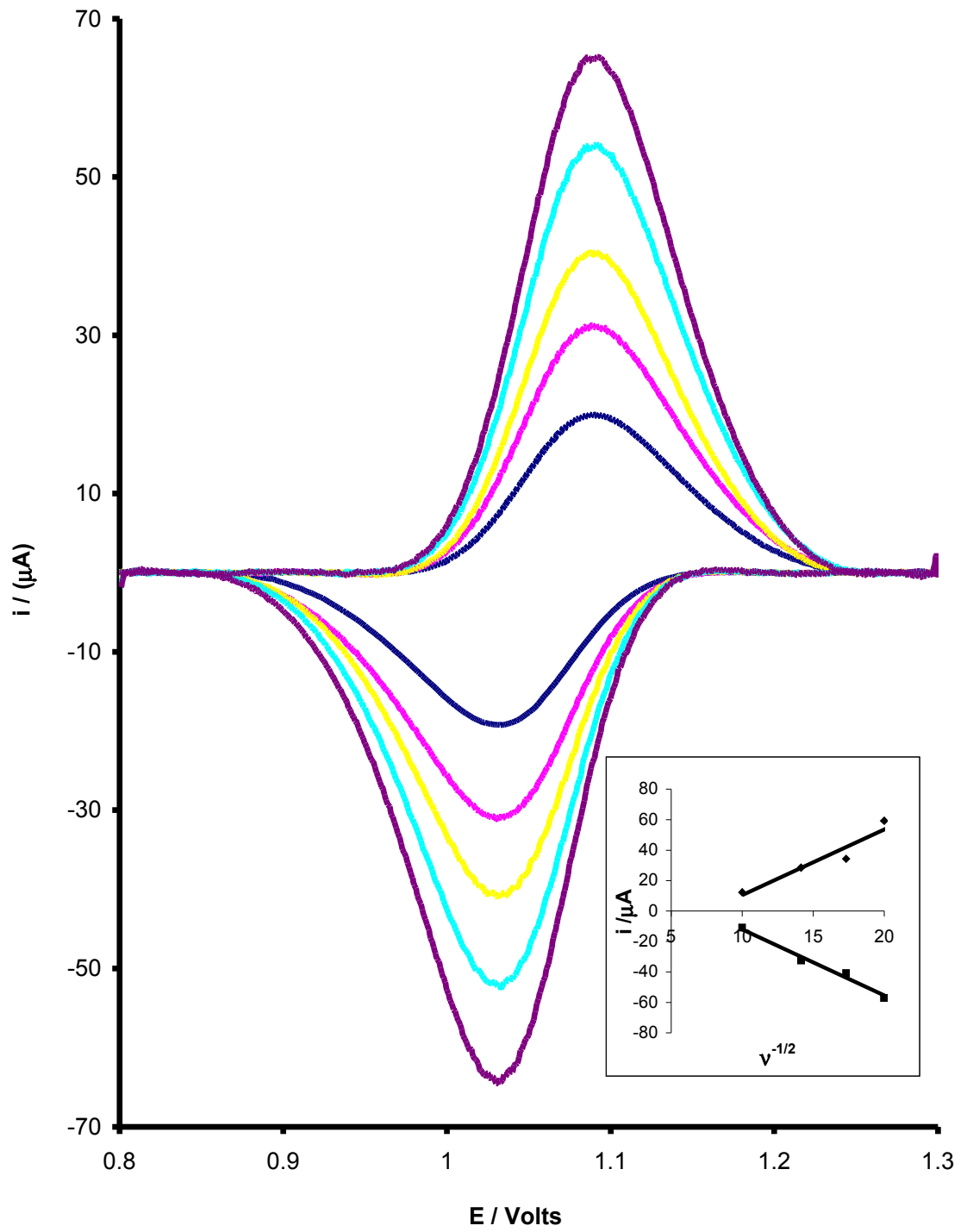


**Figure 4.4:** Background corrected cyclic voltamogram of thin films of Ru-LMWT in dry ACN containing 0.1M TBABF<sub>4</sub>.  $100 \geq v \geq 500 \text{ mVs}^{-1}$ . Insert shows plot of peak current (cathodic and anodic branches) versus  $v^{1/2}$  of this data.  $\Gamma = 6.9 \times 10^{-9} \text{ mol cm}^{-2}$

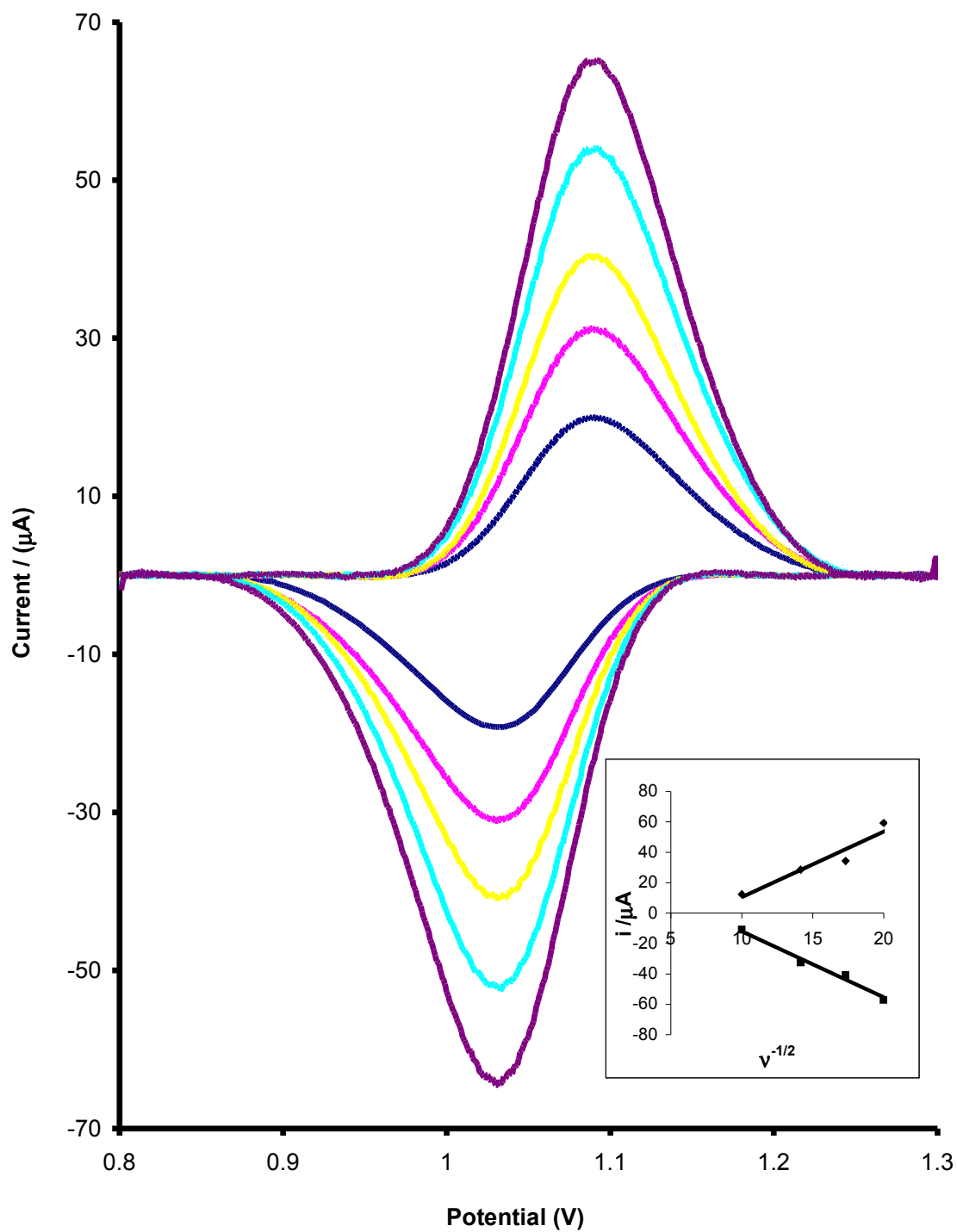


**Figure 4.5:** Background corrected cyclic voltamogram of thin films of Ru-LMWT in dry ACN containing 0.1M TBABF<sub>4</sub>.  $100 \geq v \geq 500 \text{ mVs}^{-1}$ . Insert shows plot of peak current (cathodic and anodic branches) versus  $v^{1/2}$  of this data.  $\Gamma = 6.9 \times 10^{-9} \text{ mol cm}^{-2}$

### 4.3.3 Steady state luminescence of Ru-PMAS Composite Films.

As previously detailed in chapter 2 both fractions of PMAS display significantly different electrochemical and photophysical properties with the LMWT PMAS fraction displaying significantly more luminescence with excited with a 355nm laser pulse. Previous emission studies on Ru-PMAS composites were carried out on an electrochemically grown composite film. UV-Vis spectral studies showed these films to contain approximately 70 % w/v HMWT PMAS and 30 % w/v LMWT PMAS. This type of film resulted in a reduced ruthenium based luminescence when compared to films containing a non-conducting polymer, such as PVP, poly(4-vinylpyridine), when excited at 355 nm. To further elucidate the effect of each specific PMAS fraction on the ruthenium based emission composite films were prepared on clean FDTO electrodes and the emission response for each composite following excitation at 355 nm. When the emission intensities are matched by absorption matching at 355 nm as can be seen from Figure 4.6 the emission response for the Ru-LMWT fraction is significantly higher than that of the Ru-HMWT fraction. This lower ruthenium emission in the HMWT system may be due to two factors, firstly as previously demonstrated the HMWT polymer provides a number of acceptor states for electron transfer from the excited  $[\text{Ru}(\text{bpy})_3]^{2+}$ . While this provides a mechanism of excited state electron transfer it also serves to deactivate the ruthenium excited state by providing an alternative pathway to radiative emission. Secondly as can be seen from Figure 4.7 both  $[\text{Ru}(\text{bpy})_3]^{2+}$  and HMWT PMAS absorb at 355 nm creating a competitive effect for the absorption of light. Comparing the absorption intensities of both PMAS fractions at 355 nm (Figure 2.15, Chapter 2) it can be seen that the HMWT PMAS absorbs more light than the LMWT PMAS and as such the same competing effect is not seen for the Ru-LMWT PMAS composite.



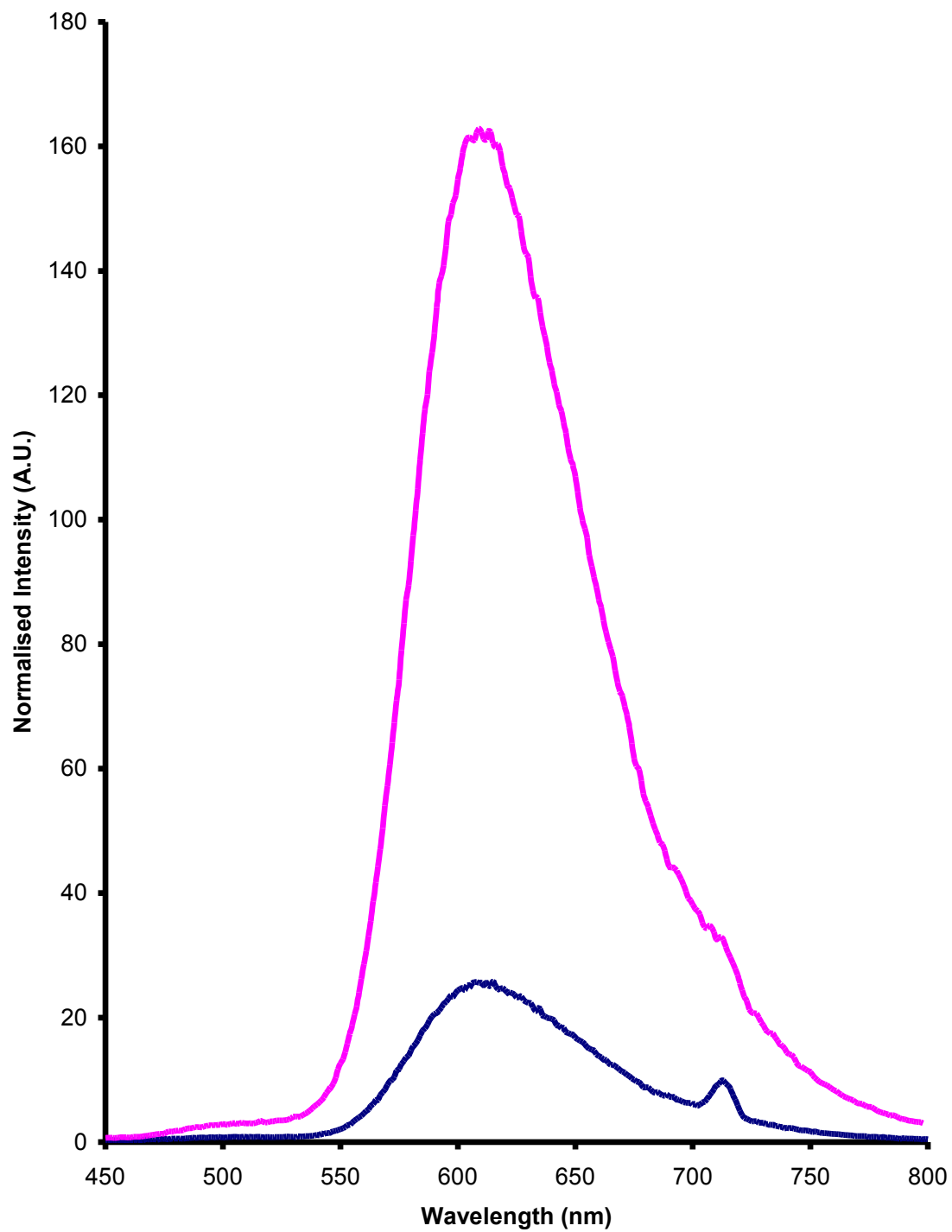


*Figure 4.6: Emission obtained for thin films of Ru-LMWT PMAS (pink) and Ru-HMWT PMAS (blue) composite films using an excitation wavelength of 355 nm.*

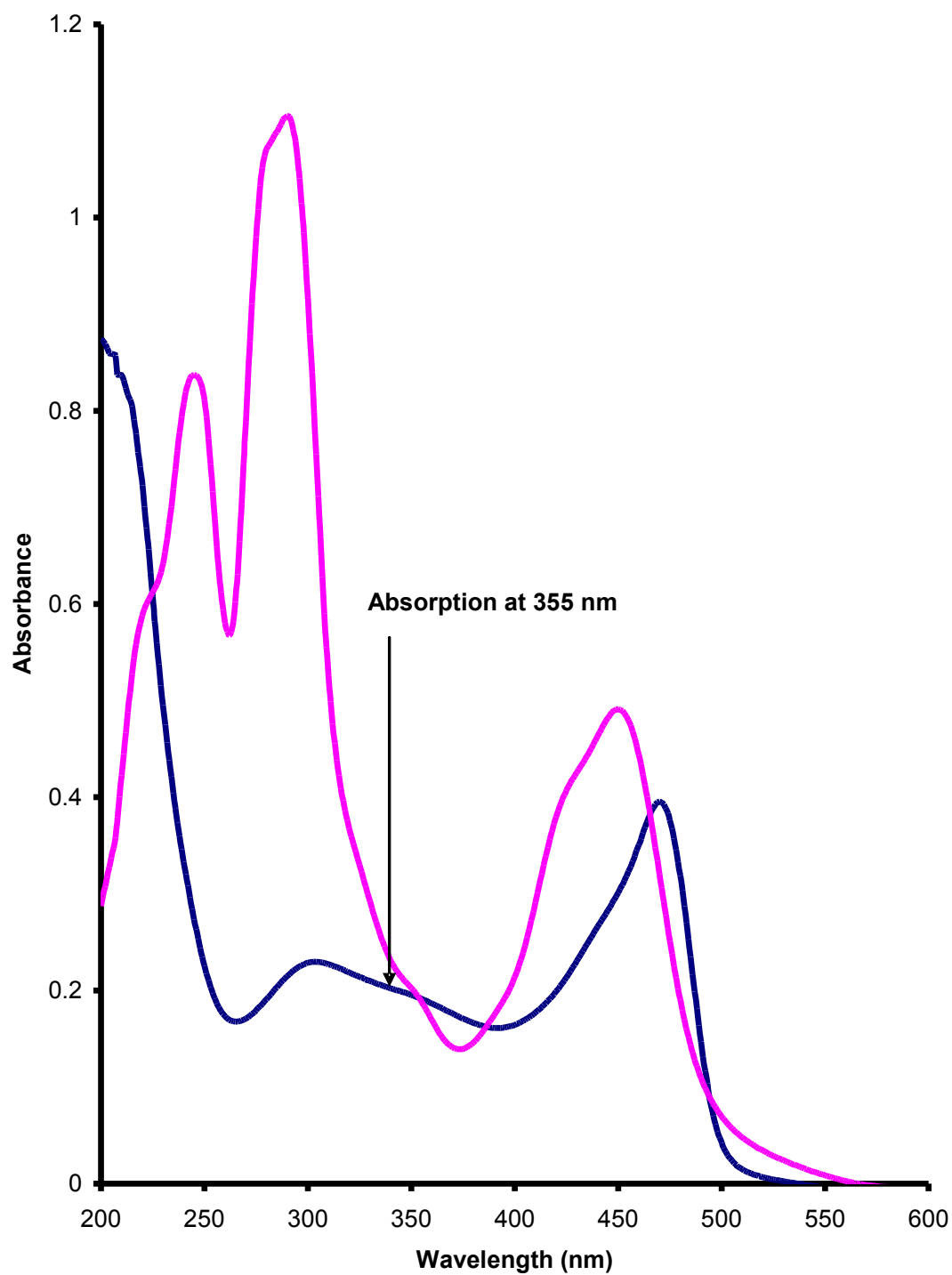


*Figure 4.7: UV absorbance spectrum of HMWT PMAS (blue) and  $[Ru(bpy)_3]^{2+}$  (pink) in ACN Solution concentrations have been adjusted to show overlap at 355 nm*

#### 4.3.4 Solution phase Quenching Studies

Much work has been published on the quenching of ruthenium by both osmium containing bipyridyl complexes and non conjugated metallopolymers.<sup>166,167,168,169,170,171</sup> As observed in the previous section significantly higher emission was observed from the Ru-LMWT PMAS composite film than that of the Ru-HMWT composite film despite both composites containing equal amounts of  $[\text{Ru}(\text{bpy})_3]^{2+}$ . To investigate if this observed emission existed solely in the solid phase a series of solution phase quenching studies were carried out. The process of quenching may arise from a number of different processes. For example, 'dynamic' quenching involves a collisional encounter between the quencher and the excited state and the lifetime and intensity of the emission both decreased. Alternatively, 'static' quenching arises where an interaction between the fluorophore and quencher exists in the ground state. Pure static quenching can be identified since it reduces the luminescence intensity but does not generally decrease the measured lifetime of emission. Dynamic quenching can be modelled using the Stern-Volmer equation;

$$I_0/I = \tau_0/\tau = 1 + k_q\tau_0 [Q] \quad (2)$$

where  $I_0$  and  $I$  are the luminescence intensities in the absence and presence of quencher respectively,  $k_q$  is the collision quenching rate,  $\tau_0$  is the luminescence lifetime without any quencher present, and  $[Q]$  is the concentration of the quencher, PMAS. It is important to note that the emission intensities must be corrected for the absorbance of the quencher at the exciting wavelength and therefore absorbance corrections were made using standard procedures.<sup>172,173</sup> If the fluorophore can form a stable complex with a quenching molecule, the resultant ground state of the fluorophore-quencher complex is said to be statically quenched. In this case, the Stern-Volmer equation is modified, where  $k_q\tau_0$  can be substituted by  $K_{SV}$ , is the Stern-Volmer constant.

The effect of adding each PMAS fraction to 100  $\mu\text{M}$  of  $[\text{Ru}(\text{bpy})_3]^{2+}$  can be seen in Figure 4.8 and 4.9. Figure 4.10 shows the Stern-Volmer plot for the quenching of  $[\text{Ru}(\text{bpy})_3]^{2+}$  by PMAS. This plot indicates that HMWT PMAS effectively quenches the ruthenium-based emission most likely via deactivation of the excited state by acceptor sites on the polymer backbone or by competing with  $[\text{Ru}(\text{bpy})_3]^{2+}$  or by a combination of both. This quenching also highlights some of the rationale for poor luminescence previously observed for the previously reported electrochemically grown Ru-PMAS composite films, which as stated above contained approximately 70 % w/v HMWT PMAS. Figure 4.8 also illustrates the influence of LMWT PMAS on the luminescence of  $[\text{Ru}(\text{bpy})_3]^{2+}$ . In sharp contrast to HMWT PMAS, the LMWT fraction resulted in an enhanced ruthenium based emission. As can be seen from the spectral overlap in Figure 4.11 this enhancement is most likely due to an electron transfer from the emissive LMWT PMAS fraction to the ruthenium metal centre. In effect, the  $[\text{Ru}(\text{bpy})_3]^{2+}$  is quenching the LMWT PMAS emission and the energy transfer from the LMWT PMAS results in an enhancement of the ruthenium emission.

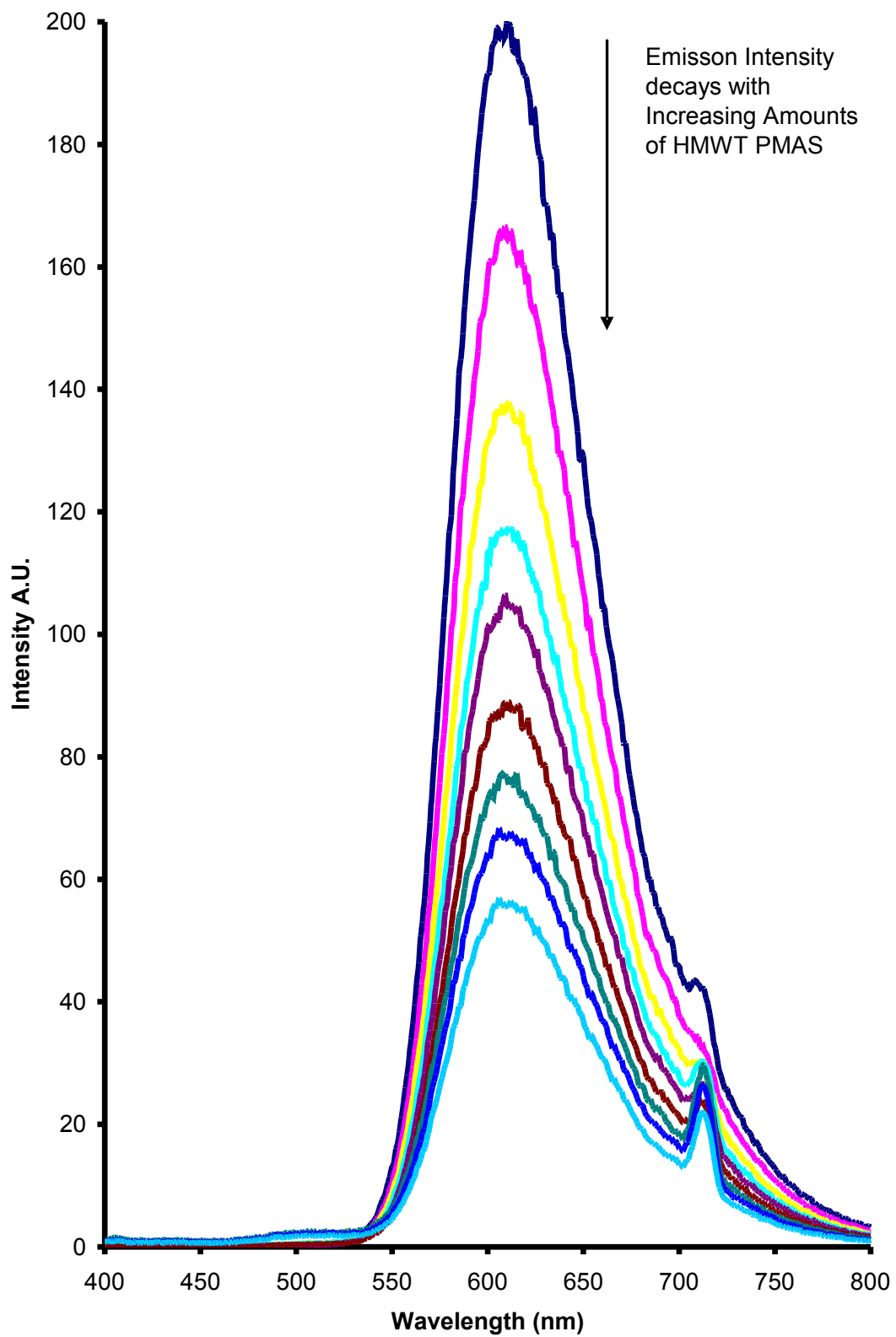


**Figure 4.8:** Effect of addition of HMWT PMAS to 100  $\mu\text{M}$   $[\text{Ru}(\text{bpy})_3]^{2+}$  in dH2O

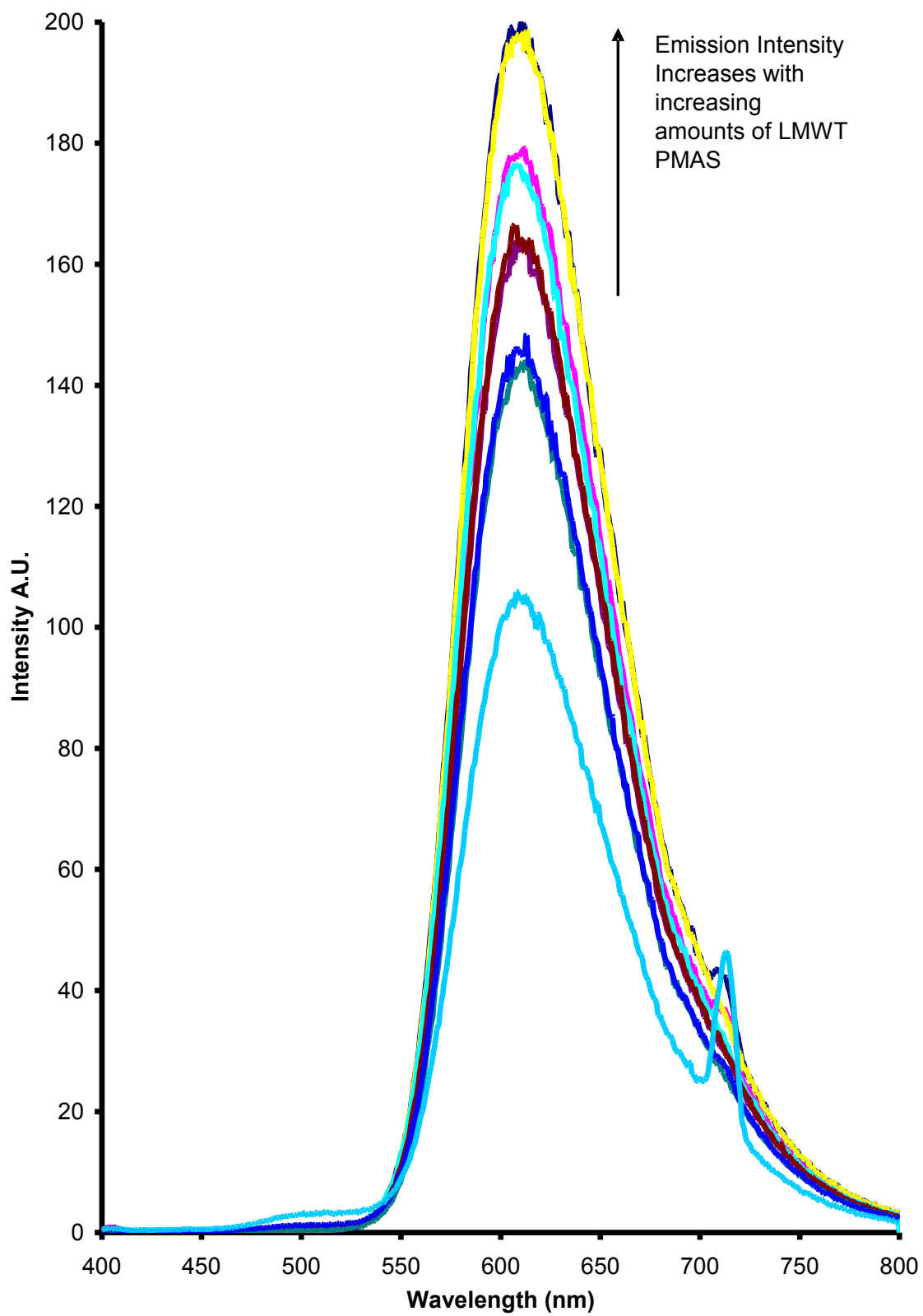


**Figure 4.9:** Effect of addition of LMWT PMAS to 100  $\mu\text{M}$   $[\text{Ru}(\text{bpy})_3]^{2+}$ .

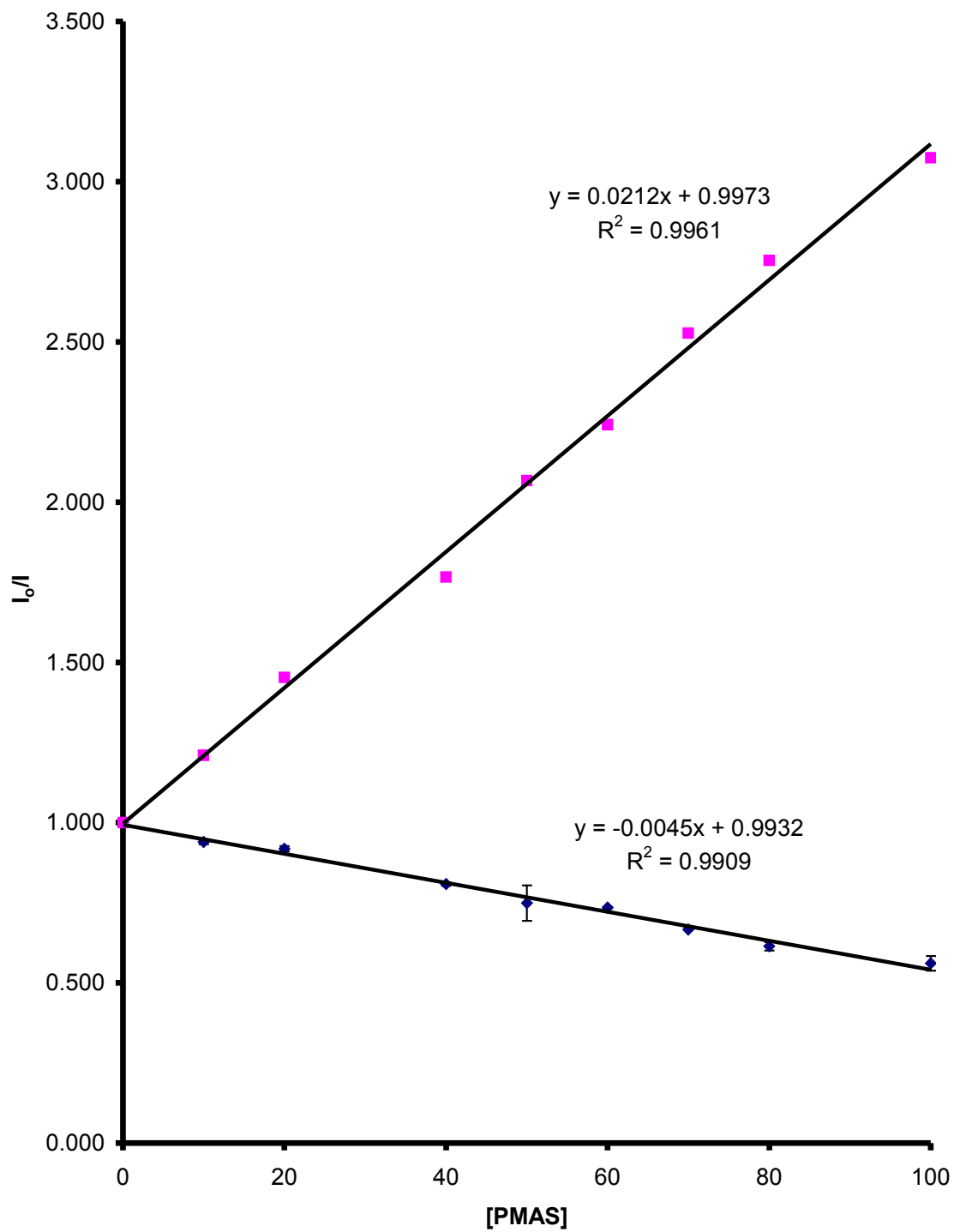


**Figure 4.10:** Stern Volmer Plot of  $I_0/I$  vs. Increasing  $[PMAS]$  HMWT PMAS indicate by pink dots.

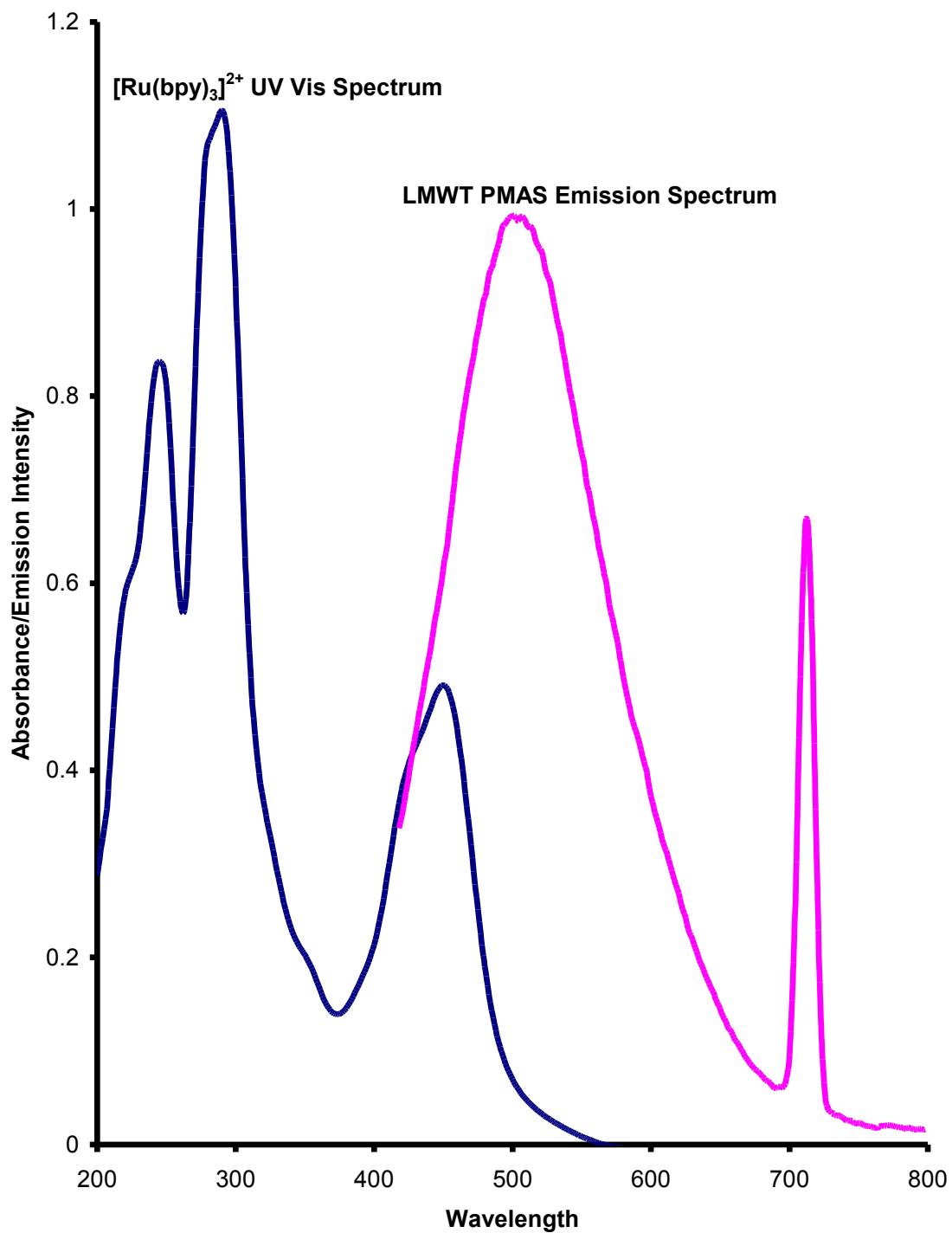


**Figure 4.11:** *Overlap of LMWT PMAS Emission (pink) with UV Visible spectrum of [Ru(bpy)<sub>3</sub>]<sup>2+</sup> (blue). Relative intensities have been altered to show overlap.*

#### ***4.3.5 Luminescent Lifetime Measurements of Ru-PMAS Composite Films***

The luminescent lifetime can provide useful insights into the mechanism of excited state energy transfer between the metal centre and the quencher. A time-correlated single photon counting (TCSPC) system was employed using a 370 nm pulsed laser sources. Typical TCSPC responses for Ru-HMWT PMAS and Ru-LMWT PMAS are shown in Figure 4.11. The TCSPC responses in each case were collected to the same photon count intensity, (10000 counts). Emission responses were analysed using PicoQuant FluoFit software employing a fitting function containing two time constants.

Like previously reported results for an electrochemically synthesised ruthenium PMAS composite film these lifetimes exhibit a complex decay characterized by at least two time constants whereby a double exponential fits adequately describe the experimental responses. . For both Ru-HMWT and Ru-LMWT films the lifetime obtained was lower than that expected for a solution containing only  $[\text{Ru}(\text{bpy})_3]^{2+}$ . The luminescent decay of the Ru-HMWT PMAS film is characterized by long and short lived components that have lifetimes of  $46 \pm 5$  ns (population fraction 0.8) and  $5 \pm 0.2$  ns (population fraction 0.2), respectively. The biexponential behavior may arise from different microenvironments within the film, e.g., poorly solvated or cross-linked chains that increase the rigidity of the complex and decrease the rate of vibrational relaxation. Examination of the lifetimes at low temperature should provide more insight into the exact origin of each of the decays. However given the electrochemical activity of the HMWT PMAS fraction it is expected to be a greater quencher of the  $[\text{Ru}(\text{bpy})_3]^{2+}$  luminescent lifetime than the LMWT PMAS. To investigate this effect the lifetime of the dominant component in the film was measured with varying degrees of HMWT PMAS.

The lifetime of the dominant component in the presence of quencher is taken as  $\tau$ . The data presented in Figures 4.10 and 4.13 clearly indicate that the presence of

HMWT PMAS causes both the luminescence intensity and lifetime to decrease, which suggests an influence from dynamic quenching. A typical Stern-Volmer plot for luminescence lifetime,  $\tau_0/\tau$  versus  $[Q]$  is shown in Figure 4.13. When luminescence quenching occurs solely by dynamic quenching the slopes of plots of  $I_0/I$  and  $\tau_0/\tau$  should be identical and the Stern-Volmer constant,  $K_{SV}$ , is equal to  $k_q$ . Figure 4.10 and 4.13 show that the slopes of the  $\tau_0/\tau$  and Stern-Volmer plots are 0.0136 and 0.0212, respectively. The fact that these slopes differ from one another indicates that while dynamic quenching occurs in this system to an extent it does not fully account for the decrease in ruthenium emission observed in the presence of the HMWT PMAS fraction. Therefore, it appears that some of the luminophores can physically move within the lifetime of the excited state, giving rise to a dynamic quenching contribution but that static quenching represents the most significant quenching mechanism.

As can be seen from the Stern Volmer Plot in Figure 4.13 the luminescence lifetime of the Ruthenium component of the Ru-LMWT PMAS composite is not as sensitive to LMWT PMAS concentration as it is to increasing amounts of HMWT PMAS. The luminescent decay of the Ru-LMWT PMAS composite film is also characterized by short and long lived components that have lifetimes of  $427 \pm 15$  ns (population fraction 0.7) and  $36 \pm 5$  ns (population fraction 0.3), respectively and display only minor variations upon increasing the concentration of the LMWT PMAS within the composite film while maintaining the Ru concentration. The large lifetime obtained for the Ru-LMWT PMAS composite with that of the Ru-HMWT is consistent with previous studies showing that the LMWT PMAS was chemically inert and therefore is not as strong a quencher as the HMWT PMAS. The LMWT PMAS may also serve to better encapsulate the  $[\text{Ru}(\text{bpy})_3]^{2+}$  thereby preventing quenching from atmospheric oxygen. While the HMWT PMAS may also encapsulate the  $[\text{Ru}(\text{bpy})_3]^{2+}$  in the film thereby protecting it from atmospheric oxygen this effect is negated by its greater quenching properties. Although the LMWT PMAS enhances the emission of the ruthenium metal centre it does not significantly influence the excited state lifetime.

Alternatively the presence of a decay in both films of approximately 40 ns may be due to LMWT PMAS as it has previously been reported that the HMWT PMAS does not emit luminescence and that any luminescence observed is due to trace amounts of the LMWT PMAS fraction in the mixture, however further analysis of populations at increasing concentrations of both HMWT and LMWT PMAS would be required to confirm this.

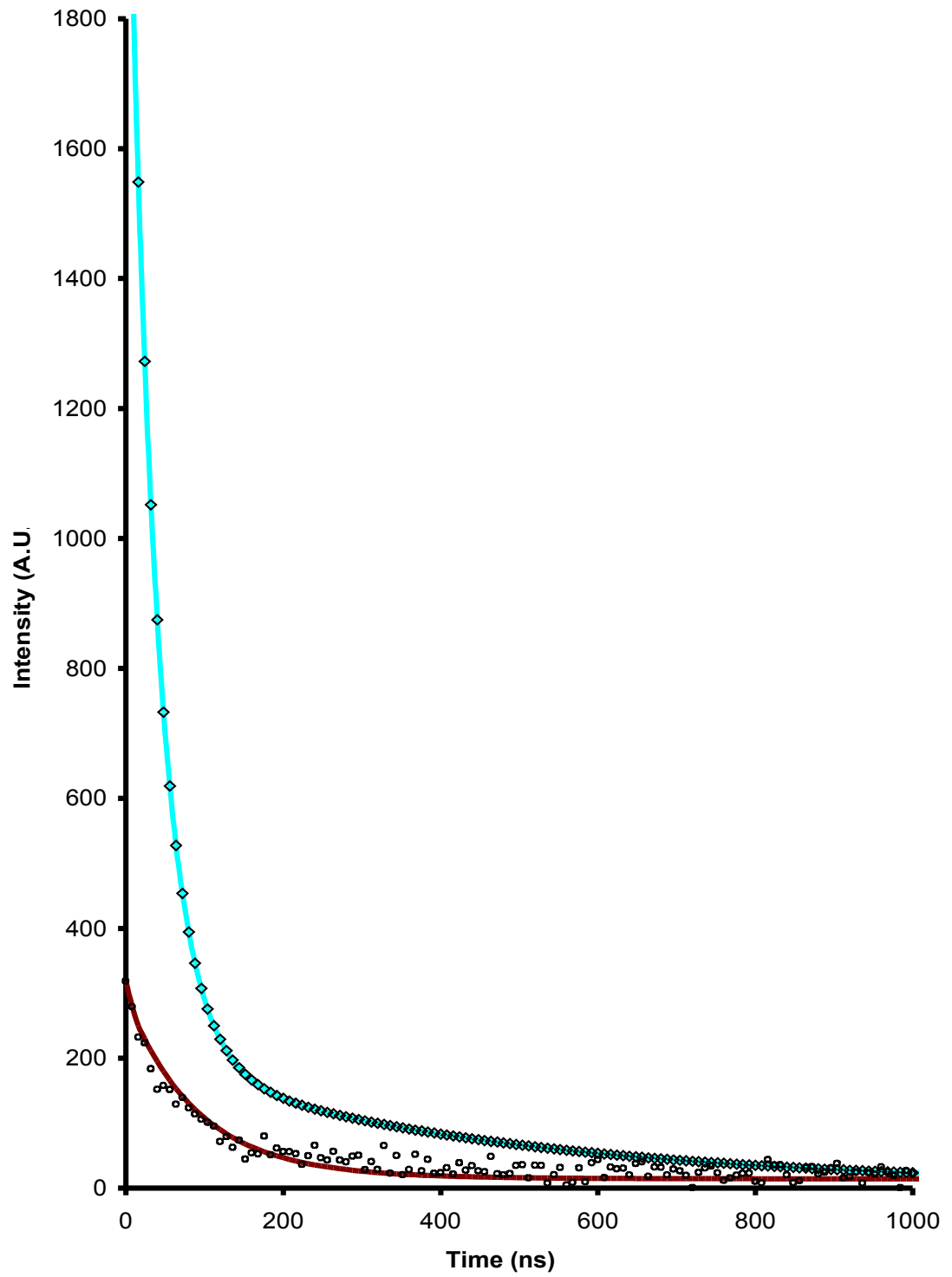


*Figure 4.12: Luminescent Lifetime decays for Ru-LMWT PMAS (blue) and Ru-HMWT PMAS (brown) composite films*

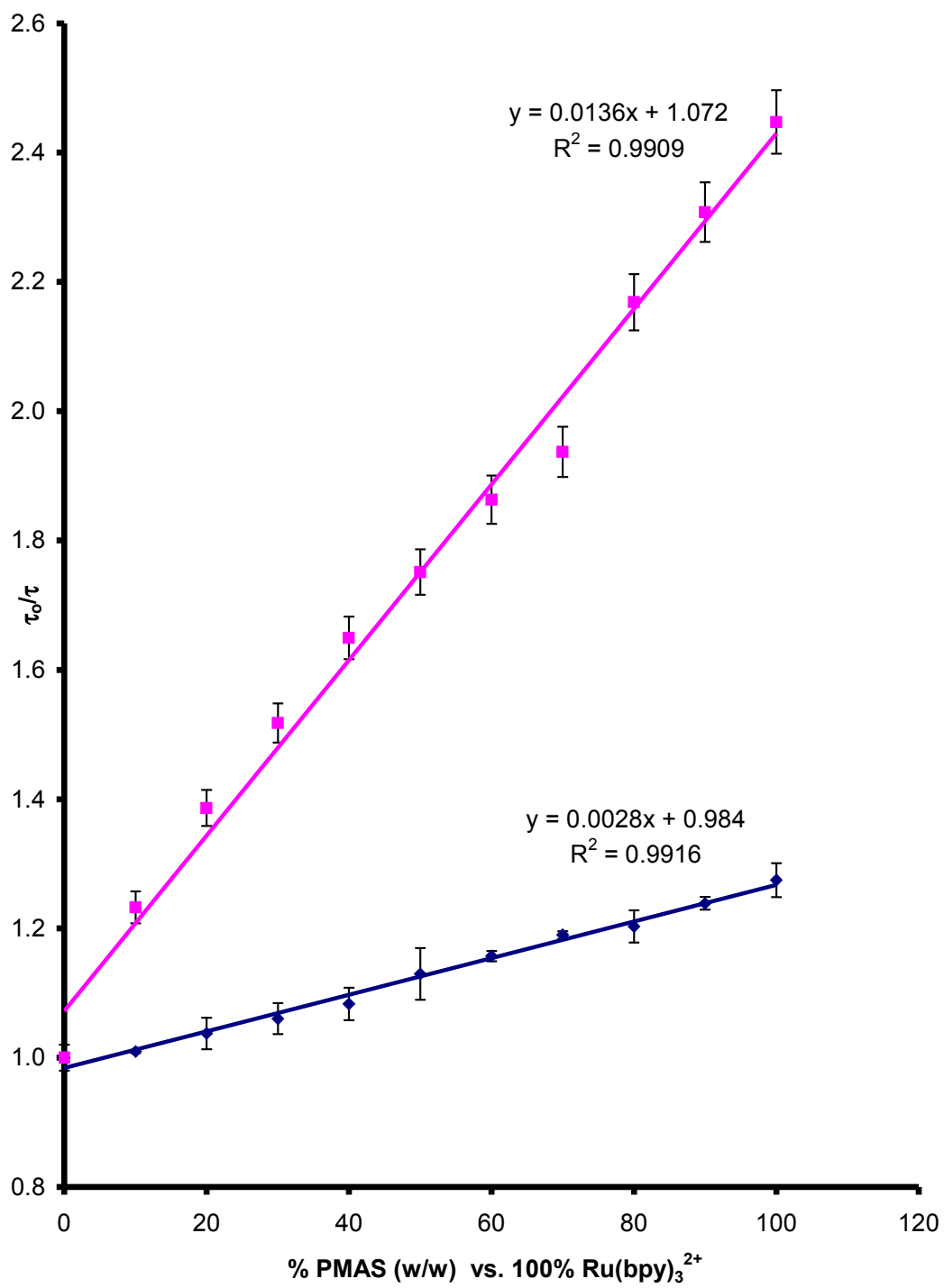


**Figure 4.13:** Stern Volmer Plot of  $\tau_0/\tau$  vs. Increasing [PMAS]. Ru-HMWT PMAS (pink), Ru-LMWT PMAS (blue). All solutions  $d\text{H}_2\text{O}$

#### ***4.3.6 Fluorescent Lifetime Imaging Microscopy of Ru-PMAS Composite Films***

Since its introduction in the early 90s Fluorescent Lifetime Imaging Microscopy has initiated a breakthrough in biomedical imaging.<sup>174,175,176,177,178</sup> The applicability of multi-photon excitation, the optical sectioning capability and the superior contrast of these instruments make them an ideal choice for fluorescence imaging of both biological, organic and inorganic samples. A significant advantage of this form of microscopy lies in the fact that the fluorescence of molecules is not only characterised by the emission spectrum but it has also a characteristic lifetime. Any energy transfer between an excited molecule and its environment in a predictable way changes the emission lifetime. Since the lifetime does not depend on the concentration of the chromophore fluorescence lifetime imaging is a direct approach to all effects that involve energy transfer.<sup>179,180,181,182</sup> Typical examples are the mapping of cell parameters such as pH, ion concentrations or oxygen saturation by emission quenching, or fluorescence resonance energy transfer (FRET)<sup>179,180</sup> between different chromophores in the cell. Furthermore, combined intensity lifetime imaging is a powerful tool to distinguish between different fluorescence markers in multi-stained samples and between different natural fluorophores of the cells themselves. These components often have ill-defined fluorescence spectra but are clearly distinguished by their fluorescence lifetime.<sup>183</sup> As such Fluorescent Lifetime imaging microscopy is a powerful tool.

The images in Figure 4.14 show the Fluorescence obtained from a thin film of both Ru-HMWT PMAS and Ru-LMWT PMAS. The fluorescence from the film is represented by the red colour. As can be observed from the image significantly more emission is seen from the Ru-LMWT composite film than from the Ru-HMWT film (approximately 60%). This observation reinforces what has been previously observed for these composite films. As previously mentioned a key advantage of this technique is that the fluorescent lifetime of a compound can also be obtained from various sections of the observed image. Figure 4.15 shows a FLIM image of a Ru-LMWT

PMAS Composite Film. The luminescent lifetime of which has been extrapolated from two different areas of the film, e.g. An area of high luminescence possibly indicating an area of high ruthenium concentration within the film and an area of low luminescence, possibly indicating an area containing a high concentration of LMWT PMAS. These areas are represented by the concentric circles overlaid on the image. The lifetimes obtained from this region of the image correspond to 280 ns and 35 ns respectively for the Ru-LMWT composite film and 60 ns and 21 ns for the Ru-HMWT film.

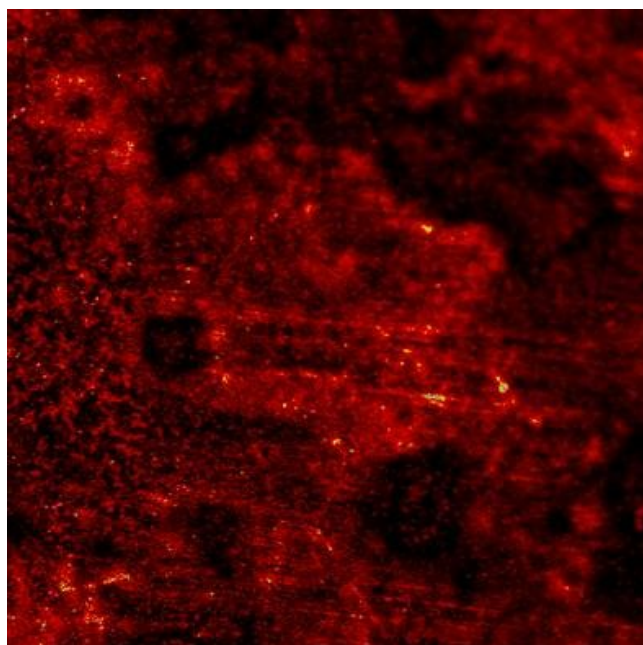
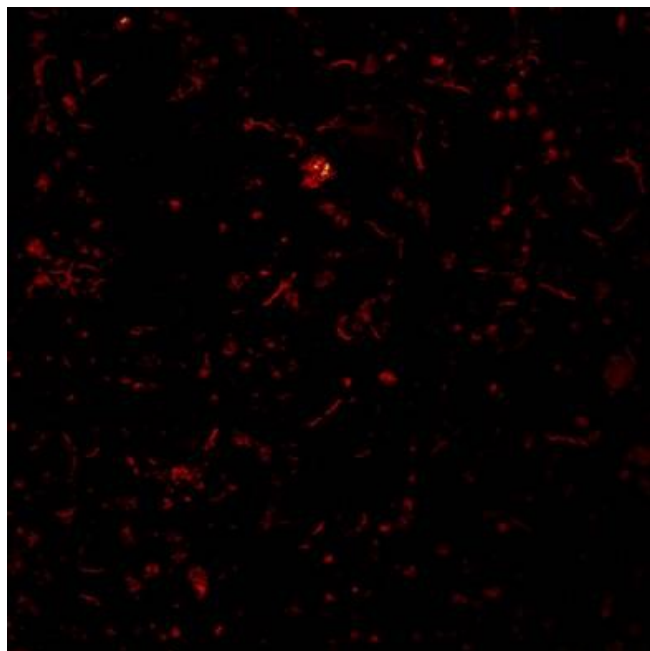


*Figure 4.14: LSM Image of Ru-HMWT PMAS (top) and Ru-LMWT PMAS (bottom) Composite films, Excitation 457 nm.*

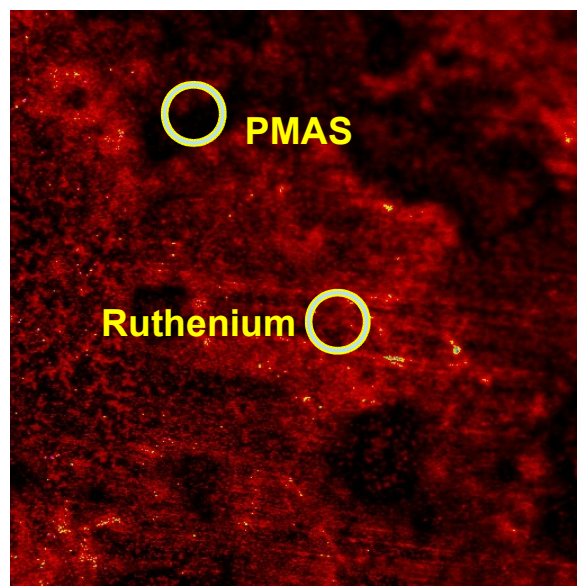


**Figure 4.15:** *Fluorescent Lifetime Imaging Microscopy of Ru-LMWT film. Lifetimes calculated from the areas within the yellow circles.*

#### ***4.4 Conclusions***

By isolating the two fractions of the conducting polymer, Poly(2-Methoxyaniline-5-Sulfonic Acid), PMAS, the effect of each fraction on the electrochemical and photochemical properties  $[\text{Ru}(\text{bpy})_3]^{2+}$  can be investigated. Both Ru-HMWT and Ru-LMWT composite films showed good communication in both the ground and excited states. However, electrochemical analysis reveals that the HMWT PMAS emeraldine salt supports a more rapid electron transfer within the film compared to the Ru-LMWT PMAS composite whereas the LMWT PMAS serves to enhance the  $[\text{Ru}(\text{bpy})_3]^{2+}$  centered luminescence by means of electron transfer. The relatively low luminescence observed for the Ru-HMWT composite can be attributed to overlapping absorption spectra of  $[\text{Ru}(\text{bpy})_3]^{2+}$  and that of HMWT PMAS at 355 nm leading to competitive absorption of light and also to acceptor states on the polymer backbone accepting electron transfer from the  $[\text{Ru}(\text{bpy})_3]^{2+*}$  thereby effectively “quenching” the ruthenium based emission. However quenching from dynamic and static mechanisms may also play a part in the observed reduction in luminescence.

The luminescent lifetime of the composite films is somewhat more complicated and further work may be required to determine if the dominant decay in the Ru-HMWT composite film is attributed to ruthenium based emission or trace amounts of the LMWT PMAS in the film. However given the relatively high purity of the HMWT PMAS any trace amount of LMWT PMAS would be very low. This in conjunction with the high concentrations of  $[\text{Ru}(\text{bpy})_3]^{2+}$  in the film it is reasonable to assume that the dominant decay is due to the ruthenium based lifetime. In each film the dominant decay was less than that expected for a solution containing solely  $[\text{Ru}(\text{bpy})_3]^{2+}$  so in each case no significant enhancement of the ruthenium based lifetime is observed. As PMAS concentrations in each film were increased a reduction in lifetime was observed however the dominant component of the Ru-HMWT composite was more susceptible to HMWT PMAS concentration increases than in the Ru-LMWT film. Given the electrochemical activity of the HMWT PMAS

it is expected to be a better quencher of the ruthenium lifetime than the non conducting LMWT PMAS thereby resulting in a significantly lower lifetime than that observed for Ru-LWMT film, the PMAS component of which is non conducting. The immobilization of  $[\text{Ru}(\text{bpy})_3]^{2+}$  within specific PMAS fractions illustrates that both the photochemical and electrochemical properties of the luminescent metal centre can be modulated to enhance either the photoluminescence or the rate of charge transfer by interacting with either the LMWT or HMWT PMAS. This may allow each fraction to be utilized in very different applications depending on the desired function. The ability to tune both the charge transport properties as well and the photoluminescent characteristics demonstrate the many possible applications that these composites can be exploited for, including both luminescence and electrochemical based sensors.

## *Chapter 5*

### *Electrochemiluminescent Properties of [Ru(bpy)<sub>2</sub>(PPyBBIM)<sub>n</sub>]<sup>2+</sup> Metallopolymers and Ru-PMAS Composite Films.*

## 5.1 Introduction

As previously discussed in Chapter 1 the luminescence arising from the electron transfer recombination of electrogenerated reactants is known as electrochemiluminescence (ECL). ECL has been the subject of extensive study for the past three decades.<sup>184,185</sup> The production of light from intermediates generated during electrolysis occurs when the energy liberated by reaction between the electrogenerated precursors is sufficient to generate a product in an electronically excited form.<sup>186</sup> Studies of inorganic ECL have been dominated by transition metal complexes,<sup>187,188,189,190</sup> particularly ruthenium poly(pyridyl) species, e.g., those of the general formula  $\text{Ru}(\text{L})_3^{2+}$ , e.g., where L = 2,2'-bipyridine,<sup>191,192,193</sup> 4,7-diphenyl-1,10-phenanthroline<sup>194</sup> or 2,2'-bipyrazine.<sup>195</sup> This is due to the attractive photophysical and electrochemical properties that these compounds typically exhibit.

Electrochemiluminescence combines the inherent sensitivity, selectivity and linear range advantages of chemiluminescence methods with increased temporal and spatial control over the chemiluminescent reaction making ECL a powerful analytical tool. Systems utilising both organic and inorganic complexes have been developed.<sup>196,197</sup> The majority of early ECL systems investigated involved species dissolved in the solution phase with emission occurring in the diffusion layer near the electrode surface. The advent of chemically modified electrodes allowed ECL to be generated in films constrained to the surface of an electrode, e.g. as thin layers produced by electropolymerisation of vinyl containing monomeric species or by electrostatic incorporation of the luminescent species into a preformed polymer matrix. The ability to modify electrode surfaces with ECL producing complexes has greatly increased the scope of potential ECL applications within biomedical sensor design.

As with all sensors there is a constant drive to improve sensitivity and selectivity. The future health industry in conjunction with point of care health monitoring will

demand the detection of life threatening diseases before critical stages have been reached. This will require a new breed of biomedical sensors capable of measuring disease biomarkers down to the pico molar range. In order to design such sensors, it is necessary to consider the limitations of current biomedical sensors. As previously discussed in Chapter 1 the basic requirements for efficient annihilation ECL to occur are the formation of stable radical ions of the precursor molecules in the electrolyte of interest, good photoluminescence efficiency of a product of the electron transfer reaction and sufficient energy in the electron transfer reaction to produce the excited state. Once these criteria are met ECL is typically observed.

Depending on the nature of a specific ECL reaction the sensitivity of film ECL based systems may be limited by certain factors. These include slow rates of charge transfer ( $D_{CT}$ ) through the film. A slow rate of charge transfer will lead to slow regeneration of the  $Ru^{3+}$  excited state that is required to react with an analyte to produce ECL. A fast rate of charge transfer will lead to an increase in the amount of  $Ru^{3+}$  available to react with a specific analyte. This should lead to increased ECL production and improved sensitivity. One appealing possibility is to wire the luminophores using a conjugated polymer backbone. Charge transfer between ruthenium centres in a non-conjugated metallopolymer typically consists of a through space mechanism and introduction of a conjugated backbone has been known to enhance charge transfer rates between metal centres.<sup>198</sup> As previously stated for ECL to occur it must be thermodynamically feasible, e.g. the reaction between the oxidised and reduced species should have a negative  $\Delta G^\circ$  value. As the formal potential for most ruthenium polypyridyl complexes ranges between 1.4 and 0.8 eV the range of co-reactants that can produce ECL with these systems can sometimes be limited. ECL production is also greatly affected by film porosity or “swelling”. Swelling of a film allows enhanced diffusion of the analyte through the film to the ruthenium metal centres. If a film is compacted an analyte may have difficulty diffusing thru that film and hence less may come into contacting the ruthenium metal centres for creation for the emitting excited state.

The level of swelling in a metallopolymer film can be influenced greatly by pH changes and the use of certain electrolytes.

This chapter will give an account of the ECL properties of the conjugated metallopolymer Ruthenium-[2,2'-bipyridyl]-poly[2-(2-pyridyl)-bibenzimidazole] ( $[\text{Ru}(\text{bpy})_2(\text{PPyBBIM})_n]^{2+}$ ) and the  $[\text{Ru}(\text{bpy})_3]^{2+}/[\text{poly}(2\text{-methoxyaniline-5-sulfonic acid})]$  (Ru-PMAS) composite films. Each approach will be evaluated based on charge transport and regeneration times within the film, ECL production and ECL efficiencies. The performance of each system will be compared not only to one another but also to that of the non conjugated metallopolymer  $[\text{Ru}(\text{bpy})_2(\text{PVP})_{10}]^{2+}$ .

## ***5.2 Apparatus and Reagents***

Electrochemiluminescent studies were performed on glassy carbon electrodes that were modified with thin films of  $[\text{Ru}(\text{bpy})_2(\text{PPyBBIM})_n]^{2+}$  and Ruthenium PMAS as previously described in chapter 2. The non conjugated metallopolymer  $[\text{Ru}(\text{bpy})_2(\text{PVP})_{10}]^{2+}$  was kindly supplied by the RFTK research group.

Electrochemical and ECL experiments were performed in a standard electrochemical cell using a CH instruments (Memphis TN.) model 660 potentiostat with equipped with an auxiliary port. ECL emission was recorded via a photomultiplier tube detector connected to the auxiliary port on the potentiostat. The PMT allowed recording of the emitted light from the electrode via an optical fiber positioned directly opposite the working electrode outside the cell. The cell was protected from light by placing it in a sealed black box to avoid external optical background and possible photodecomposition of the ruthenium complex. A graphic representation of the cell can be seen in Figure 5.1.

All other electrochemical experiments were carried out using a 3 mm diameter glassy carbon working electrode in a conventional three-electrode assembly using a platinum flag as the counter electrode. Working electrodes were cleaned by polishing with 0.3 and 0.05  $\mu\text{m}$  alumina on felt pad, followed by sonication in distilled deionised water for 30 min. Potentials were measured versus a Ag/AgCl reference electrode. All electrochemical measurements were performed in  $\text{H}_2\text{SO}_4$  or 0.1 M Sodium Oxalate (Aldrich) containing 0.1M  $\text{LiClO}_4$  electrolyte and were carried out at room temperature. All solutions were degassed using nitrogen or argon prior to measurement.

Electrodes were modified with metallopolymer films as previously described in Chapter 2. Working electrodes were modified by applying a drop ( $\approx 15 \mu\text{L}$ ) of an ethanolic solution of the metallopolymer to the electrode surface which was then allowed to dry in the dark for 10 to 12 hours. Surface coverages,  $\Gamma$ , were

determined by graphical integration of background corrected cyclic voltammograms ( $< 5 \text{ mV s}^{-1}$ ). In all cases the surface coverage was  $2 \pm 1 \times 10^{-8} \text{ mol cm}^{-2}$ , unless otherwise stated. Figure 5.2 represents a schematic of a modified electrode.

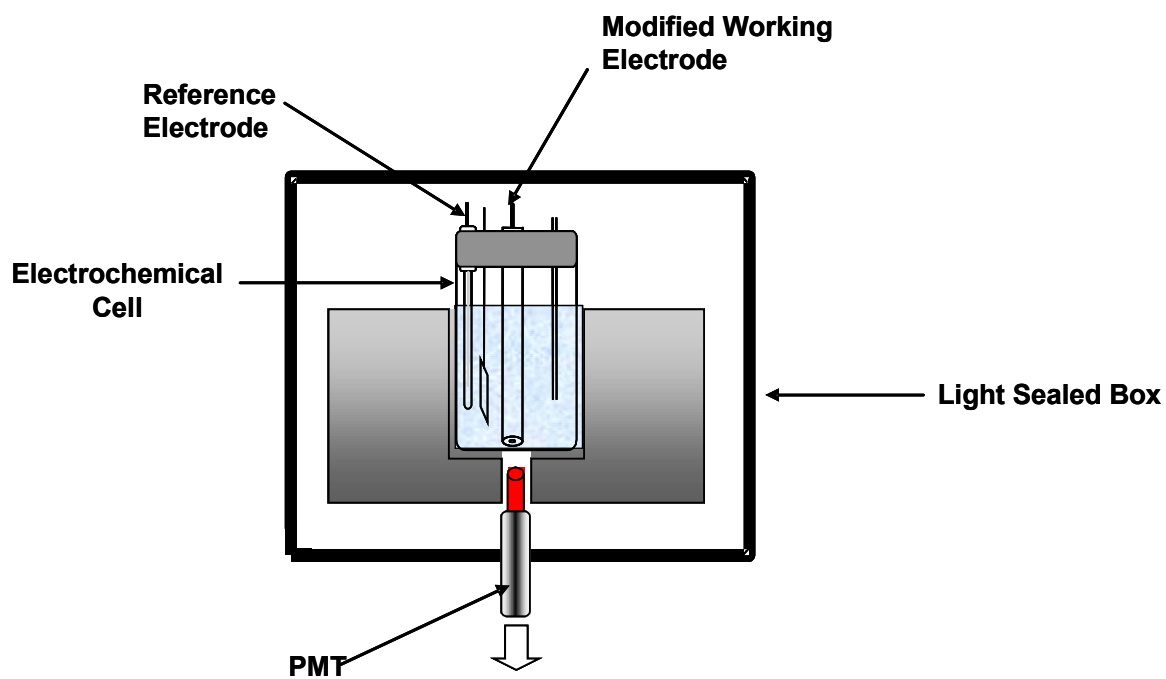


*Figure 5.1: Setup of the electrochemical cell used for ECL studies, The cell allows for dual light and current detection.*

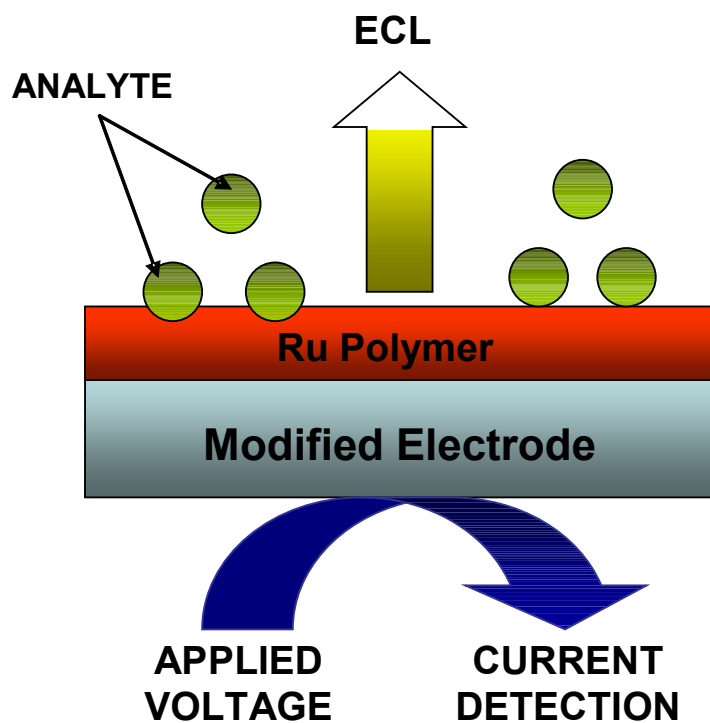


*Figure 5.2: Illustration of glassy carbon electrode modified with ruthenium polymer.*

## 5.3 Discussion

### 5.3.1 Charge transport properties of ruthenium containing polymers and composite films.

Electrochemiluminescence has many distinct advantages over conventional Chemiluminescence. However like many other transduction methods it too suffers from certain disadvantages. ECL production is highly dependent upon the rate of charge transfer ( $D_{CT}$ ). A fast rate of charge transfer ensures sufficient  $Ru^{3+}$  will be present to react with a given analyte and produce ECL. An insufficient amount of  $Ru^{3+}$  will result in decreased ECL emission and hence decreased sensitivity. An increase in the rate of charge transfer will result in a significant increase not only in sensitivity but also the selectivity of ECL based sensors. The redox metallopolymers that have typically been used for ECL suffer from relatively slow charge transport compared to recently developed conducting metallopolymers.<sup>199</sup>

Metallopolymers currently utilised for ECL production such as  $[Ru(bpy)_2(PVP)_{10}]^{2+}$  consist of electrochemically active sites at each ruthenium metal centre tethered to a electrochemically *inactive* backbone. The ruthenium metal d-orbitals are isolated from one another and as such charge transfer occurs via a “through space mechanism” requiring polymer chain movement to allow the metal centres to collide. By incorporating a conjugated backbone the electronic interactions between the polymers  $\pi$ -system and the metals d-orbitals can modulate the properties of both components in interesting and potentially useful ways. One of the anticipated benefits is fast cycles of  $Ru^{3+}$  production and subsequent reaction with co-reactant. A faster rate of charge transfer would significantly increase the production of ECL leading to enhanced sensitivity. This coupled with increased luminescence yield from energy transfer from the polymer backbone or polymeric matrix should lead to favourable characteristics necessary for enhanced ECL production.

This faster regeneration of the  $\text{Ru}^{3+}$  species in the Ruthenium-PMAS composites and  $[\text{Ru}(\text{bpy})_2(\text{PPyBBIM})_n]^{2+}$  metallopolymers imply that the enhanced communication resulting from the incorporation of a  $\pi$  conjugated system ultimately increases the efficiency of the ruthenium metal centers. This could impact greatly on sensor design, as the faster regeneration of the  $\text{Ru}^{3+}$  species should drastically improve the sensitivity of systems involving a ruthenium redox center.

**Table 5.1:**  $D_{CT}$  and  $Ru^{3+}$  regeneration times for the  $[Ru(bpy)_2(PPyBBIM)_3]^{2+}$  metallopolymer and the Ruthenium-PMAS Composites films.

<b>Material</b>	<b><math>D_{CT} cm^2 s^{-1}</math></b>
$[Ru(bpy)_2(PPyBBIM)_3]^{2+}$	$4.56 \times 10^{-10}$
$[Ru(bpy)_2(PPyBBIM)_{10}]^{2+}$	$8.22 \times 10^{-10}$
$[Ru(bpy)_2(PPyBBIM)_{20}]^{2+}$	$7.09 \times 10^{-12}$
Ru-LMWT	$3.59 \times 10^{-10}$
Ru-HMWT	$1.44 \times 10^{-10}$
$[Ru(bpy)_2(PVP)_{10}]^{2+}$	$9.12 \times 10^{-11}$

### 5.3.2 Sodium Oxalate as a Co-Reactant

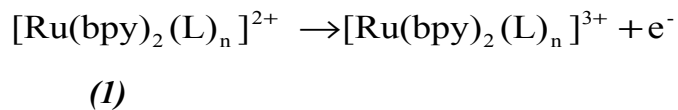
The overall aim of this work is to produce new materials that may eventually improve current electrochemiluminescent detection systems leading to increased levels in sensitivity and thus lower detection limits. Previous work within this research group has reported that oxidation of guanines in DNA by electrochemically generated  $[\text{Ru}(\text{bpy})_2(\text{PVP})_{10}]^{2+}$  in ultra thin films leads to photoexcited  $[\text{Ru}(\text{bpy})_2]^{2+}$  sites in the film that generate electrochemiluminescence (ECL) upon relaxation back to the ground state.<sup>200</sup> This thin-film ECL approach has been exploited to detect DNA damage induced by styrene oxide. The reaction is initiated by an electrochemical catalytic oxidation of guanine sites in DNA in a way that is similar to that reported by Thorp *et al.*<sup>201</sup> for  $\text{Ru}(\text{bpy})_3^{2+}$  in solution. By enhancing the ECL or luminescent efficiency of the ruthenium moiety through interactions with a conducting polymer, the sensitivity of this type of ECL sensors could be dramatically improved. Chapters 3 and 4 have documented the electrochemical and photophysical properties of these systems and have highlighted the favourable characteristics that may lead to an improvement in ECL sensor design. As with any new system it is necessary to evaluate its performance compared to previous systems using a recognised testing method. The production of ECL from reaction of ruthenium containing compounds with sodium oxalate has been well documented both within this group and outside<sup>202,203</sup> and as such was chosen as a suitable system to evaluate the electrochemiluminescent properties of the  $[\text{Ru}(\text{bpy})_2(\text{PPyBBIM})_n]^{2+}$  metallopolymers and the Ruthenium-PMAS Composite films.

High oxalate concentrations in the blood or urine accompany a number of maladies including renal failure, vitamin deficiencies, intestinal deficiencies, hyperoxaluria<sup>204</sup> and have also been implicated in the formation of kidney stones. As such, selective and precise methods for the determination of oxalate are important. A number of methods for the determination of oxalate have been described including volumetric, colorimetric, fluorimetric and enzymatic methods. HPLC<sup>205</sup> and cyclic voltammetry<sup>206</sup> have also been suggested as methods of determining oxalate. As most of these methods required a significant amount of

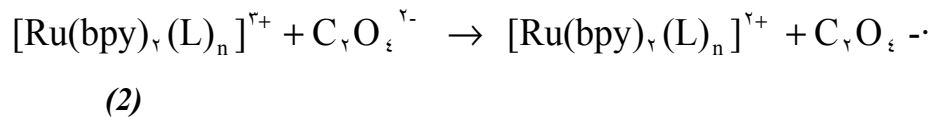
sample preparation to isolate oxalic acid from the biological matrix they were often time consuming and expensive. Therefore, a more specific and less time consuming method was required and this came in the form of electrogenerated Chemiluminescence or ECL.

Electrogenerated chemiluminescence via the reaction of sodium oxalate with the  $\text{Ru}^{3+}$  excited state was first reported by Chang *et al*<sup>207</sup> and since then has been well documented.<sup>91</sup> Ruthenium containing metallopolymers immobilised on an electrode surface such as  $[\text{Ru}(\text{bpy})_2(\text{PVP})_{10}]^{2+}$  have also been shown to produce ECL upon reaction with oxalic acid. All ECL studies were carried out at pH 6.0 for two reasons. Firstly, as previously reported sodium oxalate produces the highest ECL intensity with ruthenium at this pH. Secondly, as one of the main aims of this work is to produce a sensor that can be used for the detection of biological analytes that under normal circumstances do not exhibit extremes of pH. As such a neutral pH was chosen to simulate a biological matrix. The reaction scheme for the generation of ECL between a ruthenium containing metallopolymer and oxalic acid is as follows.

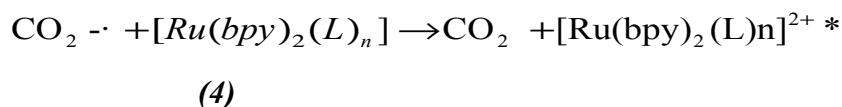
The metallopolymer is first oxidised at an electrode according to the equation:



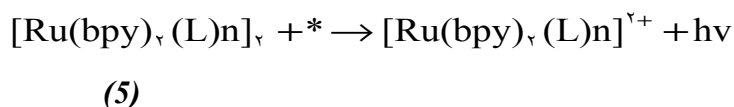
The following reactions then occur at the electrode surface:



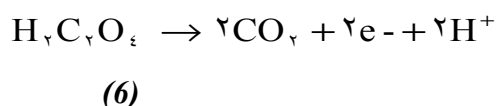
The intermediate radical anion,  $\text{CO}_2^{\bullet -}$  is a strong reducing agent and produces the excited state,  $[\text{Ru}(\text{bpy})_2(\text{L})_n]^{2+*}$  in an electron transfer reaction with the 3+ species. The amount of excited state species produced is heavily dependent upon the speed at which the oxidised  $\text{Ru}^{3+}$  species is produced.



As the excited  $[\text{Ru}(\text{bpy})_2(\text{L})_n]^{2+*}$  decays to the ground state electrochemiluminescence is produced:



As the non-conjugated metallopolymer  $[\text{Ru}(\text{bpy})_2(\text{PVP})_{10}]^{2+}$  has been previously reported to produce ECL with sodium oxalate<sup>208</sup> at pH 5.5 and as such it was picked as a standard to which the imidazole based conjugated metallopolymer were compared. The oxidation of oxalate proceeds via the overall equation



In this catalytic route, oxidation of oxalate is mainly through Ruthenium mediated reaction. Direct oxidation of oxalate at the electrode, although thermodynamically possible is known to be kinetically slow.<sup>209</sup> This behaviour arises because a significant over potential must be applied before oxalic acid can be oxidized at a bare electrode. Therefore, the direct oxidation of oxalate is generally considered to contribute little to the ECL emission in either solution or phase or immobilized ruthenium/oxalate systems.<sup>213,210,211,212</sup> Figure 5.3 shows the current responses obtained when thin films of Ru-LMWT and Ru-HMWT PMAS are placed in 0.1

M H<sub>2</sub>SO<sub>4</sub> solution containing 10 mM Na<sub>2</sub>C<sub>2</sub>O<sub>4</sub> (pH 6.1). Significant increases in current are observed for each composite film. This enhanced current arises from the mediated oxidation of oxalic acid by Ru<sup>3+</sup> centres within the film. Similar behaviour is observed for the [Ru(bpy)<sub>2</sub>(PPyBBIM)<sub>n</sub>]<sup>2+</sup>. Figure 5.4 shows the change in voltammetric response that occurs when 500mM sodium oxalate is added to a solution containing thin films of [Ru(bpy)<sub>2</sub>(PPyBBIM)<sub>3</sub>]<sup>2+</sup> the contacting solution (quiescent) during the course of a C.V. experiment. The current response increases with time due to the slow rate of equilibration upon addition of oxalate. The large increase in current at circa 1.1 V vs. Ag/AgCl, on addition of the substrate clearly demonstrates that oxalate is oxidised at potentials when Ru<sup>3+</sup> sites exist within the metallopolymer film. Also, the absence of a return peak on addition of the oxalate is an indication that catalysis is efficient and that a large number of the mediator sites are involved in the catalytic reaction.

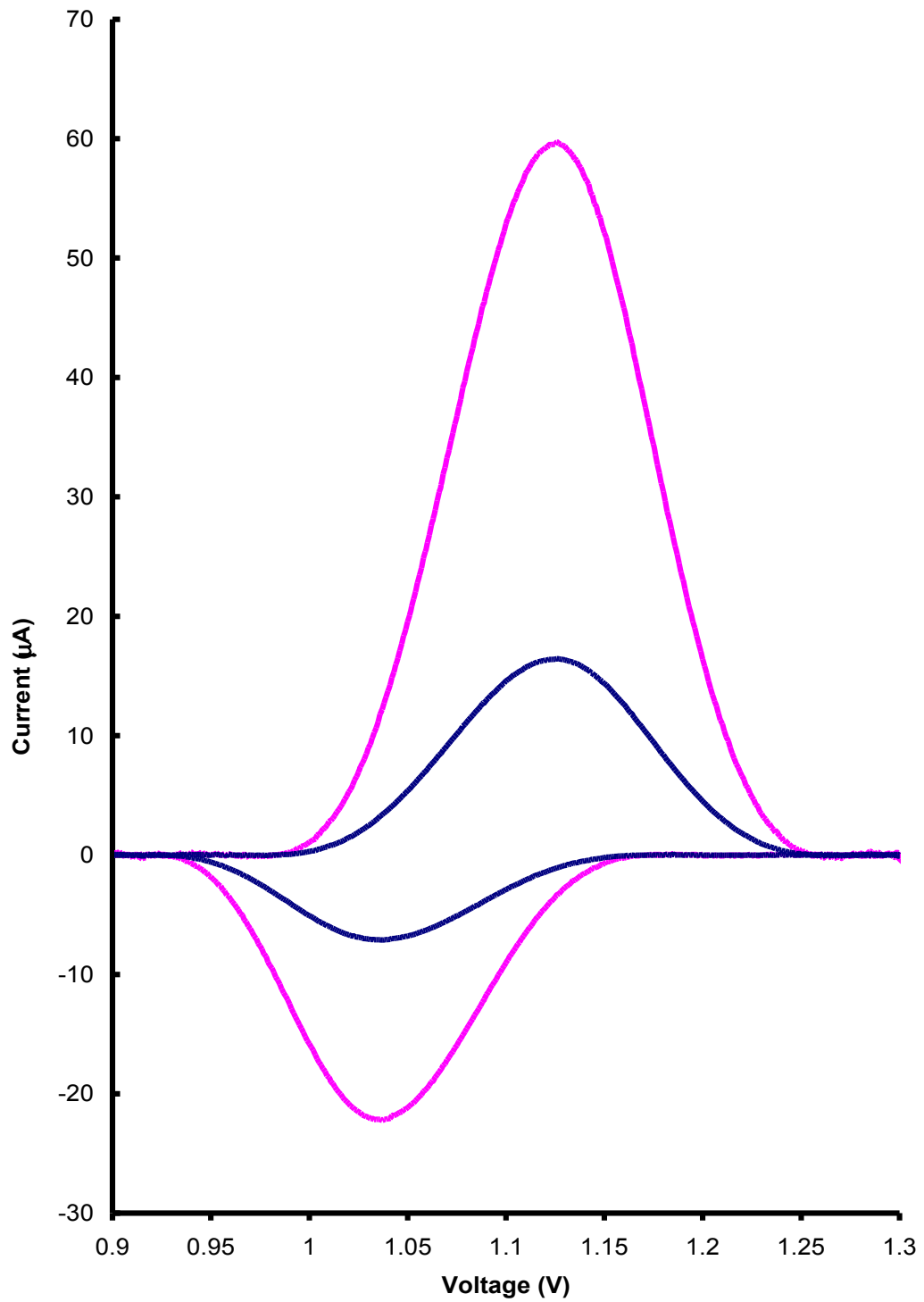


**Figure 5.3:** Background corrected Cyclic Voltammogram response of Ru-LMWT (pink) and Ru-HMWT (blue) PMAS films in the presence of 10mM

SodiumOxalate dissolved in dH<sub>2</sub>O.  $\Gamma = 4.1 \pm 1.0 \times 10^{-8}$  and  $6.9 \pm 1.2 \times 10^{-8}$  mol cm<sup>-2</sup> respectively.

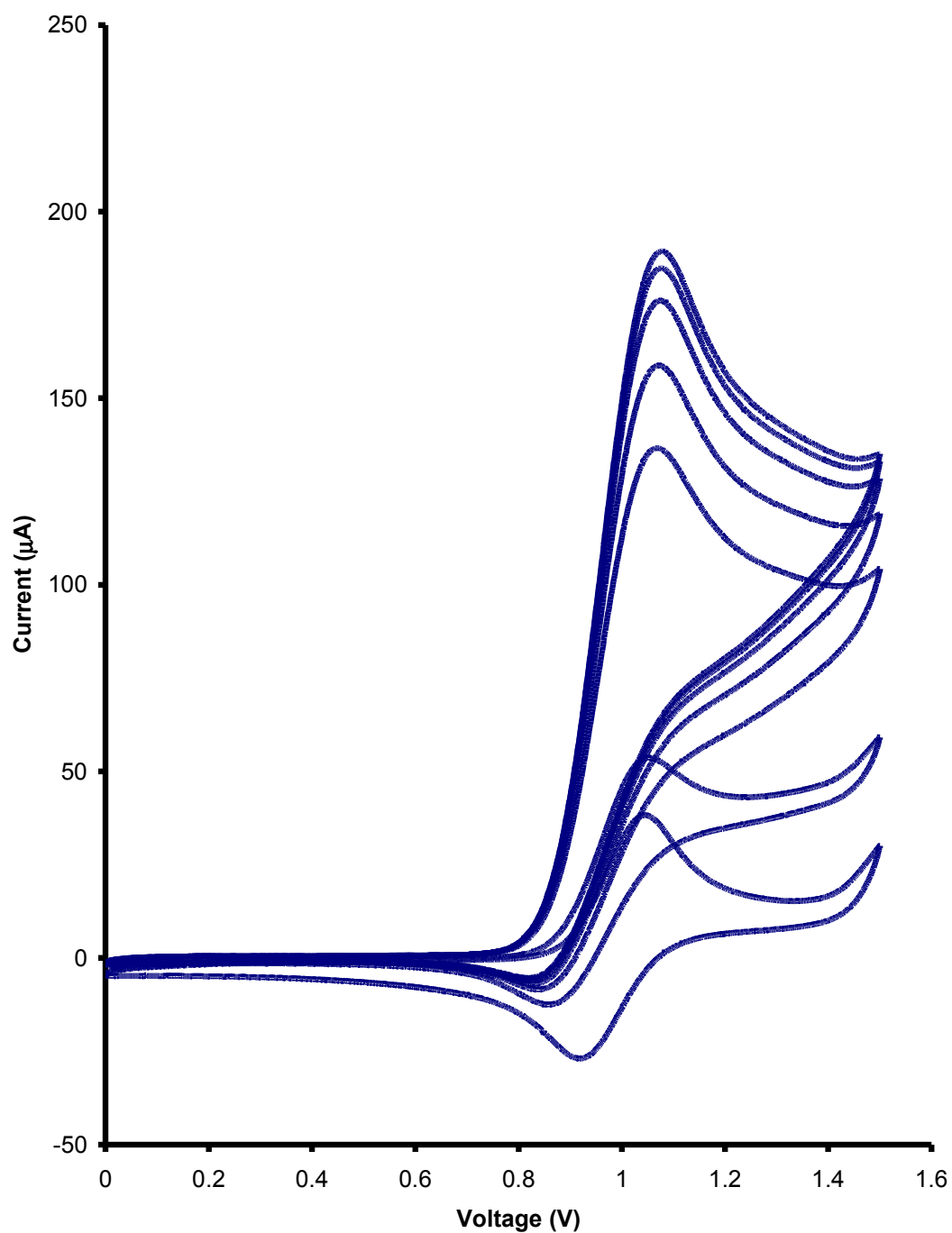


**Figure 5.4:** Increased current response when 50mM sodium oxalate is added to  $[Ru(bpy)_2(PPyBBIM)_3]^{2+}$  during the course of a C.V. experiment. Scan rate  $0.1Vs^{-1}$ .  $\Gamma = 2 \pm 0.5 \times 10^{-8}$  mol cm<sup>-2</sup>.

### 5.3.3 ECL Generation with sodium oxalate.

Electrodes were modified with thin films of each of the respective  $[\text{Ru}(\text{bpy})_2(\text{PPyBBIM})_n]^{2+}$  metallopolymers and both Ru-HMWT and Ru-LMWT PMAS composite films. To evaluate the properties of these conjugated metallopolymer systems against currently utilised non conjugated systems thin films of the non conjugated metallopolymer  $[\text{Ru}(\text{bpy})_2(\text{PVP})_{10}]^{2+}$  were also prepared, by drop casting in ethanolic solutions as described previously. ECL from the modified electrodes was easily generated *via* the co-reactant pathway using oxalate dissolved in 0.1 M  $\text{Na}_2\text{S}_2\text{O}_4$  at pH 6 as described above in equations 1 - 6. As the potential of the modified electrode in contact with such a solution approaches 1.2 V both the Ruthenium and oxalate are oxidized leading to the electrochemical production of the ruthenium excited state thereby generating luminescence as it decays to the ground state. Figure 5.5 illustrates ECL emission spectra obtained for each of the  $[\text{Ru}(\text{bpy})_2(\text{PPyBBIM})_n]^{2+}$  metallopolymer films. The highest emission was observed from the  $[\text{Ru}(\text{bpy})_2(\text{PPyBBIM})_3]^{2+}$  metallopolymer followed by the  $[\text{Ru}(\text{bpy})_2(\text{PPyBBIM})_{10}]^{2+}$  and  $[\text{Ru}(\text{bpy})_2(\text{PPyBBIM})_{20}]^{2+}$  metallopolymers respectively. The Ru-PMAS composite films also produced ECL in the presence of sodium oxalate as can be seen in Figure 5.6. The variance of peak shape between the  $[\text{Ru}(\text{bpy})_2(\text{PPyBBIM})_n]^{2+}$  and the Ru-PMAS composites can be attributed to varying kinetics under the experimental conditions between the two systems. The Ru-LMWT composite film produced approximately 30% greater ECL intensity than the Ru-HMWT composite. Despite producing a very small photoluminescent emission significant ECL emission was produced from the Ru-HMWT composite film. This can be attributed to the fact that the emission is produced without any incident light eliminating any absorption of light by the HMWT PMAS within the film. When the ECL intensities of the  $[\text{Ru}(\text{bpy})_2(\text{PPyBBIM})_n]^{2+}$  series of metallopolymer are compared to the Ruthenium-PMAS films we can see that

significantly greater emission intensity is observed from the Ru-PMAS films than  $[\text{Ru}(\text{bpy})_2(\text{PPyBBIM})_n]^{2+}$  metallopolymers as can be seen in Figure 5.7. This may be simply due to increased amounts of ruthenium within the film, therefore to fully assess the ECL performance of each of the approaches it is necessary to calculate the ECL efficiencies for each system.

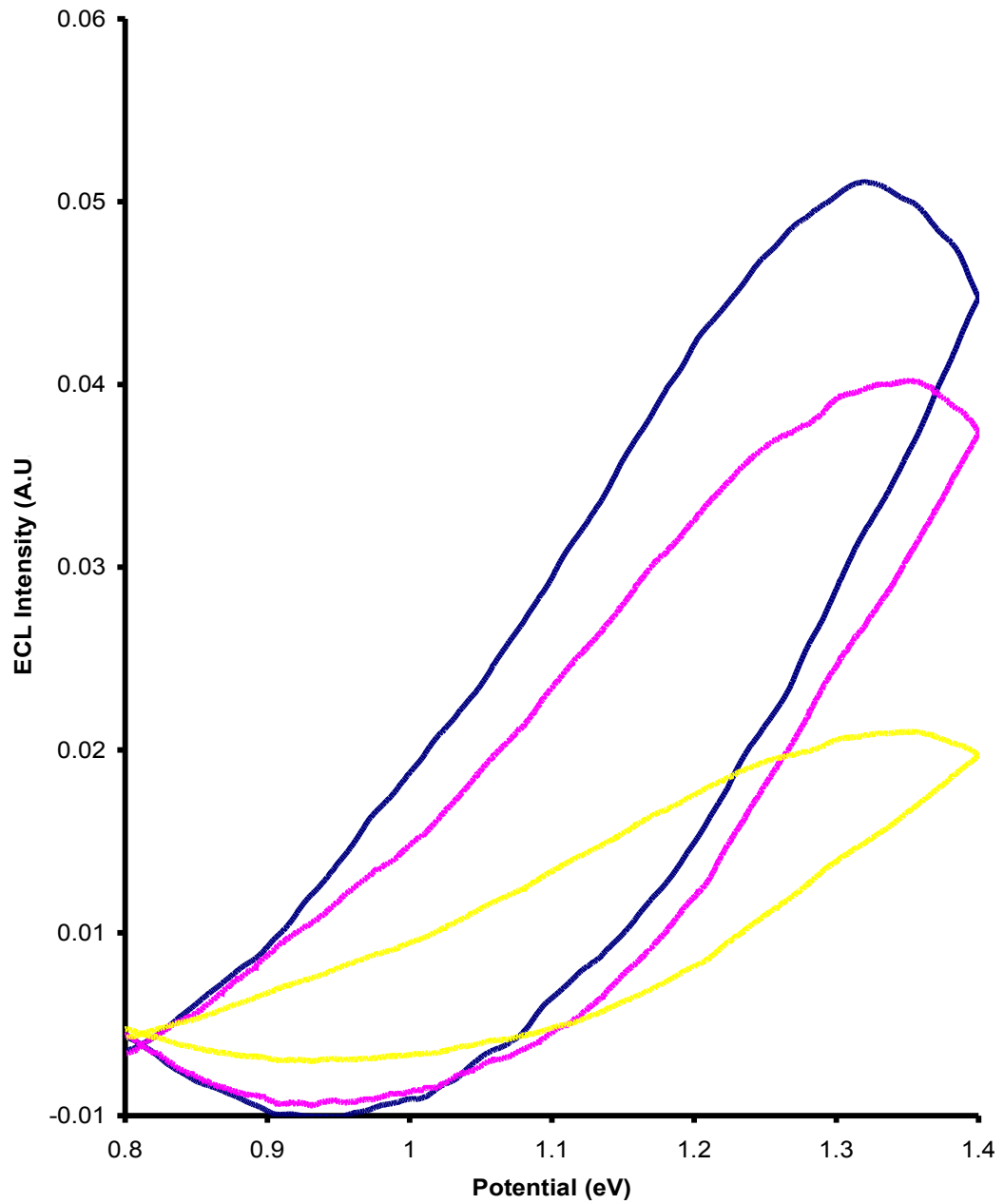


**Figure 5.5:** ECL response of  $[Ru(bpy)_2(PPyBBIM)_3]^{2+}$  (blue)  $[Ru(bpy)_2(PPyBBIM)_{10}]^{2+}$  (pink) and  $[Ru(bpy)_2(PPyBBIM)_{20}]^{2+}$  (yellow) metallopolymers respectively in the presence of 10mM sodium oxalate at pH 6.1 Scan rate  $0.1Vs^{-1}$ ,  $\Gamma = 3.1 \times 10^{-8} \text{ mol cm}^{-2}$ ,  $2.8 \times 10^{-8} \text{ mol cm}^{-2}$  and  $1.5 \times 10^{-8} \text{ mol cm}^{-2}$  respectively

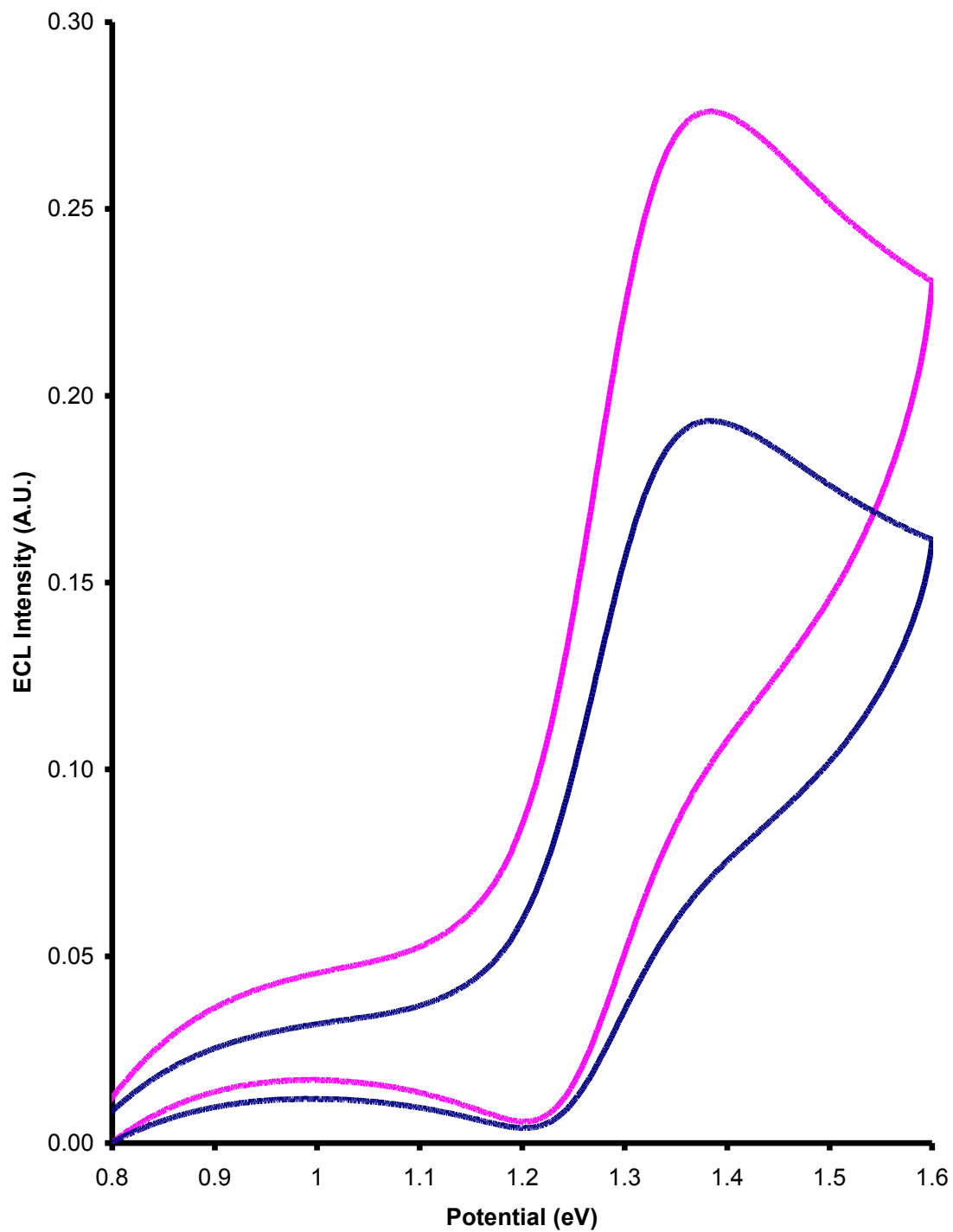


**Figure 5.6:** ECL response of Ru-LMWT and Ru-HMWT PMAS composite films in the presence of 100mM sodium oxalate, pH (6.1). Scan rate  $0.1\text{Vs}^{-1}$ ,  $\Gamma = 3.4 \times 10^{-8} \text{ mol cm}^{-2}$  and  $3.1 \times 10^{-8} \text{ mol cm}^{-2}$  respectively.

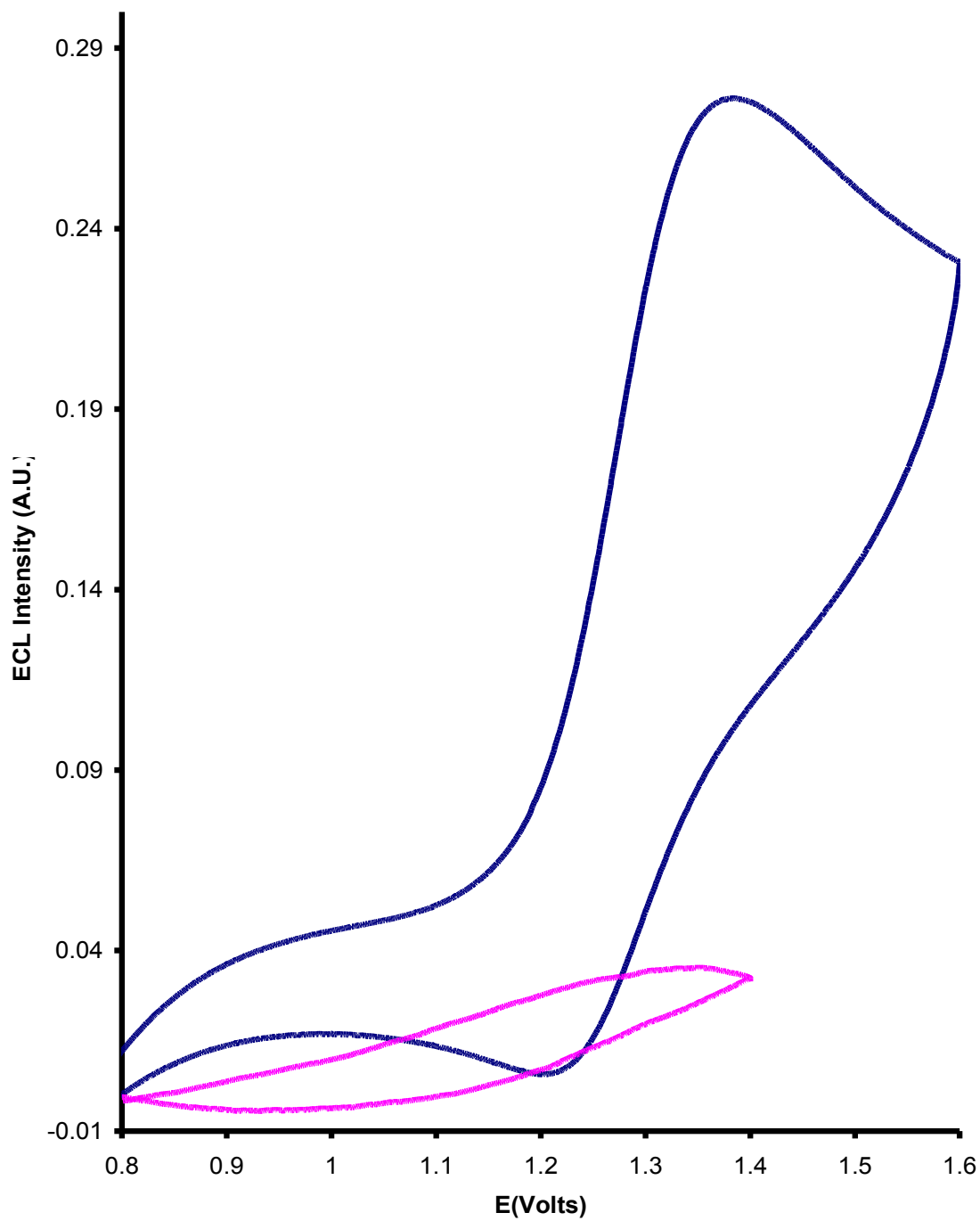


**Figure 5.7:** Comparison of ECL responses for Ru-LMWT PMAS and  $[Ru(bpy)_2(PPyBBIM)_3]^{2+}$  in the presence of 100mM Sodium Oxalate. Scan rate  $0.1 \text{ Vs}^{-1}$ . pH (6.1),  $\Gamma = \Gamma = 3.4 \times 10^{-8} \text{ mol cm}^{-2} \pm 1 \times 10^{-8} \text{ mol cm}^{-2}$

### 5.3.4 Electrochemiluminescent efficiencies of the metallopolymer films.

The ECL efficiency of this type of composite film was also compared against previous non conjugated ruthenium containing metallopolymers. The overall ECL efficiency ( $\phi_{\text{ECL}}$ ) is defined as the number of photons emitted per faradaic electron passed during the chemiluminescent reaction.<sup>213</sup> It is the product of the efficiency of populating the excited state ( $\phi_{\text{EX}}$ ) and the quantum yield of emission from that excited state ( $\phi_{\text{P}}$ ).  $\text{Ru}(\text{bpy})_3^{2+}$  was used as a relative standard for all experiments. The relative efficiency was obtained using the relation:<sup>214</sup>

$$\phi_{\text{ECL}} = \phi_{\text{ECL}}^0 (I Q_{\text{f}}^0 / Q_{\text{f}} I^0) \quad (7)$$

where  $\phi_{\text{ECL}}^0$  is the ECL efficiency of  $\text{Ru}(\text{bpy})_3^{2+}$  (1 mM and 0.1 M TBABF<sub>4</sub> / ACN) *via* annihilation, taken as 5.0%,<sup>215,216</sup>  $I$  and  $I^0$  are the integrated photomultiplier tube responses for the polymer and  $[\text{Ru}(\text{bpy})_3]^{2+}$  respectively, and  $Q_{\text{f}}$  and  $Q_{\text{f}}^0$  are the faradaic charges passed for the sample and standard.

It is important to note that as  $[\text{Ru}(\text{bpy})_3]^{2+}$  itself cannot be immobilized in a thin film format the ECL efficiencies of the films are compared to 100 $\mu\text{M}$   $[\text{Ru}(\text{bpy})_3]^{2+}$  in solution. This results in low % efficiencies overall, However as the goal of this work is to compare the ECL efficiency of conjugated and non conjugated systems the overall % value is insignificant as it is the ratio of the values with respect to one another that supplies the information required. Table 5.1 reveals that the greatest ECL efficiency is obtained from the Ru-LMWT PMAS composite film. The value is approximately 25% greater than that obtained for the non conjugated  $[\text{Ru}(\text{bpy})_2(\text{PVP})_{10}]^{2+}$  film. Surprisingly the ECL efficiency obtained for the Ru-HMWT PMAS film is approximately 10% that of the Ru-LMWT film despite similar enhanced rates of charge transport being observed. This again may be due to the reduced lifetime and emission observed in Chapter 4 caused by charge

transfer from the ruthenium excited state to the HMWT PMAS polymer. Another reason for the observed decrease in efficiency may lie in the Ru-HMWT film not being as porous as the Ru-LMWT films, thereby by inhibiting the diffusion of sodium oxalate to the ruthenium centres. This issue could be further probed through the use of Scanning Electron Microscopy or Rotating Disk Voltammetry. Interestingly the ECL emission intensities for the conjugated  $[\text{Ru}(\text{bpy})_2(\text{PPyBBIM})_n]^{2+}$  series of metallopolymers was significantly lower than that obtained for the non conjugated  $[\text{Ru}(\text{bpy})_2(\text{PVP})_{10}]^{2+}$  metallopolymer despite displaying faster rates of charge transfer. Again a possible reason of this may lie in the porosity of the metallopolymer film.

**Table 5.2:** ECL efficiencies of for the composite film compared to solution phase  $[Ru(bpy)_3]^{2+}$

<b>Material</b>	<b><math>\phi_{ECL}</math> (%)</b>
<b>SOLUTION PHASE</b>	
$[Ru(bpy)_3]^{2+}$	5.0
<b>THIN FILM</b>	
$[Ru(bpy)_2(PVP)_{10}]^{2+}$	0.152
Ru-LMWT PMAS	0.2
Ru-HMWT PMAS	0.022
$[Ru(bpy)_2(PPyBBIM)_3]^{2+}$	0.0096
$[Ru(bpy)_2(PPyBBIM)_{10}]^{2+}$	0.011
$[Ru(bpy)_2(PPyBBIM)_{20}]^{2+}$	0.033

## 5.4 Conclusions

The electrochemiluminescent properties of the  $[\text{Ru}(\text{bpy})_2(\text{PPyBBIM})_n]^{2+}$  metallopolymers and Ru-PMAS composites were investigated using sodium oxalate as a co-reactant. When analysed under the same conditions the  $[\text{Ru}(\text{bpy})_2(\text{PPyBBIM})_n]^{2+}$  metallopolymers and the Ruthenium-PMAS composite films displayed diffusion coefficient values an order of magnitude faster than the non conjugated metallopolymer  $[\text{Ru}(\text{bpy})_2(\text{PVP})_{10}]^{2+}$ . This led to faster  $\text{Ru}^{3+}$  regeneration times with anticipated increases in ECL intensity. ECL was observed for each of the systems investigated. For the  $[\text{Ru}(\text{bpy})_2(\text{PPyBBIM})_n]^{2+}$  metallopolymers the highest ECL intensity was observed for the  $[\text{Ru}(\text{bpy})_2(\text{PPyBBIM})_3]^{2+}$  metallopolymer followed by the  $[\text{Ru}(\text{bpy})_2(\text{PPyBBIM})_{10}]^{2+}$  and  $[\text{Ru}(\text{bpy})_2(\text{PPyBBIM})_{20}]^{2+}$  metallopolymers respectively. As the relative ECL intensity did not vary significantly with surface coverage it can be assumed that the intensity differences observed between the metallopolymers are due to enhanced rates of charge transfer. The ECL efficiencies obtained however were significantly lower than both non conjugated  $[\text{Ru}(\text{bpy})_2(\text{PVP})_{10}]^{2+}$  metallopolymer and the Ru-PMAS composites. A possible explanation for this may be due to the compact nature of poly-benzimidazole based polymer films. A very compact film may prevent analyte diffusion thereby reducing the amount of  $\text{Ru}^{3+}$  metal centres that come in contact with the co-reactant. Despite the enhanced rates of charge transport only the outer  $\text{Ru}^{3+}$  centres may be exposed to co-reactant leading to generation of light. Electrochemical studies consisting of rotating disk voltammetry could provide further evidence of this effect.

For the Ru-PMAS systems the highest ECL intensity was observed for the Ru-LMWT PMAS composite film, approximately 30% more than the Ru-HMWT PMAS film. Despite relatively low photoluminescent yields obtained for the Ru-

HMWT composite film significant ECL emission was observed. The reason for this lies in the method in which the ruthenium excited state is created. Due to the fact that the excitation for ECL is not luminescence based the ruthenium in the film is not competing with the PMAS for absorption of light. Despite similar rates of charge transport, ruthenium based emission and ruthenium luminescent lifetimes there existed approximately a 20 fold difference in ECL efficiency between the Ru-LMWT PMAS films and the  $[\text{Ru}(\text{bpy})_2(\text{PPyBBIM})_n]^{2+}$  metallopolymers. This result further highlights the importance of film porosity to within film based ECL systems. Significantly the ECL efficiency of the Ru-LMWT PMAS composite films was approximately 25 % greater than that obtained for the non conjugated  $[\text{Ru}(\text{bpy})_2(\text{PVP})_{10}]^{2+}$  metallopolymer.

## *Chapter 6*

### *Conclusions*

## ***6.0 Conclusions***

Electrochemiluminescence (ECL) based sensing devices have a promising future in the biomedical diagnostic industry. Such sensors offer many of the advantages of luminescent based sensing without many of the drawbacks. The primary focus of this thesis has been to improve the sensitivity of such sensors by “tuning” the specific properties that lead to the production of light from an ECL based sensor. This was done by taking advantage of new and emerging materials in the area of conducting metallopolymers. By combining a ruthenium metal complex with a conducting polymer backbone it was anticipated that in a traditional “supramolecular” approach, the electrochemical and photophysical properties of each would combine together to enhance ECL limiting factors such as charge transport and low luminescent yields. The results presented in this thesis have demonstrated that it is possible to tune the rates of charge transport, luminescent yield and luminescent lifetimes to favour ECL production however this does not necessarily translate into an ECL enhancement.

Factors affecting ECL production are both electrochemical and photophysical in nature. Provided the analyte of interest is not rate limiting, ECL production is highly dependent upon the rate of charge transfer within a film or solution. Therefore enhancing the charge transport within a film leads to a greater number of  $\text{Ru}^{3+}$  available for reaction with the co-reactant which in turn leads to increased ECL production. ECL is the product of the efficiency of populating the excited state ( $\phi_{\text{EX}}$ ) and the quantum yield of emission from that excited state ( $\phi_{\text{P}}$ ). Therefore increased ruthenium based luminescence and luminescence lifetimes would also favour ECL enhancement. In this work two approaches were adopted to meet these goals.

The first approach was to utilize a  $[\text{Ru}(\text{bpy})_2(\text{PPyBBIM})_n]^{2+}$  series of conducting metallopolymers. These materials consisted of a ruthenium-(2,2-bipyridyl) metal centre covalently bound to a conducting bibenzimidazole based polymer backbone. To further understand the contribution of fast charge transport to ECL production the metallopolymers examined had various metal loadings. These metallopolymer

displayed enhanced rates of charge transport in the ground state however the excited state charge transport was not as efficient leading to the production of dual emission. Charge transfer from the metallopolymer backbone to the excited state ruthenium was not thermodynamically feasible being exergonic by 0.2 eV. The luminescent lifetimes reported for the metallopolymer were consistent with those previously reported for non conjugated ruthenium containing metallopolymer. The enhanced rates of charge transport however did not translate into enhanced ECL production and ECL efficiencies were shown to be significantly less than those obtained using the non conjugated  $[\text{Ru}(\text{bpy})_2(\text{PVP})_{10}]^{2+}$  metallopolymer, the  $D_{\text{CT}}$  of which was over an order of magnitude smaller than that obtained for the imidazole based metallopolymer. The presence of the polymer backbone did not drastically affect the ruthenium based luminescent lifetimes with decays of approximately 120 ns on average being observed. While these factors meet the criteria for ECL production the question of such low efficiencies remains. An explanation for this may lie in the film porosity. A very rigid and compact film will prevent analyte diffusion thru itself thereby “physically” reducing contact between the  $\text{Ru}^{3+}$  mediating centres and the co-reactant. While this metallopolymer film may have been unsuitable for the analysis of sodium oxalate it should be highlighted that this does not negate its use as an ECL detection system. Given the synthetic challenges of producing a porous film while retaining favorable electrochemical and photophysical properties, it is probable that in the future the range of ECL producing materials will be wide with varying degrees of film porosity. The use of which will be dictated by the analyte of interest as opposed a generic system suitable for the detection of all analytes.

The second approach adopted not only attempted to enhance ECL by tuning the electrochemical and photophysical properties but to produce an ECL material that avoided the difficulties associated with covalently binding a ruthenium metal to a conducting polymer backbone. Like the imidazole based metallopolymer the Ru-PMAS composite films displayed enhanced charge transport properties compared to the non conjugated metallopolymer  $[\text{Ru}(\text{bpy})_2(\text{PVP})_{10}]^{2+}$ . As regards tuning the ruthenium based luminescent properties of the films both composite films displayed

contrasting results. The Ru-HMWT PMAS film was shown to effectively quench the ruthenium excited state emission via electron transfer to acceptor states on the polymer backbone. The overlapping absorption spectra of HMWT PMAS and  $[\text{Ru}(\text{bpy})_3]^{2+}$  further served to reduce ruthenium based luminescence in both the solution and solid states. This however was less of an issue as regards ECL production as the excited state is generated electrochemically as opposed to optical excitation. Within this system the effect of the HMWT PMAS on the ruthenium luminescent lifetime has a greater affect on ECL production. The dominant decay within the film had a lifetime of only 45 ns, significantly lower than that of  $[\text{Ru}(\text{bpy})_3]^{2+}$  in solution. This decay in lifetime is believed to be one of the primary reasons for the low ECL efficiency of the Ru-HMWT PMAS composite film compared to the Ru-LMWT film. The highest ECL efficiency obtained from all films examined in this work came from the Ru-LMWT PMAS film. The ECL efficiency obtained was approximately 25 % greater than that of the  $[\text{Ru}(\text{bpy})_2(\text{PVP})_{10}]^{2+}$  metallopolymer

When designing polymeric systems whereby the cooperative effects of the polymer and ruthenium metal centre are designed to enhance ECL criteria certain considerations in the choice of material should be adhered to. The charge transport properties in not only the ground state but also the excited state need serious consideration. While fast rates of charge transfer are required it should be noted that deactivation of the ruthenium excited state by the polymer backbone is also possible thereby reducing ECL as demonstrated in the Ru-HMWT PMAS system. This environment is unfavourable for ECL production. The effect of the conducting polymer backbone on the ruthenium based luminescent lifetime must also be considered as demonstrated by each PMAS fraction. While the Ru-LMWT PMAS film displayed luminescent lifetimes of approximately 427 ns the lifetimes observed for the Ru-HMWT PMAS composite displayed reduced lifetimes of 45 ns. This difference may be caused by the non conducting LMWT PMAS shielding the excited state ruthenium from atmospheric oxygen. While the HMWT PMAS may also have this affect, it provides a mechanism of excited state deactivation via acceptor states on

the polymer backbone. However the Ru-LMWT PMAS composite films showed a reduction in the charge transfer diffusion coefficient  $D_{CT}$  thereby reducing the amount of  $Ru^{3+}$  available for reaction with the co-reactant, this factor must also be considered when evaluating different systems.

The ideal material for ECL should therefore not only display fast  $Ru^{2+/3+}$  regeneration times, good quantum luminescent yield and lifetimes but should also be porous enough to allow diffusion of a range of analytes through the film itself. While two of these factors have been addressed in this work the issue of film porosity while retaining favorable electrochemical and photophysical characteristics presents a great synthetic challenge. The possibility of combining a luminescent metal complex with conducting carbon nanotubes (CNTs) is one approach that may help tackle this challenge. Provided a suitable overlap of the metal and CNT orbitals could be obtained the porous yet conducting nanotube should allow significant analyte diffusion while retaining enhanced rates of charge transfer. While promising in its approach the method of integration of the metal into the CNT would need serious consideration given the varying directions of conductivity based on tube geometry existing in CNTs.

In conclusion this thesis has demonstrated that it is possible to tune both the electrochemical and photophysical properties of a material to favor ECL production, but that there often exists a “trade off” between the two, e.g. enhanced charge transport resulting in decreased luminescent lifetime. ECL generation using conducting polymers has been demonstrated. As our understanding of not only the ground state charge transfer but also the excited state charge transfer in conducting metallopolymers continues to advance the use of such systems for ECL generation is sure to increase resulting in a promising future for ECL based detection systems.

## *References*

- <sup>1</sup> Knight, A. W.; Greenway, G. M. *Analyst* **1994**, *119*, 879-890.
- <sup>2</sup> Knight, A. W. *TrAC Trends in Analytical Chemistry* **1999**, *18*, 47-62.
- <sup>3</sup> Gooding *Electroanalysis* **2002**, *14*, 1149-1156.
- <sup>4</sup> Fanrich, K. A. P., M. Guilbault, G.G. *Talanta* **2001**, *2001*, 531-559.
- <sup>5</sup> Fleet, B. K., Kirkbright, G.F., Pickford, C.J. *The Analyst* **1969**, *94*, 847.
- <sup>6</sup> Herejik, J. H. *Chemical Listy*. **1984**, *78*, 1254.
- <sup>7</sup> Greenway, G. M. *Trends in Analytical Chemistry* **1990**, *9*, 200.
- <sup>8</sup> Rozhitskii, N. N. *Journal of Analytical Chemistry* **1992**, *47*, 1288.
- <sup>9</sup> Velasco, J. G. *Electroanalysis* **1991**, *3*, 261-271.
- <sup>10</sup> J, K. L. *Luminescence* **1999**, *3*, 261.
- <sup>11</sup> Lee, W.-Y. *Mikrochimica Acta* **1997**, *127*, 19-39.
- <sup>12</sup> Gerardi, R. D.; Barnett, N. W.; Lewis, S. W. *Analytica Chimica Acta* **1999**, *378*, 1-41.
- <sup>13</sup> Benjamin, P. C., C.A.M., Loyc, J. Blum., *Analytica Chimica Acta* **2005**, *538*, 1-7.
- <sup>14</sup> Yuanhong Xua, Y. G., B.C. Hui Wei, A. Erkang, Wang A. *Journal of Chromatography* **2006**, *1115*, 260-266.
- <sup>15</sup> Jianguo L., H., *J. Analytica Chimica Acta* **2006**, *575*, 57-61.
- <sup>16</sup> Marcus, R.A.J. *Chem. Phys.* 1965, *43*, 2654.
- <sup>17</sup> Maloy, J. B., A.J. *Journal of American Chemical Society* **1971**, *93*, 5959.
- <sup>18</sup> Abruna, H. D. *Journal of Electrochemical Society* **1985**, *132*, 842
- <sup>19</sup> Lee, C. B. A. *J. Electroanalytical Chemistry, Interfacial electrochemistry* **1988**, *244*, 319.
- <sup>20</sup> Maguire N.A.P., O. N., P.J. *Inorganic Chemistry* **1987**, *26*, 2340.
- <sup>21</sup> G., X. *Analytica Chimica Acta* **2000**, *12*, 235
- <sup>22</sup> Vogler A., A., K.H. *Chemical Int.* **1981**, *20*, 469.
- <sup>23</sup> M.M. Richter. Stiplin D.R. Crosby G.A. Bard, A. J. *Analytical Chemistry* **1996**, *668*, 4370.
- <sup>24</sup> Taverna, P. J. A., A.R.J. *Analytica Chimica Acta* **1998**, *373*, 111.
- <sup>25</sup> Vogler A., A., K.H. *Journal of American Chemical Society* **1987**, *333*, 155.
  
- <sup>26</sup> Wilson, R. W. B., L., Cubitt, R., Gonsalves, M., Gilde., A. Hillman, R.A. Vos, J.G. Hogan, C.,
- <sup>27</sup> Reddinger, J. L., Reynolds, J.R. *Chemical Materials* **1988**, *10*, 3-5.
- <sup>28</sup> Campell, A. K. *Chemiluminescence* **1988**, *10*, 3-5.
- <sup>29</sup> Wallace, W. L.; Bard, A. J. *Journal of Physical Chemistry* **1979**, *83*, 1350-1375.
- <sup>30</sup> Noffsinger, J. B., Danielson, N. D. *Analytical Chemistry* **1987**, *59*, 865-868.

- <sup>31</sup> Knight, A. W.; Greenway, G. M. *Analyst* **1996**, *121*, 101R-106R.
- <sup>32</sup> Uchiyama, K., Sugii, A., *Analytical Science* **1993**, *9*, 223.
- <sup>33</sup> Holeman, J. A., Danielson, N.D. *Analytica Chemica Acta* **1993**, *277*, 55.
- <sup>34</sup> Rubinstein, I.; Bard, A. J. *Journal of American Chemical Society* **1981**, *103*, 5007-5513.
- <sup>35</sup> Ege, G. B., W.G.; Bard, A. J *Journal of Analytical Chemistry* **1984**, *56*, 2413.
- <sup>36</sup> Chen, X. C., W.; Jiang, Y.; Jia, L.; Wang, X *Journal of Microcheem.*, **1998**, *59*, 427.
- <sup>37</sup> Yocoyama, K. S., S.; Ikebukuro, K.; Taceuchi, T.; Karube, I.; Tokitsu, Y.; Masuda, Y. *Talanta* **1994**, *41*, 1035.
- <sup>38</sup> Mikkelsen, S. R. *Electroanalysis* **1996**, *8*, 15-19.
- <sup>39</sup> Yang M., M., M.E., M. Thompson, M. *Analytica Chemica Acta* **1997**, *346*, 259-274.
- <sup>40</sup> Thorp, H. H. *Trends in Biotechnology* **1998**, *16*, 117-121.
- <sup>41</sup> C. G. Cameron, T. J. P. A. P. G. P. *Journal of Physically Chemistry* **2001**, *105*, 8838-8834.
- <sup>42</sup> Arnold, J., F. E.; Arnold, F. E. *Advances in Polymer Science* **1994**, *117*, 257.
- <sup>43</sup> Techagumpuch, A. N., Miyata, S., **1961**, *Vol.2*.
- <sup>44</sup> Vogel, H. M., C. S. *Journal of Polymer Science* **1961**, *117*, 257.
- <sup>45</sup> Roberts, M. F. J., S. A. *Journal of Chemical Materials* **1994**, *6*, 135.
- <sup>46</sup> Chiang, C. K. P., Y. W.; Heeger, A. J.; Shirakawa, H.; Louis, E. J.; Macdiarmid, A. G. *Phys. Rev. Lett.*, **1977**, *39*, 1098.
- <sup>47</sup> Roncali, J. **1986**, *Vol 1,2*.
- <sup>48</sup> Wagner, J., Pielichowski, J., Hinsch, A., Pielichowski, K., Bogdal, D., Pajda, M., Kurek, S.S., Burczyk, A., *Synthetic Metals* **2004**, *146*, 159-165.
- <sup>49</sup> Skompska, M., Chmielewski, M.J., Tarajko, A., *Electrochemistry Communications* **2006**, *67*, 165.
- <sup>50</sup> Wan, Q., Wang, X., Wang, X., Yang, Y., *Sensors and Actuators* **2006**, *118*, 228-253.
- <sup>51</sup> Belosludov, R. V., . Farajian, A.A., Kikuchi, Y., Mizuseki, H., Kawazoe, K **2006**, *578*, 59-74.
- <sup>52</sup> Kingsborough , R. P. S., T. M. *Progress in Inorganic Chemistry* **1999**, *48*, 123.
- <sup>53</sup> Bard, A. J. **1994**, 89-241.
- <sup>54</sup> Lyons, M. E. G. **1994**.
- <sup>55</sup> C. G. Cameron and P. G Pickup *Journal of American Chemical Society* **1999**, *121*, 7710-7711.
- <sup>56</sup> M. Haga, M. M. A., S. Koseki, A. Yoshimura, K. Nozaki and T. Ohno, *Analytica Chemica Acta* **1994**, *226*, 17.

- <sup>57</sup> E. Sable, H. L. H. *Electrochim. Acta*, **1991**, 36, 15.
- <sup>58</sup> B. Ballarin, S. M., R. Seeber, D. Tonelli, *Journal of Electroanalytical Chemistry* **1998**, 449, 173.
- <sup>59</sup> G. Zotti, S. Z., G. Schiavon, A. Berlin, G. Pagani, A. Canavesi, *Journal of Chemical Materials*, 7, 2309.
- <sup>60</sup> Mirrazaei, R., Parker, D.S., Munro, H.S. *Journal of Materials Chemistry* **1989**, 30, 265.
- <sup>61</sup> Bauerle, P., Scheib, S., *Advanced Materials* **1993**, 5, 848.
- <sup>62</sup> Chayer, M., Faid, K., Lecleric M., *Chemical Materials* **1997**, 9, 2902.
- <sup>63</sup> Zotti, G., Schiavon G., Berlin A., Canavesi, A. *Synthetic Materials*, 76, 255.
- <sup>64</sup> King, G., Higgins, S.J., Price, N., *The Analyst* **1992**, 117, 1243.
- <sup>65</sup> C. G. Cameron and P. G Pickup *Journal of American Chemical Society* **1999**, 121, 11772-11779.
- <sup>66</sup> B. J. Mclean and P. G. Pickup *Journal of Physical Chemistry* **2002**, 106, 4658-4662.
- <sup>67</sup> J. R. Nitschke, S. Z. A. T. D. T. *Journal of American Chemical Society* **2000**, 30, 179-186.
- <sup>68</sup> I. Tomita, A. N., T. Igarashi and T. Endo *Polymer. Bull* **1993**, 30, 179.
- <sup>69</sup> M. Kurashina, M. M., T. Watanabe and H. Nishihara, *Journal of American Chemical Society* **2003**, 125, 10345-10352.
- <sup>70</sup> H. Nishihara, M. K. A. M. M. *Macromolecules Symposium* **2003**, 196, 27-38.
- <sup>71</sup> S. S. Zhu and T. M. Swager *Advanced Materials* **1996**, 8, 497-500.
- <sup>72</sup> P. L. Vidal, B. D.-B., G. Bidan, J. L. Hazemann, J. M. Kern and J. P. Sauvage, *Journal of European Chemistry* **1996**, 6, 1663-1673.
- <sup>73</sup> L. Dennany; E. J. O'Reilly; P. C. Innis; G. G. Wallace; R. J. Forster *Electrochimica Acta* **2008**, 53, 4599-4605.

- <sup>74</sup> Nguyen, M.T., Leclerc. M., Diaz, A.F. **1995** 186. Adv Polym Sci
- <sup>75</sup> Evans, G.P.; Advances in Electrochemical Science and Engineering, vol. 1, VCH, New York, **1990**
- <sup>76</sup> Samuelsen E.; (Ed.) Science and Applications of Conducting Polymers, Hilger, Bristol, UK, **1991**
- <sup>77</sup> Inzelt, G.; Bard, A.J.; (Ed) Electroanalytical Chemistry, vol, 18, M. Dekker, New York, **1994**, p. 89
- <sup>78</sup> Pickup, P.G.; (Ed) Modern aspects of Electrochemistry, vol. 33. Kluwer Academic Publishers, Boston, MA, **1999**. p 549
- <sup>79</sup> Marcel, c.; Tarascon, J.M.; Solid State Ionics 143, **2001**, 89-101
- <sup>80</sup> Falcao. E.H.L.; de Azevedo, W.M. Synth. Met. **2001**, 128
- <sup>81</sup> Wolfbeis, O.S.; Anal. Chem. 74, **2002** 2663-2678
- <sup>82</sup> S. Cosnier, Biosensors Bioelectron. 14, **1999**, 443
- <sup>83</sup> Pickup, P.G.; J. Mater. Chem. Chem. 9, **1999**, 1641
- <sup>84</sup> G. Cameron and P. G Pickup *Journal of American Chemical Society* **1999**, 121, 7710-7711.
- <sup>85</sup> Arnold, J., F. E.; Arnold, F. E. *Advances in Polymer Science* **1994**, 117, 257.
- <sup>86</sup> Osaheni, J. A., Jenekhe, S. A. *Journal of Chemical Materials* **1992**, 1282.
- <sup>87</sup> Knödler. A, Hübler, K. Sixt, T. Kaim. *Inorganic Chemistry Communications, Volume 3, Issue 4, 1 April 2000, Pages 182-184*
- <sup>88</sup> Albrecht, A. Scheiring. Sixt, T. Kaim *Journal of Organometallic Chemistry, Volume 596, Issues 1-2, 29 February 2000, Pages 84-89*
- <sup>89</sup> Vogel, H. M., C. S. *Journal of Polymer Science* **1961**, 117, 257
- <sup>90</sup> Thorne, J.R.G., Masters, J.G., Williams, S.A., MacDiarmid, A.G., Hochstrasser, Synth Met. **1992**, 49. 159
- <sup>91</sup> Kim. K., Lin, L.B., Ginder, Gustafson, T.C. Epstein, A.J., Synth Met. **1992**. 50, 423.
- <sup>92</sup> Yue, J. Epstein A.J.; J. Am. Chem. Soc. **1990**. 112. 2800
- <sup>93</sup> Shimizu, S. Saitoh, T., Uzawa, M. Yano, K., Maruyama,. T. Watanabe, K. Synth. Met. **1997**. 1337
- <sup>94</sup> Masdaraloomor, F.; Innis; P.C.; Ashraf, S.; Wallace, G.G.; Synthetic Metals 153, **2005**, 181-184
- <sup>95</sup> Tallman, D.E., Wallace, G.G., Synth Met. **1997**, 90, 13.

- <sup>96</sup> Kane-Maguire, L. A. P., Causley, J.A., Kane-Maguire, N.A.P., Wallace, G.G., *Current Applied Physics* **2004**, 4, 394-397.
- <sup>97</sup> Innis, P.C. Masdarolomoor, F. Kane Maguire, L.A.P, Forster, R.J.; Keyes. T.E. Wallace G.G. *J.Phys. Chem. B.* **2007**, 111, 12738-12747
- <sup>98</sup> Lay, P. A. S., A. M.; Taube, H. *Inorganic Chemistry* 1986, 24.
- <sup>99</sup> Guo, R.; Barisci, J. N., Innis, P.C. ; Too, C. O.; Wallace, G.G.; Zhou, D.; *Synth Met*, **2000**, 114, 287
- <sup>100</sup> Seddon, E. A., Seddon, K.R., **1984**, Ch15, p1180.
- <sup>101</sup> Durham, B., Casper, J.V., Nagle, J.K. Meyer, T.J., *Journal of American Chemical Society* **1982**, 104, 4803.
- <sup>102</sup> Casper, J. V., Meyer, T.J *Journal of American Chemical Society* **1983**, 104, 4803.
- <sup>103</sup> Haas, O., Kriens, M., Vos, J.G., *Journal of American Chemical Society*, **1981**, 103, 1318.
- <sup>104</sup> Clarke, A. P., Vos, J.G., Bandey, H.L., Hillman, A.R., *Journal of Physical Chemistry* **1995**, 99, 15973.
- <sup>105</sup> Forster, R. J., Vos, J.G., *Macromolecules Symposium* **1990**, 23, 4372.
- <sup>106</sup> Kane-Maguire, L. A. P., Causley, J.A., Kane-Maguire, N.A.P., Wallace, G.G., *Current Applied Physics* **2004**, 4, 394-397.
- <sup>107</sup> *Ch2* 1985, 49.
- <sup>108</sup> Masdaralomoor, F.; Innis,; P.C.; Ashraf, S.; Wallace, G.G.; *Synthetic Metals* 153, **2005**, 181-184
- <sup>109</sup> MacDiarmid, A. G.; Epstein, A.J. *Synth Met.* **1994**, 65, 103.
- <sup>110</sup> MacDiarmid, A. G.; Epstein, A.J. *Synth Met.* **1995**, 69, 85.
- <sup>111</sup> Xia, Y. ; Wiesinger, J.M. ; MacDiarmid, A.G. ; *A. J. Chem. Mater.* **1995**, 7, 4435
- <sup>112</sup> Son. Y.; Patterson, H.; Carlin, C.M. *Chem. Phys. Lett.* **1989**, 162, 461.
- <sup>113</sup> Karpacheva, G.; Orlov, A, V.; Rykov, S.V., Skakovsky, E.D.; *ANTEC* **1992**, 56, 1340
- <sup>114</sup> Yue. J.; Wang. Z.H.; Cromack. K, R.; Epstein, A.J., Mac Diarmid. A.G., *J. Am. Chem. Soc.*, 113, **1991**, 2665;
- <sup>115</sup> Dennany, L.; O'Reilly, E.J.; Innis, P.C.; Wallace, G. W.; Forster, R. J.; *Electrochemica Acta.* **2007** (in press)
- <sup>116</sup> Jortner. J.; Bixon. M; *Adv. Chem. Phys.* **1999** 106,
- <sup>117</sup> Barbara. P.F.; Meyer, T.J.; Ratner, M.A.; *J. Phys. Chem.* **1996** 100,
- <sup>118</sup> Jortner. J.; Ratner. J. *Molecular Electronics*, Blackwell Science Ltd., Oxford, 1997
- <sup>119</sup> Newton, M.D. *Chem Rev.* **1991** 91, 767

- <sup>120</sup> Hush, N.S.; J. Electroanal. Chem. **1999**, 460, 5
- <sup>121</sup> Ward, M.D. Chem Soc Rev. **1997**, 26, 365.
- <sup>122</sup> Nazeeruddin, M.K.; Kay, A.; Rodicio, I.; Humphry-Baker, R.; Muller, E.; Liska, P.; Vlachopoulos, N.; Gratzel M.J.; J. Am. Chem. Soc. **1993**, 115, 6382
- <sup>123</sup> Knox, R.S. Photosynth. Res. **1996**, 48, 35
- <sup>124</sup> Cameron, C. G; Pickup P. G, J.; Am. Chem. Soc. **1999**, 121, 11773-11779.
- <sup>125</sup> Cameron, C.G.; Pickup, P.G.; J. Phys Chem. **2001**, 105, 8838-8834.
- <sup>126</sup> Cameron, C.G., Pickup, P.G.; J.; Am. Chem. Soc. **1999**, 121, 7710-7711.
- <sup>127</sup> Cameron, C.G., Pickup, P.G.; J. Am. Chem. Soc **1999**, 121, 11772-11779.
- <sup>128</sup> B. J. Mclean and P. G. Pickup J. Am. Chem. Soc. **2002**, 106, 4658-4662.
- <sup>129</sup> Dennany, L.; O'Reilly, E. J.; Keyes, T. E.; Forster, R.J.; Electrochem Comm. **2006**, 8, 10. 1588- 1594
- <sup>130</sup> Dennany, L.; Forster, R.J.; Rusling, J, F.; J. Am. Chem. Soc. **2003**, 125, 5213-5218
- <sup>131</sup> Kaneko, M.; Prog. Polym. Sci. 26 **2001** 1101-1131
- <sup>132</sup> McClean, B. J.; Pickup, P.J; J. Phys. Chem. B **2002**, 106, 4658-4662
- <sup>133</sup> R. J. Forster and J. G. Vos in Comprehensive Analytical Chemistry, Ed. G. Svehla, Elsevier, Amsterdam, **1992**, vol. XXVII, p. 465.
- <sup>134</sup> Paul, E.W.; Ricco, A.J.; Wrighton, M.S.; J. Phys. Chem. **1985**, 89, 1441.
- <sup>135</sup> Thackeray, J.W.; White, H.S.; Wrighton, M.S.; J. Phys. Chem. **1985**, 89, 5133.
- <sup>136</sup> Ofer, D.; Crooks, R.M.; Wrighton, M.S.; J. Am. Chem. Soc., **1990** 112, 7869.
- <sup>137</sup> Dahms, H.; J Phys. Chem., 72 **1968** 362.
- <sup>138</sup> Ruff, I.; Friedrich, V.J.; Demeter, K.; Csillag, K.; J. Phys. Chem. **1971** 75, 3303.
- <sup>139</sup> Terrill, R.H, Hutchinson, J.E.; Murray, R.W.; J. Phys. Chem. B, **1997**, 101, 1535.
- <sup>140</sup> Wuelfing, W.P.; Green, S.J.; Pietron, J.J.; Cliffel, D.E.; Murray, R.W.; J. Am. Chem. Soc. **2000** 122, 11465.
- <sup>141</sup> Kasha, M.; Discuss. Faraday Soc., **1950**, 9, 14 – 19
- <sup>142</sup> Keyes, T. E.; O'Connor, C; Vos, J.G; Chem. Commun., **1998**, 889
- <sup>143</sup> Blakely, M. R.; DeArmond, K. M.; J. Am. Chem. Soc. **1987**, 109, 4895-4901
- <sup>144</sup> Rehm, D.; Weller, A. Israel J. Chem., **1970**, 8, 259.
- <sup>145</sup> Lyons, C. H.; Abbas, E. D.; Lee, J.-K.; Rubner, M. F. *J. Am. Chem. Soc.* **1998**, 120, 12100.
- <sup>146</sup> Mikkelsen, S. R. *Electroanalysis* **1996**, 8, 15-19.
- <sup>147</sup> Thorp, H. H. *Trends Biotechnol.* **1998**, 16, 117-121.
- <sup>148</sup> Palek, E.; Fojta, M. *Anal. Chem.* **2001**, 73, 75A-83A.
- <sup>149</sup> Lee, J.; Wu, A.; Handy, S.; Rubner, M. F. *Appl. Phys. Lett.* **1996**, 69, 1686.
- <sup>150</sup> Zotti, G.; Schiavon, G.; Zecchin, S.; Berlin, A.; Pagani, G.; Canavesi, A. *Synth. Metals* **1996**, 76, 255-258.
- <sup>151</sup> Cameron, C. G.; Pickup, P. G. *J. Am. Chem. Soc.* **1999**, 121, 7710-7711.
- <sup>152</sup> Cameron, C. G.; Pickup, P. G. *Chem. Commun.* **1997**, 3, 303-304.
- <sup>153</sup> L. Dennany; E. J. O'Reilly; P. C. Innis; G. G. Wallace; R. J. Forster *Electrochimica Acta* **2008**, 53, 4599-4605.

- 154 Masdarolomoor, F.; Innis, P. C.; Ashraf, S.; Wallace, G. G. *Synth. Metals* **2005**, *153*, 181-184.
- 155 Masdarolomoor, F.; Innis, P. C.; Ashraf, S.; Wallace, G. G. In *ICSM 2004*: Wollongong, Australia, 2004.
- 156 Forster, R. J.; Vos, J. G. *Langmuir* **1994**, *10*, 4330-4338.
- 157 Tokel, N. E.; Bard, A. J. *J. Am. Chem. Soc.* **1972**, *94*, 2862-2863.
- 158 Tallman, D. E.; Wallace, G. G. *Synth. Metals* **1997**, *90*.
- 159 Hogan, C. F.; Forster, R. J. *Anal. Chim. Acta* **1999**, *396*, 13-21.
- 160 Denny, R. A.; Sangaranarayanan, M. V. *J. Phys. Chem. B* **1998**, *102*, 8670-8677.
- 161 Lyons, M. E. G. In *Electroanalytical chemistry, Part I: Fundamentals*; Lyons, M. E. G., Ed.; Plenum Press: New York, **1994**, pp 89-241.
- 162 Inzelt, G. In *Electroanalytical Chemistry*; Bard, A. J., Ed.; Marcel Dekker: New York, **1994**; Vol. 18, pp 89-241.
- 163 Haga, M.-A.; Meser Ali; Koseki, S.; Yoshimura, A.; Nozaki, K.; Ohno, T. *Inorganica Chimica Acta* **1994**, *226*, 17-24.
- 164 Forster, R. J.; Vos, J. G. *J. Electroanal. Chem.* **1991**, *314*, 135-152.
- 165 Forster, R. J.; Vos, J. G.; Lyons, M. E. G. *J. Chem. Soc., Faraday Trans.* **1991**, *87*, 3761-3768.
- 166 Fleming, C.N. Maxwell. K.A. DeSimone, J.M. Meyer. T.J. and Papanilolas, J.M. *J. am. Chem. Soc.*, **2001**, *123*, 10336-10347
- 167 Huynh, M. H. V. Dattelbaum, D.M. Meyer, T.J. *Coord. Chem. Rev.*, **2005**, *249*, 457-483
- 168 Ward M.D. Barigelletti, F. *Coord. Chem. Rev.* **2001**, 216-217,
- 169 Haas, O. Kriens. M. Vos, J.G. *J. Am. Chem. Soc.*, **1981**, *102*, 1318-1319
- 170 Kelly. D.M. Vos. J.G. in *Electroactive Polymer Chemistry, Part 2, Methods and applications*, ed. M. Lyons, Plenum Press, New York, **1996**. Ch. 8.
- 171 Ziessel R. in *Advances in Chemical Conversions for Mitigating Carbon Dioxide*, ed. T. Inui, M. Anpo, S. Yanagida and T. Yamaguchi, **1998**, vol. 114, p 219
- 172 J. N. Demas, A. W. Adamson, *J. Am. Chem. Soc.* **1973**, *95*, 5159.
- 173 *G. Chem.* **1974**, *13*, 2159.
- 174 Minsky M.: *Scanning* **1998**, *10*, 128-138.
- 175 White, J.G. Amos W.B. Fordham, M : *J. Cell Biol.* **1987** *105*, 41-48.
- 176 Denk, W. Strickler, J.H., Webb, W.W. *Science* **1990**, *24* 73-76
- 177 A. Periasami, M. Elangovan, H. Wallrabe, J.N. Demas, M. Barroso, D.L. Brautigan, R.N. Day, *Methods in cellular imaging* (ed. by A. Periasamy), 295-308, Oxford University Press, New York
- 178 B. Herman, *Fluorescence Microscopy*, 2nd. edn. Springer-Verlag, New York 1998

- <sup>179</sup> J.R. Lakowicz, Principles of Fluorescence Spectroscopy, 2nd. Ed., Plenum Press, New York 1999
- <sup>180</sup> A. Periasami, R.N. Day, Visualizing protein interactions in living cells using digitized BFG imaging and FRET microscopy, in: Green Fluorescent Proteins, ed. by K.F. Sullivan, S.A Key, Academic Press, 1999
- <sup>181</sup> Elangovan, M., Day, R.N., Periasami. A., J. Microsc. **2002**, 205, 3-14
- <sup>182</sup> M.R. Eftink, Fluorescence quenching: Theory and application, in: J.R. Lakowicz, Topics in fluorescence spectroscopy, Vol. 2 **1991**, 53-126
- <sup>183</sup> Koenig, K., Peuckert, C., Riemann, I, Wollina, U. SPIE 4620-36
- <sup>184</sup> Knight, A. W.; Greenway, G. M. *Analyst* **1996**, 121, 101R-106R.
- <sup>185</sup> Knight, A. W. G., G.M. *Analyst* **1994**, 119, 879-890.
- <sup>186</sup> J.-K. Lee; D. S. Yoo; E. S. Handy; Rubner, M. F. *Applied Physical Letters* **1996**, 69, 1686-1688.
- <sup>187</sup> Ward, W. K. *ASAOI* **1999**, 45, 555-561.
- <sup>188</sup> Weisner, A. Current Pharmaceutical Biotechnology **2004**, 2004, 45-67.
- <sup>189</sup> Kojima, K. H. A. S. H., Yano, K., Ikebukuro, K. Kraube I. *Analytical Chemistry* **2003**, 75, 1116-1122.
- <sup>190</sup> Wilson, M. S. *Analytical Chemistry* **2005**, 77, 1496-1502
- <sup>191</sup> A.E., A. *Analytical Chemistry* **1984**, 56, 667-671.
- <sup>192</sup> Masdarolomoor, F.; Innis, P. C.; Ashraf, S.; Wallace, G. G. In *ICSM 2004: Wollongong, Australia*, 2004.
- <sup>193</sup> Haas, O.; Kierns, M.; Vos, J. G. *Journal of American Chemical Society* **1981**, 103, 1318-1319.
- <sup>194</sup> Qu, P.; Thompson, D. W.; Meyer, G. J. *Langmuir* **2000**, 16, 4662-4671.
- <sup>195</sup> Swager, R. P. *Journal of American Chemical Society* **1999**, 121, 1100-1104.
- <sup>196</sup> Lee, C. B. A. J. *Electroanalytical Chemistry, Interfacial electrochemistry* **1988**, 244, 319.
- <sup>197</sup> G., X. *Analytica Chimica Acta* **2000**, 12, 235.
- <sup>198</sup> C. G. Cameron and P. G Pickup *Journal of American Chemical Society* **1999**, 121, 11772-11779.
- <sup>199</sup> C. G. Cameron, G. P. *Journal of Physically Chemistry* **2001**, 105, 8838-8834.
- <sup>200</sup> Dennany, L.; Forster, R. J.; Rusling, J. F. *J. Am. Chem. Soc.* **2003**, 125, 5213-5218.
- <sup>201</sup> Johnston, D. H.; Glasgow, K. C.; Thorp, H. H. *J. Am. Chem. Soc.* **1995**, 117, 8933-8941.
- <sup>202</sup> Hogan, C. F.; Forster, R. J. *Anal. Chim. Acta* **1999**, 396, 13-21.
- <sup>203</sup> Dennany, L.; Hogan, C. F.; Keyes, T. E.; Forster, R. J. *Anal. Chem.* **2006**, 78, 1412-1417.

- <sup>204</sup> Hodgkinson, A. *Academic Press* **1977**, 230-253.
- <sup>205</sup> Murray, J. F., Nolen, H., Gordon, G.R., Peters, J.H., *Analytical Biochemistry* **1982**, *121*, 301-309.
- <sup>206</sup> Thiruvikraman, K. V. K., Wolfson S.K., Yao, S.J., Morgenlander, J.C., **1982**, *9*, 357-364.
- <sup>207</sup> Chiang, C. K. W.; Heeger, A. J.; Shirakawa, H.; Louis, E. J.; Macdiarmid, A. G. *Phys. Rev. Lett.*, **1977**, *39*, 1098.
- <sup>208</sup> Hogan, C. F.; Forster, R. J. *Anal. Chim. Acta* **1999**, *396*, 13-21.
- <sup>209</sup> Obeng, Y.S. Bard, A.J., *Langmuir* 1991, *7*, 195
- <sup>210</sup> Sato, Y. Uosaki, K. *J. Electroanal. Chem.* **384** (1995) 57.
- <sup>211</sup> Calvert, J.M. Meyer. T.J., *Inorg. Chem.* **20** (1981) 27
- <sup>212</sup> Zu, Y. Bard, A.J. *Anal. Chem.* **72**, (2000) 3223
- <sup>213</sup> Bard, A. J.; Keszthelyi, C. P.; Tachikawa, H.; Tokel, N. E. *Chemiluminescence & Bioluminescence* **1973**, *3*, 193-199.
- <sup>214</sup> Richter, M. M.; Debad, J. D.; Striplin, D. R.; Crosby, G. A.; Bard, A. J. *Anal. Chem.* **1996**, *68*, 4370-4376.
- <sup>215</sup> Wallace, W. L.; Bard, A. J. *J. Phys. Chem.* **1979**, *83*, 1350-1375.
- <sup>216</sup> Van Houten, J.; Watts, R. J. *J. Am. Chem. Soc.* **1976**, *98*, 4853-4858.